Analytical and Experimental Investigation of Overtesting during Assembly-Level Shock Testing

Jean-Philippe Deblois

A Thesis

in

The Department

of

Mechanical and Industrial Engineering

Presented in Partial Fulfillment of the Requirements
for the Degree of Master of Applied Science (Mechanical Engineering) at
Concordia University
Montreal, Quebec, Canada

May 2009

Your file Votre référence
ISBN: 978-0-494-67257-0
Our file Notre référence
ISBN: 978-0-494-67257-0

Abstract

Analytical and Experimental Investigation of Overtesting during Assembly-Level Shock Testing

Jean-Philippe Deblois

Mechanical shocks induced by the detonation of pyrotechnics ordnances are known to be highly detrimental to the integrity of spacecraft components. As a result, it is desirable to qualify these components as early as possible to prevent failures during launch. Assembly-level shock tests are usually performed on these components. However, these tests are suspected to be the cause of several failures that would not occur during flight. The knowledge acquired in vibration testing suggests that the overtesting is mainly due to the rigidity of the mounting interface between the component and the testing device. Consequently, the test configuration lacks the dynamic absorber effect which should naturally occur in flight configuration. While the Force Limited Vibration (FLV) technique has been developed to reduce the overtesting occurring in vibration testing, no systematic methodology have been proposed to measure and to reduce the shock overtesting to this date.

The objective of this study is to conduct systematic analytical and experimental sensitivity investigation on the overtesting occurring in the assembly-level shock testing. A reconfigurable prototype of an electronic box and a mounting structure have been designed and modeled using the finite element method. The prototype is then fabricated and tested to demonstrate the

occurrence of overtesting experimentally. The vibration overtesting and the C^2 coefficients of the semi-empirical method are evaluated using FLV technique. The shock overtesting is evaluated similarly using an acceleration excitation generated for the shaker test. The results show that no significant correlation between the vibration and the shock overtesting exist. Finally, a method to reduce the shock overtesting is proposed in which the shock specification is notched at the main frequencies to limit the response of the structure.

Acknowledgements

I wish to express my profound gratitude to my supervisors Dr. Ramin Sedaghati and Dr. Yvan Soucy for their constant encouragement and guidance; Dr. Soucy who identified this original problematic and drove me toward this glimpse of solution and Dr. Sedaghati who acted as a mentor and pushed me to confront my new ideas with reality.

I would like to thank Steeve Montminy at the Canadian Space Agency (CSA) who has made invaluable suggestions of design and has provided me with examples of electronic boxes. I want to express my appreciation to Sébastien Brunel, also at the CSA, whose advice and skills have considerably added to the FE modelling. I am also grateful to CSA machine shop personnel, namely Pierre Lortie, Philippe Vincent and Ralph Nolting, for manufacturing the test articles, Dr. Raj Singhal and Richard Poirier at DFL for allowing to perform the experiments, Dr. Jim Olmstead and Dr. Gérard Carrier at MDA Space Missions for their discussions about mechanical shock testing and design requirements.

Also, I would like to show my appreciation to my friends and my family who have kept my life cheerful and entertaining all this time. At last, I am exceptionally grateful to my father and mother, Réjean Deblois and Nicole Naud, for their incessant love and support throughout my life.

TABLE OF CONTENTS

LIST OF FIGURES

LIST OF TABLES

LIST OF ACRONYMS

APSD:	Acceleration Power Spectral Density
CS:	Coupled System
CSA:	Canadian Space Agency
DLF:	David Florida Laboratory
d.o.f.	Degree-of-freedom
DUT:	Device Under Test
FE:	Finite Element
FLV:	Force-Limited Vibration
FPSD:	Force Power Spectral Density
I/F:	Interface
IES:	Input Energy Spectrum
MS:	Mounting Structure
ms:	Millisecond
PVSS:	Pseudo-Velocity Response Spectrum
PSD:	Power Spectral Density
RRS:	Random Response Spectrum
SDOF:	Single Degree-Of-Freedom
SRS:	Shock Response Spectrum
TA:	Test Articles
TDOF:	Two Degrees-Of-Freedom
TI:	Test Item

NOMENCLATURE

f	Frequency	(Hz)
f_n	Natural Frequency	(Hz)
$y(t)$	Relative Displacement	(m)
$\ddot{z}(t)$	Ground Acceleration	(m/s²)
E	Young's Modulus	(Pa)
ω	Angular Frequency	(rad/s)
ω_n	Angular Natural Frequency	(rad/s)
ζ	Critical Damping Fraction	
ρ	Density	(kg/m^3)
λ	Wavelength	(m)

Chapter 1

Introduction

1.1 Motivation and Objective

Launch vehicles and spacecrafts often use several pyrotechnic devices during their mission. Such devices usually serve to separate the spacecraft from the launch vehicle and/or to deploy appendages. However, pyrotechnics detonation induces severe transient shock on the surrounding structure. This high frequency transient event is known as pyroshock and has high amplitude (up to 10 000 g or more), short duration (less than 20 ms) and high frequency content (up to above 10 kHz) that can be detrimental to many spacecraft equipments while they are resistant to a variety of lower frequency environment, including random vibration. Pyroshocks are known to be the cause of many failures in the past [1, 2] and are still regarded as a major threat to space mission success [3, 4, 5]. Qualifying flight hardware for pyroshock environment is deemed an effective mean of protection against this threat.

At the spacecraft and large subsystem level-of-assembly, such testing is usually performed utilizing flight pyrotechnic devices and flight or flight-like structure. Tests at lower levels-of-assembly, such as electronic components, mechanical devices, components and small subsystems, commonly referred to assembly-level tests, are performed using a variety of mechanical devices to

simulate the shock input. The input is usually specified in the form of the envelope of the shock response spectrum (SRS) of the expected in-flight environment. These assembly-level tests are suspected to cause severe overtesting mainly related to the vibration absorber effect and could potentially cause severe damage to delicate space hardware which would have not occurred in flight configuration. To date, there is not precise estimate of shock overtesting.

Considering the above, the overall objective of this thesis is to conduct fundamental study on the overtesting phenomenon occurring during assembly-level shock testing, to investigate possible means of estimating this overtesting and to modify the shock test strategy in order to reduce the overtesting occurring in test.

1.2 Literature Review of the Pertinent Works

The purpose of this section is to provide a digest on the current state-of-the-art of pyroshock testing and analysis. It also provides a survey of the state-of-the-art in the field of force limited vibration (FLV) testing and on the current knowledge of shock overtesting. Moreover, it is intended to establish a common terminology between two different areas, namely random vibration and pyroshock testing. These two fields of structural dynamics have matured separately and thus, showing parallels between understanding of both

communities is pertinent. It should be noted that most of the relevant work is from the space industry with some addition from the earthquake community.

1.2.1 The Pyrotechnics Shock Problem

This section provides details about the pyrotechnics ordnance usages in the space industry, pyroshock physical characteristics, shock level prediction methods available and methods employed to qualify equipment especially at assembly-level.

1.2.1.1 Pyrotechnics Ordnances Usage

Many space programs use pyrotechnics ordnance for purpose as diverse as to separate launch vehicle stages, to separate spacecraft from launch vehicle, to deploy appendages like solar arrays and antennas and to activate components like valves and switches [3]. The lightweight and high reliability of these ordnances make them perfect for space system. Most of the time, the ordnance is used to break the mechanical link between two parts. For example, an explosion rips apart the bolts retaining a solar array which then deploys itself using the energy stored as a pre-load. A similar method is used in V-band clamps to retain the spacecraft during launch and to separate it from the launch vehicle once in space.

There are several types of pyrotechnics ordnances used in space applications. They can be grouped by their geometrical configuration. Each of

these sources produces a particular shock wave. A line source is generally more intense than a point source [3].

Here are some examples of point and line sources:

- Point sources: Explosive bolt, separation nut, pin puller, pyrovalve.
- Line sources: V-band clamp, mild detonation fuse, explosive transfer line.

Bement and Schimmel [6] provide detailed explanations about the usage of pyrotechnics in the aerospace industry. The explanations focus on the proper design and integration of ordnances in a design. It also contains useful explanations concerning testing methods.

Chang [7, 8] conduct in-depth investigation of the characteristics of widely used pyrotechnic devices. These studies provide comparison of the specification provided by their respective manufacturer with data observed on actual aerospace hardware. Specially, in the case of a V-band release mechanism, Chang [7] shows that the shock energy is mostly provided by the strain energy released and not from the ordnance's chemical reaction.

1.2.1.2 Shock Induced Failures

Moening [1] has documented the cause of failure of major space programs for the 1960-82 period. Of the 85 observed failures, 19 are directly attributed to pyroshock, while 22 more are very likely induced by pyroshock and another 31

are potentially caused by pyroshock. Most of the shock induced failures reported had magnitude in excess of 3000 g at frequency higher than 2000 Hz. These levels are also reported by Luhrs [9]. Prior to these early failures, such high frequency excitations were disregarded as a threat to structural integrity or to the good operation of any equipment. It is important to mention that these magnitudes and frequency contents are out of reach of usual sine and random vibration test performed on electrodynamics shaker. Shock sensitive components and their possible mode of failures can be summarized in three categories as given in Table 1:

Table 1: Shock sensitive components and their failure modes [1]

Components	Examples	Failure mode
Relay and switch		Chatter and transfer
		Permanent damage
Brittle material	Crystals, ceramis, brittle epoxies, glass diodes, wire leads	Cracks and breakage
		Loss of seal
		Bond fractures
		Shorts
Light-weight structural member		Deformation

As a corrective action, the importance of testing equipment at system level and, if possible, at sub-system level is particularly stressed. Analysis can be performed in order to assed equipment damage risk to shock as explained by Ref. [10].

1.2.1.3 Categories of Pyroshock

There is a frequency rule, which helps judging if equipment needs qualification [11]. The frequency damage rule-of-thumb is the shock acceleration level in g times its frequency in Hz. Damages were observed in military grade equipment when subjected to a SRS shock level of 1.6 times frequency. Therefore, systematic testing when the SRS shock level reaches 0.8 times frequency is recommended.

$$\begin{aligned} G\,level &\geq 0.8f \Rightarrow Qualification \\ G\,level &\geq 1.6f \Rightarrow Observed\ Damage \end{aligned} \qquad \textbf{Eq. (1)}$$

For example, if an acceleration level of 1500 g is encountered at a frequency of 1000 Hz, the frequency damage rule-of-thumb suggests that the exposed component should undergo a qualification campaign (1500 > 0.8 x 1000).

Pyroshock environments can be divided into three categories: near-field, mid-field and far-field, according to their magnitude and spectral content [11]. A summary of the pyroshock categories is presented in Table 2. It should be emphasized that no shock sensitive hardware should be exposed to near-field environment in a good design. Therefore, most space works focus on far-field regime.

Table 2: Pyroshock Regimes [11]

Zone	Near-field	Mid-field	Far-field
Response governed by	Structure material stress wave propagation effects	Combination of the two effects	Structural resonance response effects
Distance from with intense	< 15 cm	15-60 cm	> 60 cm
with less intense	< 7.5 cm	7.5-15 cm	> 15 cm
pyrotechnic device	(no intervening structural discontinuities)		
Peak accelerations	> 5000 g	1000-5000 g	< 1000 g
Spectral content	> 100 000 Hz	> 10 000 Hz	< 10 000 Hz
Test device	Explosive	Explosive or impact	Impact or shaker

Various studies [3, 12, 13] have shown that the amplitude level of the pyroshock decreases with the distance from the source. This well-known phenomenon is greatly affected by the type of structure. The attenuation is more important in the higher frequency range and explains why the spectral content of the pyroshock decreases with distance (far-field versus near-field). Many empirical relations have been developed to predict the attenuation with distance [3, 12, 13]. Among these relations, the so-called NASA relation is illustrated in Figure 1 and has been generally employed for a point-source ordnance in a complex structure as [3]:

$$att = \exp\left[\left(-8\times10^{-4} f_n^{\left(2.4 f_n^{-0.105}\right)}\right)\right]\Delta D \qquad \textbf{Eq. (2)}$$

Where f_n is the oscillator natural frequency and ΔD is the distance from the source. It should be noted that the name attenuation may be misleading. In fact, it may be more proper to name attenuation as transmission or the remaining content of the initial shock after a given distance.

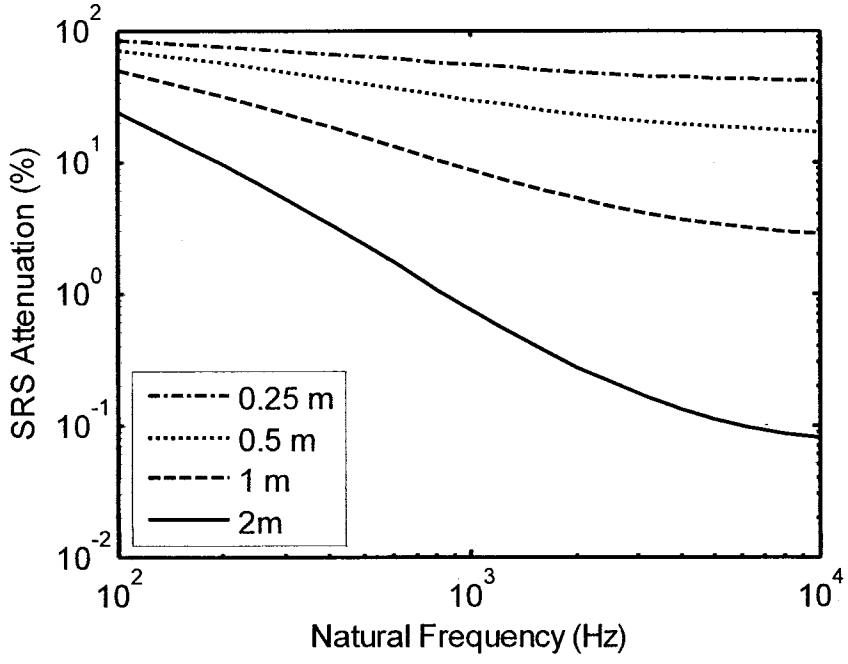

Figure 1: SRS attenuation for different distances by NASA relation

It is also shown that the number and the type of mechanical junctions also induce a strong attenuation on the pyroshock level [3, 12, 13]. More explanations about the finite element modelling of a mechanical junction can be found in Refs. [14, 15].

Also, the most widespread definition of the duration of a pyroshock event is the 10 percent duration [3]. It is measured between the instant the shock first rises above 10 percent of the maximal absolute acceleration to the last time before it decays below this value. This definition determines the duration of a transient event in an objective fashion. Pyroshocks are complex transient and do not fit into the conventional definition of the shock. It should be noted that the

excitation duration can be longer than the fundamental period of a structure, especially in the far-field regime.

1.2.1.4 Shock Response Spectrum

In 1932, Biot [16] proposed an analysis method to quantify the response of buildings to earthquake. His work has been adopted to judge the damageability of a transient event and is now known as the Shock Response Spectrum (SRS). Details about the SRS usage in the space industry are given by Irvine [17].

Essentially, a SRS is a plot showing the response of many single degree of freedom (SDOF) systems to a base excitation as shown in Figure 2. Different SDOF systems are tuned to a specific frequency. Together, these oscillators cover the entire frequency range of interest. The SRS basically demonstrates the maximal absolute acceleration response of each SDOF at its natural frequency. A damping value must be selected for the analysis and is generally taken as ζ=0.05 or Q=10. The SDOF natural frequencies are normally spaced with a proportional bandwidth.

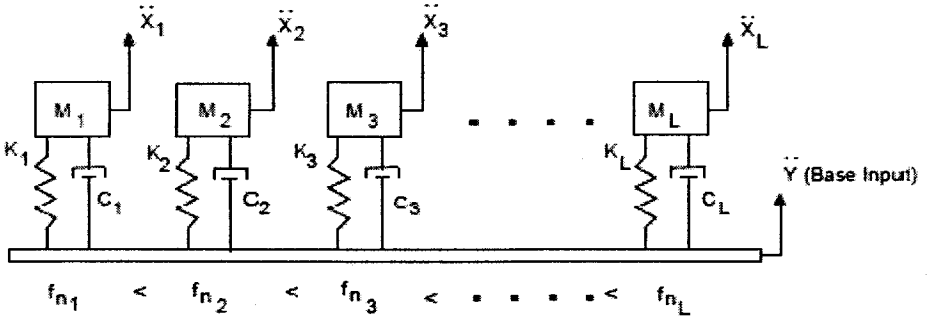

Figure 2: Symbolic SRS representation [17]

A typical acceleration waveform and corresponding SRS are shown in Figure 3. Negative and positive curve in the SRS plot corresponds to the maximal negative and positive accelerations of the SDOF system.

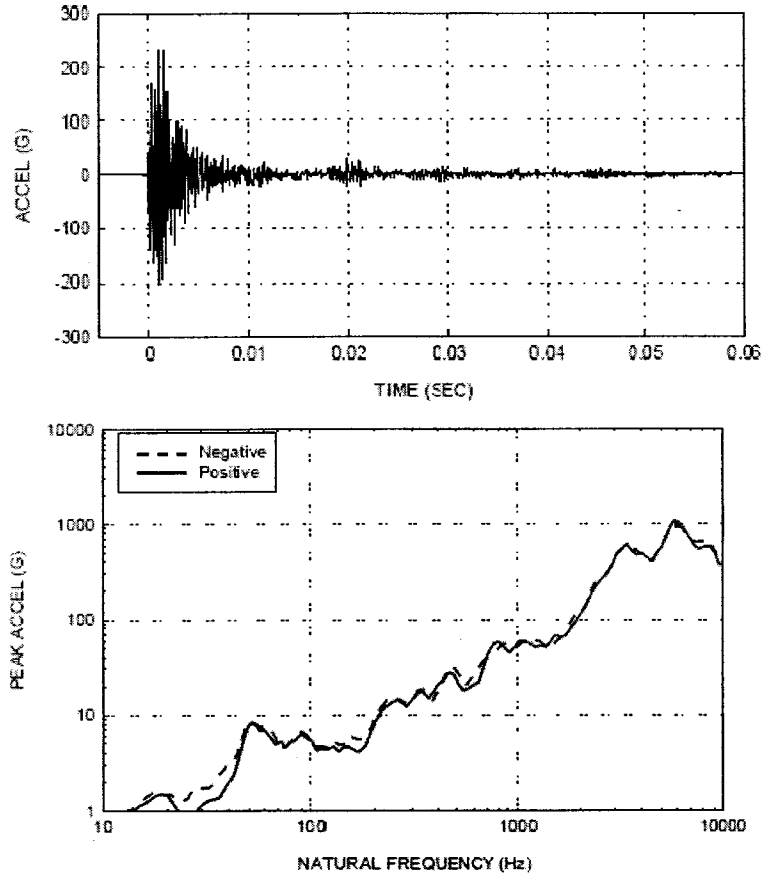

Figure 3: Typical acceleration waveform (above) and corresponding SRS (below) [17]

Matsuzaki [18] provides in-depth literature review of the SRS concept. Based on analytical demonstrations, it is shown that SRS is a useful tool to quantify transient loading for both linear and non-linear system.

Numerical integration of a linear convolution integral can be performed in order to evaluate the acceleration response of a SDOF system to the input shock

and thus, it can be used to evaluate the SRS [19]. Since the calculation is performed in the time domain, at least 8 samples per cycle of the highest frequency of interest are required to obtain accurate results [3]. For example, if the highest frequency is 10 000 Hz, the sampling frequency must be at least 80 000 Hz.

The relative time of several dedicated SRS calculation algorithm have been studied by Filippi [20] and the main results of his study are summarized in Table 3. It should be noted that direct integration of convolution integral has been disregarded in this study as it was considered too much time consuming. The Smallwood algorithm [21] is shown to be the fastest.

Table 3: Relative time comparison of SRS calculation method [20]

Method	Relative Time
Smallwood	100%
Cox	210%
Newmark	290%

All these methods result in equally valid solution. However, the result of these methods is not exactly the same, mostly due to numerical errors. These small discrepancies result in added uncertainty between different facilities. To avoid these discrepancies, NASA pyroshock handbook [3] recommends using the Smallwood algorithm as a standard calculation tool. This algorithm makes use of recursive digital filter to achieve a fast and accurate calculation.

1.2.1.5 Pseudo-Velocity Shock Spectrum (PVSS)

Some studies have demonstrated the link between modal velocity and the stress limits in mechanical vibration [22] and shock [23]. The pseudo-velocity (PV) is defined as the maximal displacement times the oscillator's natural angular frequency as [24]:

$$PV = x_{\max}\omega_n \qquad \textbf{Eq. (3)}$$

Gaberson [24] shows that the pseudo-velocity relates to the strain energy and the kinetic energy of an oscillator. Due to this relationship, Gaberson [25] recommended to use the Pseudo-Velocity Shock Spectrum (PVSS) plotted on four-coordinate paper with pseudo velocity as the main axis instead of the SRS to judge the severity of pyroshock events. Gaberson [24] also advocates that simple pulse shocks (half-sine, trapezoidal, saw tooth) can be adjusted properly to qualify equipment for pyroshock environment.

Finally, even though the PVSS indicator has been known for some time, it has not been adopted by the space industry. However, it is not uncommon to encounter a constant velocity line on SRS plots of investigations conducted by the space industry [26]. Moreover, Ref. [10] suggests using PVSS along with other tools, i.e. SRS, frequency damage rule-of-thumb (0.8*f*), to evaluate shock severity. It is important to note that the SRS cannot simply be translated to a

PVSS because both acceleration maxima, for SRS, and displacement maxima, for PVSS, don't occur at the same time.

1.2.1.6 Input Energy Spectrum (IES)

Smallwood and Edwards [27] suggest the concept of the energy method to investigate pyroshock in the space industry. The energy method allows characterizing the shock independent of the structure. It also allows evaluating the damage potential, or strain energy, as a function of structural response. These two facts are desirable characteristics of shock specification. Therefore, the authors suggest using the input energy spectrum (IES) as a specification of pyroshock. One duration indicator is also required because, for equivalent IES, shorter shock duration generally involves higher peak strain energy, thus more damageable shock.

Zahrah and Hall [28] investigate the energy distribution, and finally the energy absorption, of SDOF structures subjected to ground motion. This method was established for and is still in use in the earthquake community [29, 30]. The equation of relative motion, $y(t)$, per unit mass of a linear elastic oscillator to a ground motion, $z(t)$, can be described as [28]:

$$\ddot{y}(t) + 2\zeta\omega_n \dot{y}(t) + \omega_n^2 y(t) = -\ddot{z}(t) \qquad \textbf{Eq. (4)}$$

The different energy terms are defined as the integration of the force acting through the displacement. It is also possible to use the relationship $dy = \dot{y}dt$ to simplify the numerical integration as:

$$\int_0^Y \ddot{y}(t)dy + 2\zeta\omega_n \int_0^Y \dot{y}(t)dy + \omega_n^2 \int_0^Y y(t)dy = -\int_0^Y \ddot{z}(t)dy$$
$$\int_0^T \ddot{y}(t)\dot{y}(t)dt + 2\zeta\omega_n \int_0^T \dot{y}(t)\dot{y}(t)dt + \omega_n^2 \int_0^T y(t)\dot{y}(t)dt = -\int_0^T \ddot{z}(t)\dot{y}(t)dt \quad \textbf{Eq. (5)}$$

The input energy, E_I, to the SDOF oscillator is on the right-hand side of Eq. (5). On the left-hand side, the first term is the kinetic energy, E_K, the second term is the energy dissipated by viscous damping, E_D, and the third term is the strain energy, E_S. In the case of a non-elastic oscillator, the third term also includes the hysteretic energy, E_H. This concept can be extended to handle more general non-linear cases. Time integration technique based on the Newmark's Beta-method was used to determine the solution.

As the energy distributions between the different terms are examined in the time-domain, different indicators such as number of yields excursions, cycle reversals and effective motion have been defined to quantify the damage imparted by the earthquake to the structure [28]. All these quantities can also be plotted as a spectrum when they are investigated for different oscillator's natural frequency. The Input Energy Spectrum (IES) is thus defined as the total energy

imparted to a SDOF system by the ground motion as a function of the SDOF natural frequency.

The earthquake design spectra in the form of pseudo-velocity response spectra (PVSS), its usage as an indicator of the frequency content of the ground motion and as an analysis tool for building designer is reviewed by Hall and McCabe [29]. They also highlighted the principal limitation of PVSS, which is the lack of indication regarding the effective motion duration. In fact, the PVSS cannot distinguish between one short energy burst earthquake and a sustained long-duration motion earthquake. Considering this, the examination of the input energies in the time-domain is suggested. Moreover, the relation between the absorbed energy and the number of cycle to fracture of a structure and finally the ability of the IES to relate to cyclic induced damage are also emphasized.

Ordaz et al [30] has developed a methodology to compute the IES from Fourier amplitude spectrum. The IES can be computed exactly from the integration of the Fourier amplitude spectrum, $A(\omega)$ and the real part of the transfer function, H_v , relating the ground acceleration to the relative velocity, as [30]:

$$E_I(\omega,\zeta) = -\frac{1}{\pi}\int_0^{\infty} |A(\omega)|^2 \,\mathrm{Re}\left[H_V(\omega;\omega_n,\zeta)\right] d\omega$$

$$\text{where } H_V(\omega;\omega_n,\zeta) = -\frac{2\zeta\omega_n\omega^2}{\left(\omega_n^2-\omega^2\right)^2+\left(2\zeta\omega_n\omega^2\right)^2} \qquad \textbf{Eq. (6)}$$

1.2.2 Shock Prediction Techniques

Over the years, many techniques have been implemented to predict the pyroshock levels at different locations of a spacecraft. A summary of these techniques can be found in Ref. [31, 32] and the important conclusions are listed in Table 4. Of these, only the methods of interest for the present research study are further reviewed. Empirical models method is reviewed because it shows insight into the physical properties of pyroshock. Finite element prediction method is also reviewed as it is used in this study

Table 4: Summary of pyroshock prediction techniques [31]

Technique \ Merits	Analytical Models	Empirical models	Transient SEA and VMSS analyses	Extrapolation procedures	Measurements in flight on flight vehicle	Measurements in lab. on prototype or flight vehicle	Measurements in lab. on similar structure
Relatively easy to accomplish	No	Yes	No	Yes	No	No	No
Applicable in preliminary design	No	Yes	Yes	Yes	No	No	No
Applicable before first launch	Yes	Yes	Yes	Yes	No	Yes	Yes
Applicable to radical new vehicle design	Yes	No	Yes	No	Yes	Yes	No

1.2.2.1 Empirical Prediction Method

The empirical and extrapolation methods are up-to-now the most widespread pyroshock prediction methods [3, 31]. Empirical models employ loading function in the form of SRS at the pyrotechnic source location. This loading SRS is then attenuated with respect to the distance and the number of junction between the source and the component of interest. This attenuation is

calculated with attenuation function as presented in the section 1.2.1.3. Extrapolation method scales previous results from related spacecraft to new spacecraft using similar attenuation function. The complete procedure can be summarized as follow:

1. Establish the loading SRS for each pyrotechnic source.
2. Establish the attenuation for distance and structural discontinuity between the source and the component as shown in Figure 1.
3. Calculate the attenuated SRS using data from step 1 and 2 for all sources and all components.
4. Combine all the SRS in a zone using the procedure explained in section 1.2.2.3.
5. Add the appropriate safety margin.

1.2.2.2 Finite Element Prediction Method

Recent advances in computational capacity have spread the use of finite element (FE) analysis as a mean of predicting pyroshock levels [32]. One of the most important benefits of FE models is their ability to identify local responses; they are not averaged as empirical methods.

Series of articles by Kiryenko et al. [12, 33], which are summarized and expanded in Ref. [32] , and by De Benedetti et al. [15, 34, 35] provide FE formulation reviews, modelling best practices and experimental validation for

space structures. They show that the implicit FE method has limitations but can be used effectively to predict structure response due to pyroshock.

Kiryenko et al. [12, 33] stresses that linear implicit models created for modal survey, sine or random analysis are able of predicting the shock level within usual test tolerance (3 dB) for frequencies up to 1500 Hz, which is deemed to incorporate the most stringent environment. De Benedetti et al. [34, 35] show that the frequency range can be further extended to far-field frequency range (10 kHz) with only little loss in accuracy at certain frequencies.

Still, both studies reveal that non-linear modelling and explicit dynamics solver are important to precisely predict the high-frequency content of the shock, especially in the presence of mechanical junctions. Insight into the modelling techniques for those non-linearities can be found in references [14, 15].

The transient response calculation is performed using implicit direct integration formulation by Kiryenko et al. while De Benedetti et al. employ implicit modal formulation. As for any analysis using SRS, the time step size is set to incorporate at least 8 times the highest frequency of interest. Both studies recommend using at least 4 to 6 elements per wavelength. Also, the analysis should properly represent the modes of frequency at least ½ octave higher, or ideally 1 octave higher, than the maximal frequency of interest.

Practically, Kiryenko et al. [12] seek a valid response up to 1200 Hz, so the modes should be well represented for frequencies up to 2000 Hz. Assuming that waves associated with bending modes in panel have a speed of 1000 m/s at 2000 Hz, this lead to a maximal element length of 8.3 cm while using 4 to 6 elements per wavelength. The time step of the analysis is 0.025 ms.

1.2.2.3 Zoning practices

SRS levels possess points-to-points (spatial) and events-to-events variations [3]. It would be impractical of having one shock specification for every component present in a spacecraft. For this reason, the spacecraft is cut down in zones where the shock specifications are deemed comparable. The rational behind the selection of zone limit can be summarized as [3]:

> *"The SRS magnitudes for the responses at all points within each zone can be described by a single SRS that will exceed most or all of the SRS magnitudes at the individual points without severely exceeding the SRS magnitude at any one point."*

Ref. [33] presents the complete zoning process for the ESA SMART-1 project. In this case, the spacecraft has been divided in three zones, each of which has its own specification and attenuation.

The computation of zone specifications involves statistical combination, most commonly the P95/50 limit [3, 32]. This combination covers the SRS magnitude for at least 95% of the location in the zone with a confidence coefficient of 50%. This is the preferred method when sufficient data, i.e. at least 3 sets of data, is available. The specification is usually simplified by piecewise line envelope of the environment.

1.2.3 Shock Testing Practices

It has been emphasized by various studies [1, 3, 9, 36] that pyroshock testing is essential to space mission success. Pyroshock testing is a broad field: it can be carried out at different levels of assembly, for different pyrotechnics sources, for different pyroshock regimes, etc. Each of these pyroshock environments implies very specific conditions that need to be replicated in the test lab. As a consequence, there is no established testing method that can readily be applied for every single case. When selecting a test method, special consideration has to be paid to practical considerations, like the value of early qualification and the amount of work involved.

1.2.3.1 Level of Assembly

One important parameter when planning a pyroshock test is the level of assembly being tested. Level of assembly has special implication in testing because of its relation with the source of the pyroshock. Most system or subsystem assembly pyroshock events are self-induced whereas most unit

assembly pyroshock events are externally induced [3]. As a result, it is possible to test a system firing the most stringent pyrotechnics source when it does not lead to structural failure of the system. This has the advantage of testing at the actual flight level. The main disadvantage of this method is the time required to clean and to reactivate the pyrotechnics device and the risk of jeopardizing the entire structure. Inversely, unit assembly level shocks are most of the time mechanically simulated using various test methods and are of specially interest for this research study. General definition of all 5 hierarchic levels of assembly are provided in Ref. [31] and listed in Table 5.

Table 5: Level-of-assembly hierarchy [31]

Level of Assembly	Examples
System	Payload, Spacecraft, Space Vehicle
Subsystem	Instrument, Attitude Control, Propulsion
Unit	Electronic box, Gyro Package, Actuator, Transmitter, Valve Regulator
Subassembly	Assembly (Power Amplifier, Gyroscope) Subassembly (Wire Harness, Loaded Printed Circuit Card)
Part	Resistor, Capacitor, IC, Switch, Bolt, Screw, Bracket, Gasket

1.2.3.2 Test Equipment

Many test equipments exist, each of them involving different test strategy and having particular strengths and weaknesses. This section provides a review of the most common test methods used with particular focus on their applicability. A more exhaustive summary is provided in Ref. [36]

Although a summary of the major pyroshock testing facilities is provided, it should be noted that the focus of this research study is on far-field mechanical pyroshock testing; that is, test method not involving pyrotechnics source. Mechanically simulated pyroshock testing methods are therefore reviewed in more details.

1.2.3.2.1 Pyrotechnics Devices

This method employs pyrotechnics devices as the source of excitation. It can provide important high frequency content required for near-field testing [31]. This method can properly excite all directions at once. On the other hand, it can take time to tailor and is hazardous because of ordnances manipulation.

The most commonly used configuration is the pyrotechnics ringing plate [20, 37]. It consists basically of a steel plate on which the device under test (DUT) is mounted. The explosive material is placed with a gap on the other side of the plate. For large assembly, the DUT can be configured in a flight or flight-like manner and ordnances can be fired providing a realistic test.

1.2.3.2.2 Impact Devices

Impact devices collide a moving mass onto a resting mass in order to transfer momentum into vibratory energy, thus inducing the transient shock. These devices offer a highly repetitive means of delivering the transient.

Drop Table

The most conventional shock testing equipment is the drop table. However, it is disregarded as a pyroshock testing method due to the large net velocity change induced [9, 20]. This large velocity change is not present in real pyrotechnics event and is a threat to the primary structure.

Accelerated Drop Table

Gaberson [25] shows that one way to get rid of the large velocity change of the drop table is to accelerate the free-fall of the DUT with a pneumatic piston, a spring or other devices. This reduces the low frequency content of the shock. The value of the acceleration can be adjusted, and therefore the required displacement, to make the shock suitable for pyroshock qualification [24]. Its behaviour is also repeatable and can be described by few parameters. However, it cannot match closely most pyroshock specification because its SRS shape is dictated by simple pulse shape.

Mechanical Impact Pyroshock Table

Mechanical Impact PyroShock tables (MIPS) are typically large aluminium plate resting on foam [31]. The DUT is attached to the plate while an impacter strikes the plate with high velocity to deliver the shock. The shock profile can be adjusted through the velocity, material and weight of the impacter, the location of impact and the location of the DUT [33, 38]. The shock waveform is very well adapted to far-field testing and has been used extensively [36]. One of the advantages of this device is that it delivers a complex shock close in aspect to

pyrotechnics shock. Its behaviour is repeatable but is described by many parameters, making the test tailoring process longer.

This concept can be extended to various types of resonant test structures. Those structures, such as beams or plates, are mostly designed to respond at their longitudinal or bending modes. The main advantage is that one can tune the dominant mode for a specific test. In some cases, the shock may also be suitable for mid-field testing [33].

1.2.3.2.3 Electrodynamics Shaker

Electrodynamics shakers are standard equipment employed for vibration environment qualification. They are widely available and their high adaptability allows them to perform transient event required for pyroshock qualification [3]. Electrodynamics shakers may be especially convenient because they allow to test directly for shock after a vibration test while the unit is already installed and instrumented, thus allowing for important time saving [36]. Moreover, the test is highly repeatable and can consist of simple pulse or complex waveform. However, each shaker has its inherent limitations like maximal displacement, force rating and frequency content. Yet, far-field environment can be simulated in regular facilities with frequency content up to 2-3 kHz while specialized systems can reach frequency up to 5 kHz [36].

A shaker can closely simulate a complex waveform if the acceleration time-history is known. However, a shaker cannot readily and directly simulate a SRS specification. It has to go through some form of shock synthesis algorithm. These algorithms can use anything from decaying cosines or wavelets in order to create a time-history matching the specified SRS [31, 36, 39]. One has to remember that unlike the FFT, the SRS is irreversible. In other words, a given SRS equally relates to a variety of acceleration time-history and it is impossible to directly retrieve one time-history from a SRS. However, it can be done using shock synthesis algorithm. Foss et al. [40] emphasises that these algorithms should also account for extra parameters like the shock duration and/or maximal acceleration to make the synthesis shock more realistic.

1.2.4 Force Limited Vibration Testing

The force limited vibration (FLV) testing technique has been introduced by the Jet Propulsion Laboratory (JPL) in the 1990s to reduce the overtesting associated with conventional vibration tests [41]. This overtesting is due to the lack of dynamic absorber effect on the shaker configuration (rigid mounting) compared to in-flight configuration (flexible mounting) and is thus defined as the ratio of the force in these configurations. The FLV technique seeks to reduce the response of the test item at its main resonances on the shaker in order to replicate the environment condition of the system resonances of the coupled assembly. Practically, the input acceleration profile, or acceleration PSD (S_{aa}), is notched so that the force does not exceed a prescribed limit, which is

representative of the flight force level. Realistic estimation of the C^2 coefficient is essential and is between 2 and 5 for most typical space structures. The semi-empirical method is the most common method for computing force limit. For random vibration test, the force limit (S_{ff}) is defined with respect to the fundamental frequency (f_o), the physical mass (M_0) and the roll-off ratio (n) as:

$$\begin{aligned} S_{ff} &= C^2 M_0^2 S_{aa} && f < f_0 \\ S_{ff} &= C^2 M_0^2 S_{aa} \left(f_0 / f\right)^n && f \geq f_0 \end{aligned} \qquad \text{Eq. (7)}$$

Different methods to estimate the force limit are compared by Soucy et al. [42]. The exact C^2 coefficient for a complex structure is compared with the equivalent C^2 coefficients obtained by 1) the simple two degree of freedom (TDOF) method based on effective mass, 2) the simple TDOF method based on residual mass and 3) the complex TDOF method. When possible, it is suggested to use these more analytical methods as guideline while relying on the semi-empirical method to estimate the force limit.

An analytical sensitivity study to investigate the range of value taken by the C^2 is undertaken by Soucy et al. [43]. It uses a reconfigurable test item attached to a mounting structure and measures the forces and acceleration at the interface for a total of 134 cases. The parameters on which C^2 depends are 1) the effective mass ratio between the test item and the mounting structure at the fundamental frequency of the test item, 2) the number and the position of the

interface attachment points between the test item and the mounting structure, and 3) the direction of excitation [43]. The C^2 value is basically independent of the damping value.

The force-limited vibration testing technique makes use of either the effective or the apparent masses of the structure. The effective masses can be obtained in test configuration by the method described by Sedaghati et al. [44]. This way, they accurately represent the actual test item and are not derived from an analytical model.

The force-limited vibration testing technique usually notches in-test the input acceleration profile to limit the interface force to a prescribed value aimed to be more representative of the in-flight force. Fitzpatrik and McNeill [45] suggest pre-modifying the input acceleration profile to meet the force limit. The advantage is that no force sensors are required in testing. However, it does not allow the measurement of the interface force. Two methods are proposed: 1) Notching method: reduce the input acceleration power spectral density (APSD) by (C^2/Q^2) around the fundamental frequencies of the test item, and 2) Random Response Spectrum (RRS) method: create an APSD so that the resulting RRS of the test item on the shaker meet the RRS at the interface of the coupled assembly obtained either analytically or experimentally.

1.2.5 Current Knowledge of Overtesting in Shock

This section investigates the current knowledge of overtesting in shock test. Few references make statements related to overtesting due to difference of impedance, or rigidity, of the source; fewer have studied directly this effect.

One can find explanations about different test equipment in Ref. [3]. It suggests that the shock test performed with rigid mounting produces overtesting related to the different impedances of the test and flight structures. The paragraph treating of shaker transient states:

> *"Vibration shakers and some impact devices may simultaneously cause under and over-testing: under-testing due to uniaxial excitation compared to the triaxial service environment; over-testing due to a massive shaker table and fixture compared to the service installation, plus accelerometer control in the case of a shaker."*

Ref. [46] states that the shock test carried with impact simulation resulted in overtesting. Also, they suggest using system-level test to counter the overtesting at assembly-level.

> *"Impact test pyrotechnic simulations always produced severe overtests, destroying many test items. The pyrotechnic shock simulation requirements were continuously reduced and, ultimately,*

were abandoned in favor of system-level demonstrations. Only system or subsystem pyrotechnic shock tests should be conducted, using the actual or closely simulated structure."

Luhrs [47] tested a structure for shock using a flight-like structure with pyrotechnics ordnances with a maximum input spectrum of 2500 g without any failures. The same structure is also tested on a shaker with an equivalent spectrum, resulting in unit failure. This example clearly illustrates an overtesting resulting from the rigidity of the structure on which the unit is tested (rigid shaker vs flexible spacecraft). It was demonstrated that the test method greatly influences the severity of a test for an equivalent spectrum. It suggested that a shock test performed on a rigid fixture is about five times more severe than a test on flight or flight-like structure.

The effect of different test equipments on the test severity is investigated by Luhrs [48]. The internal response of a structure is studied for three excitations: 1) actual spacecraft pyrotechnic, 2) pyrotechnic structural simulation, and 3) vibration table simulation. These three excitations produce input SRS approximately equivalent. Little information is provided regarding the structure or exact configuration. The SRS inside the structure for the pyrotechnic structural simulation follows well the shape of the actual spacecraft pyrotechnic. The SRS at same locations for the vibration table simulation is well above the internal SRS

for other method: 4000 g compared to 800 g around 1500 Hz, thus showing a higher response.

Ferebee et al. [49] experienced structural failure of the Integrated Electronics Assembly of the Space Shuttle Solid Rocket Booster (SRB) when the unit is tested for shock on shaker. The shock to qualify for is induced by the impact of the booster on the ocean at re-entry. Its SRS contains important low-frequency components (250g at 80 Hz). The authors attempt to test for the flight-measured spectrum without any enveloping: while no unit failed due the re-entry shock, units failed the shaker-simulated shock. Because the electronics assembly's housing failed at its bracket interface, the authors concluded that the failure was due to higher mounting structure compliance in-test compared to in-flight.

Larue et al. [50] examined the effect of equipments mass and stiffness on the SRS and the interface loads when subjected to shock. Both finite element and test are used in parallel for the study. They show that the equipment dynamics has a strong influence on the response of the interface. Also, the load on the equipment interface is computed for the test configuration using the response spectrum method and modal effective mass. The method does not allow computation of the load when the equipment is mounted on the panel. The authors suggest that shock overtesting occurs although it is to be quantified in upcoming studies.

Smallwood et al. [27] suggested the concept of energy method, IES, to investigate pyroshock in the space industry. This concept has been explained in the section 1.2.1.6. In addition to the previous arguments, it should be stressed that the IES can be computed from Fourier amplitude spectrum, thus opening the way to force limiting in shock testing.

1.3 Expected Contribution

This thesis constitutes a fundamental study on the overtesting phenomenon occurring during assembly-level shock testing. Versatile test item and mounting structure have been designed using the finite element method and numerous sensitivity studies have been conducted to demonstrate the overtesting assumed to occur in assembly-level shock testing. Linear regressions have been performed to produce statistical model of the shock overtesting.

The first contribution of the current research project is the measurement of overtesting during assembly-level shock testing. This overtesting is mainly due to the absence of dynamics absorber effect in assembly-level testing. Also, the procedure involved in creating the shock environment, or enveloping, does not reflect this phenomenon. These facts are similarly the same as in vibration testing for which one can rely on Force-Limited Vibration (FLV) technique to measure and reduce the overtesting.

The second contribution of this research project is to attempt to relate the overtesting in shock testing to the one observed in random vibration testing. To do so, the overtesting occurring in vibration testing is also investigated. Because techniques to estimate the overtesting in vibration testing such as FLV are much more mature, they might offer a reliable background for predicting the overtesting in shock testing. Finally, vibration overtesting and others variables relevant to shock testing are to be used to estimate the shock overtesting.

The third contribution of this research project is to generate a modified specification, which results in reduced overtesting in shock test. Techniques such as force limiting to notch the input acceleration at the main resonances of the test item are used during vibration testing to reduce the adverse effects of overtesting. Unfortunately, contrarily to vibration testing for which one can readily force the control system to notch the input acceleration at certain frequencies by simply limiting some measurements channels, e.g. input interface force, this cannot be done for shock testing due to difficulty in controlling the input load and the very short duration of the event. For this reason, the assembly-level shock test is usually accomplished without any attempt to reduce the overtesting. Finally, the shock overtesting estimate could allow generating a modified specification resulting in reduced overtesting in shock test. This should lead to more frequent assembly-level test and thus, earlier qualification of hardware against shock environment.

The strategy to meet those objectives is to design test structures representative of space structure and to measure the overtesting for both vibration and shock tests based on finite element analysis. Detailed examination of the overtestings needs to be carried to predict the shock overtesting and to generate the modified specification. The design of the test structures takes into account that these analyses are to be validated experimentally using an electrodynamics shaker.

1.4 Thesis Organization

The first chapter addresses the motivation, the objectives and review of the pertinent literature. The focus is on the pyrotechnics shock problem, the shock prediction methods and the shock test methods. It also encompasses overview of the force-limited vibration testing technique and a survey of the current knowledge of overtesting in shock testing.

The second chapter is devoted to the requirements of the test articles design. These requirements dictate the fundamental characteristics of the structures, i.e. test item (TI) and mounting structure (MS), designed and analysed for this research study. The third chapter describes the designs implemented to meet these requirements. It also shows the development and the correlation of the finite element models.

Chapters 4 and 5 are dedicated to the investigation of overtesting in vibration and shock testing, respectively. The vibration overtesting investigation makes use of the force-limited vibration (FLV) technique. The shock overtesting investigation derives a similar method for shock and introduces a shock synthesis algorithm.

Chapter 6 investigates relations between the shock overtesting and the vibration overtesting or other variables relevant to shock testing. Chapter 7 proposes a method to produce the modified shock specification leading to reduced overtesting.

Chapter 8 experimentally demonstrates the validity of the current study. It presents the setup employed to correlate the finite element model. Also, it shows the measurement of the vibration and shock overtesting for three cases. The last chapter concludes with a summary of the main findings along with several recommendations to improve the current state-of-the-art.

Chapter 2

Design Requirements of the Test Articles

2.1 Introduction

The main goal of this chapter is to present a set of requirements to ensure the pertinence of the Test Articles (TA) design. The test articles consist of the test item (TI) and the mounting structure (MS). The specific objectives are:

1. To guarantee that the test articles are representative of space hardware tested against pyroshock environment. The test item dynamic characteristics should be typical of space hardware at unit level and the mounting structure should be consequently at subsystem level.

2. To provide a large enough variability on the key parameters to allow for a significant sensitivity analysis on the dynamic absorber effect occurring in Force Limited Vibration (FLV) testing [41] and expected to occur in simulated-pyroshock testing [3].

2.2 Definitions

In the following, some terminologies needed to properly define the design requirements are clearly explained.

2.2.1 Level of Assembly

System-level and assembly-level pyroshock tests, as defined in literature review, correspond to spacecraft or large subsystem level and subsystem or unit level, respectively. In addition, most system-level pyroshock events are self-induced, whereas most assembly-level pyroshock events are externally induced [3, 4]. Consequently, simulated-pyroshock testing is more commonly possible at assembly-level. The test articles are to be representative of assembly-level structures. These level-of-assemblies are defined in the section 1.2.3.1.

More specifically, the test item refers to the structure being subjected to random vibration and pyroshock testing, the mounting structure refers to the immediate structure to which the test item is being attached, and the assembled structure, or the coupled system assembly, is a combination of both the test item and the mounting structure. For example, in the case when the test item is an instrument, the mounting structure would be the rest of the spacecraft (without the instrument), and the assembled structure would be the complete spacecraft. The generic term 'test article' or TA refers to either the test item or the mounting structure.

2.2.2 Requirement Weighting

A requirement containing the verb 'shall' refers to a condition which must be met. However, a requirement containing the verb 'should' refers to a condition

which ideally would be met, but is not necessary if the implication or cost is too significant.

2.3 Test Articles Requirements

Design requirements for test articles, which include the test item and the mounting structure, are categorised according to consistent characteristics.

2.3.1 Fundamental Frequency

1. The fundamental frequency of the test item shall be between 300 to 1200 Hz.

   This frequency range is fairly representative of where the fundamental frequencies of a unit containing pyroshock sensitive parts can be expected. The test item first significant modes are normally affected with FLV notching.

2. The design of the test item shall allow the attachment of an internal subassembly with different mounting configurations.

   One common case of typical shock sensitive unit is an electronic box containing printed circuit boards (PCB). These PCBs are themselves loaded with electronic components, some of which are shock sensitive parts. The internal subassemblies should represent these loaded PCBs.

3. The design of the internal subassembly shall allow the attachment of various numbers of masses at different locations of the internal subassembly.

   Pyroshock sensitive parts, such as relays, crystals, ceramics, diodes..., are components sensible to excitation of high frequency content [1]. Pyroshock test precisely aims at qualification of these components. These masses are to represent these sensitive parts and at the same time, act as additional residual mass of the test articles. Also, the distribution of these masses should not result in undue moments at the attachment points of the test item.

4. In order to simulate real-life situations, the fundamental frequency of the mounting structure shall be less than half the fundamental frequency of the test item.

   Independently of the level of assembly of the test article, the mounting structure normally exhibits more flexibility and lower fundamental frequencies than the test item. For example, the fundamental frequency of a spacecraft would normally be above 25 Hz, while the fundamental frequency of an instrument could be above 100 Hz. Separating the fundamental frequencies of these two structures by a two folds factor is satisfactory to avoid major dynamic interactions.

5. In order to simulate real-life situations, some of the design configurations should contain coupled modes between the test item and the mounting structure.

   Space hardware at any hierarchy level is normally very complex and is likely to exhibit modes, which are close between the test item and its mounting structure. Consequently, this requirement is imposed in order to ensure relevance to possible space hardware dynamic characteristic.

2.3.2 Sensitivity Study

6. It should be possible to modify the flexibility of both test articles, in order to simulate a wide range of different frequency and amplitude of the most significant effective masses.

   This requirement leads to a larger scope of the sensitivity studies and thus brings added value to the present research. It includes the stiffness and the mass of the test item, its internal subassembly and of the mounting structure.

7. The design of the mounting structure shall allow the attachment of various numbers of masses at different locations. These masses are to represent additional residual mass of the mounting structure.

The addition of the masses to the mounting structure represents an easy way of increasing the residual masses. This increase of residual mass is on top of the ones associated with the modes having a frequency above the excitation frequency. It should be noted that the distribution of these masses should not result in undue moments at the attachment points.

2.3.3 Attachment Points

8. The design of both the test item and the mounting structure shall have sufficient interface attachment points to allow different combination of these points to be used in the various attachment configurations. The maximum number of attachment points used in a configuration shall not be more than twelve.

   This number of attachment point is deemed to be sufficient to fulfil the objectives of the project. Moreover, there are presently a total of twelve triaxial force sensors that belong to the Spacecraft Engineering facilities of CSA.

9. The moments at the interface attachment points shall never exceed the maximum allowable moments of the force sensors which is 14 Nm about the axes in the shear plane and 18 Nm about the normal axis, or as per the requirements specified in Ref. [51].

The values of allowable moments on the forces sensors are specified by their manufacturer [51]. In fact, the value of 14 Nm is for the case when the bolt preload corresponds to the manufacturer recommended value of 25 kN, which is seldom reached. Also, the value of 18 Nm is when no simultaneous shear load is present. Under these conditions, exceeding the maximum allowable moments could result in breaking the force sensor. In any case, moments in the force sensors should be minimized whenever possible to reduce the possibility of breakage of the force sensors.

10. The means of attachment between the test articles, as well as between each of the test articles and the fixture shall be through bolts.

This requirement is based on the fact that bolts are the standard means of attachment between the various parts of spacecraft. Also the use of bolts, as opposed to other means of attachment such as clamps, ensures a better control and repeatability of the interface characteristics. These are very suitable characteristics in the present sensitivity study, since it eliminates undesirable uncertainties in the factors affecting the interface force exercised by the test item during the vibration and shock test of the assembled structure.

2.3.4 Physical and Operational Properties

11. The mass of the test item should be between 0.5 to 2 kg.

    This mass range is fairly representative of where the mass of electronic unit can be expected.

12. The mass of the mounting structure should be significantly higher than the mass of the test item.

    Test articles having larger mass are likely to be more representative, at least from a mass point of view, of typical space hardware at the subsystem level.

13. Both test articles shall be made of materials representative of those typical of space hardware.

    This requirement is imposed in order to ensure that this study is relevant, from structure material point of view, to real space applications. Examples of representative materials are aluminium for structure and glass fiber reinforced plastic (FRP) laminated with aluminium for electronic board (PCB).

2.4 Conclusion

This chapter explained the requirements for the relevant design of the test item and the mounting structure. The main objectives of these requirements are to ensure that the test articles are representative of space hardware, have a wide range of characteristic for the sensitivity study and can accommodate future fabrication and testing. The requirements are presented accordingly: natural frequency related requirements, sensitivity study related requirements, attachments points related requirements and physical and operational properties related requirements. Details of the experiment can be found in the chapter 8.

Chapter 3

Design and Modelling of the Test Articles using the Finite Element Method

3.1 Introduction

The purpose of this chapter is to provide detailed explanations about the design and modeling process of the test articles using the finite element method. The final design has to meet all requirements exposed in chapter 2.

Many requirements are geometry based and thus can be met only by proper design. For example, the requirement R.10 about the assemblage through bolts is straightforward and easy to incorporate. However, some requirements necessitate a detailed analysis in order to meet them. These are mostly the requirements relating to the natural frequency of the test articles. Therefore, a Finite Element (FE) model has been developed to design the test articles. The modelling practices adopted in this study and the final FE models are presented in the third part of this chapter. The second part of the chapter is devoted to the design process of the test item and mounting structure. The fourth section presents the cases examined in the sensitivity study.

3.2 *Design of the Test Articles*

In order to effectively design the structure to meet all the objectives stated in the requirements, it is decided to design the test item and then to design the mounting structure. The final design of the test articles is shown in Figure 4. In the coupled system (CS) configuration shown, the test item (TI) sits on the top of the mounting structure (MS) and is attached through bolts. The force sensors are sandwiched between the test item and the mounting structure, as in test configuration. The mounting structure consists of a bolted assembly of panels and masses. The test articles overall dimensions are set so that their scales and masses are representative of typical hardware.

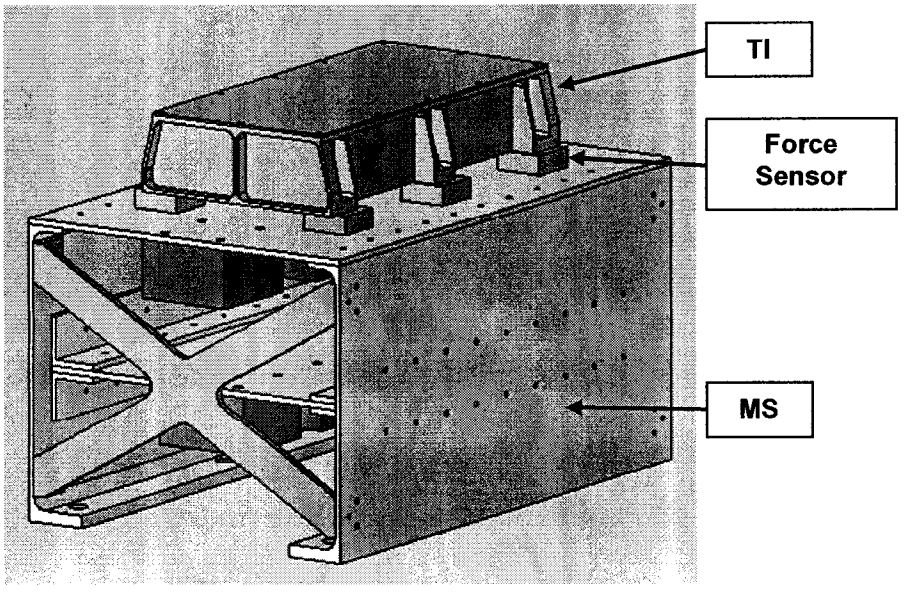

Figure 4: Isometric view of the coupled assembly

3.2.1 Test Item Design

While designing the test item, it is very important to respect the requirements listed in chapter 2. These requirements state crucial goals of the test articles. Therefore, the test articles incorporate features which are designed to meet these requirements. The test item final design is shown in Figure 5. The overall dimensions of the test item are approximately 205 x 115 x 40 mm and its mass range from 0.42 kg to 1.17 kg for different cases.

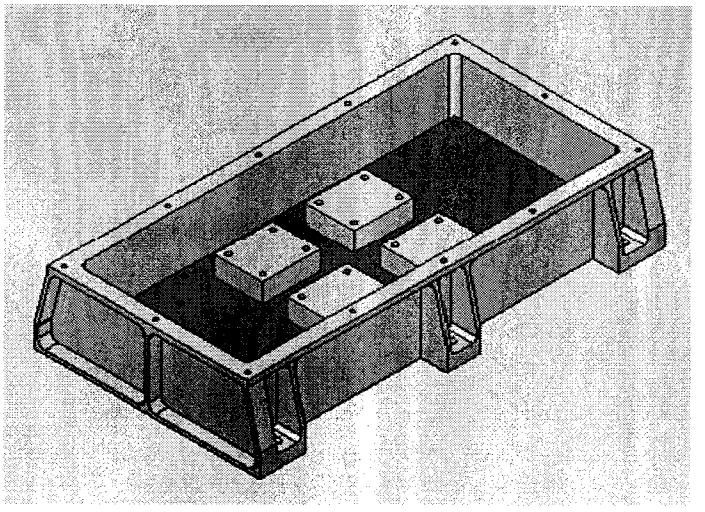

Figure 5: Isometric view of the test item (cover not shown)

It is noted that the parametric CAD model of the test item is developed within Solid Edge V18 software and transferred into the FE software PATRAN / NASTRAN to conduct detailed FE analysis. The FE model is presented in the third section of this chapter.

3.2.1.1 Example of a Test Item Design (Electronic Box)

An electronic box, shown in Figure 6, is deemed typical of a representative test item [15]. The electronic box shown is part of RadarSat-2, which has been launched successfully in 2007. The electronic box integrates 2 modules incorporating a total of 5 printed circuit boards (PCB). The overall dimensions of the box are 288 mm × 315 mm × 140 mm. The structure is made of aluminium. The mass is not mentioned.

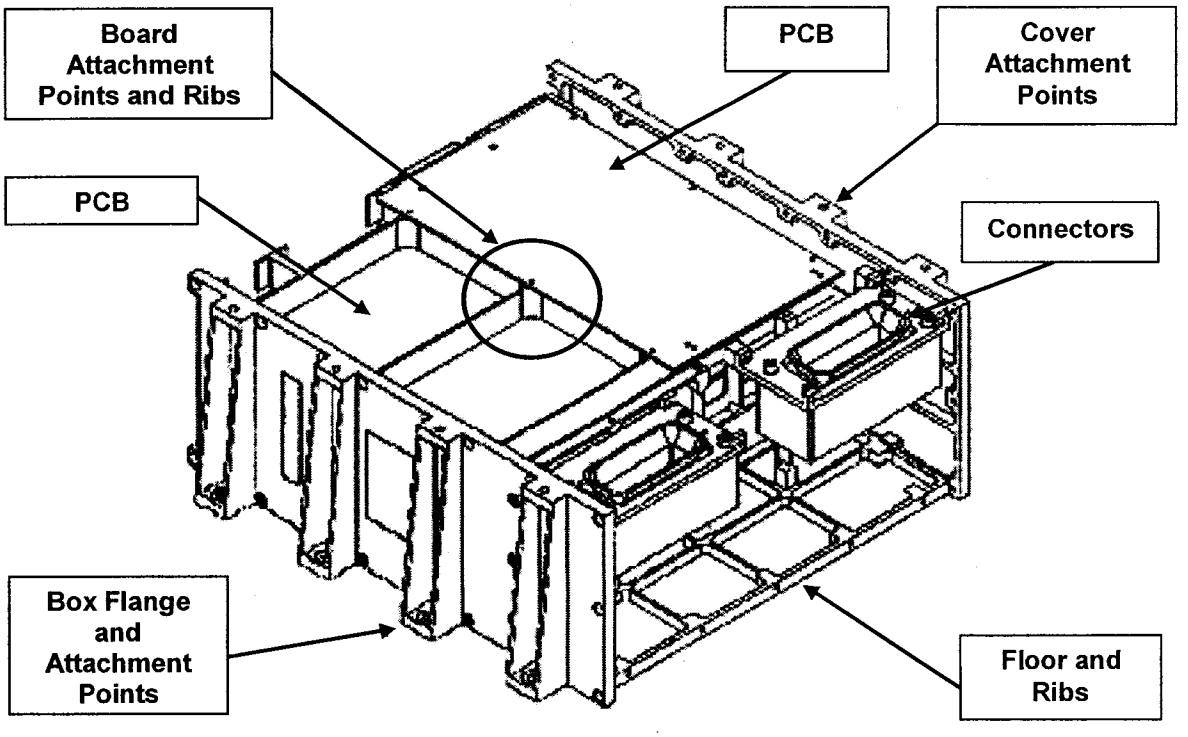

Figure 6: Example of electronic box assembly [15]

As it can be seen, the structure of the box is made of one piece and is composed of a thin-walled structure stiffened by many ribs. The box is entirely seated on a panel (not shown) in order to transfer heat flux. Also, the box is fixed by 8 attachment points, which are stiffened by flanges to transfer the mechanical

load. The PCBs are supported at various locations by a ribs network. This network is linked to the box walls and finally, to the attachment point flanges. A cover (not shown) completes the structural integrity of the box and is mounted through bolts with the attachment point's flanges. Electrical interface is accomplished through connectors disposed around the box.

Figure 7 and Figure 8 show two additional examples of electronic box design from the Quicksat satellite. The same features can be observed on these assemblies. The overall dimensions of the C&DH assembly are approximately 250 x 300 x 75 mm and its mass is 2 kg. The overall dimensions of the CPU box assembly are approximately 115 x 100 x 35 mm and its mass is 0.3 kg.

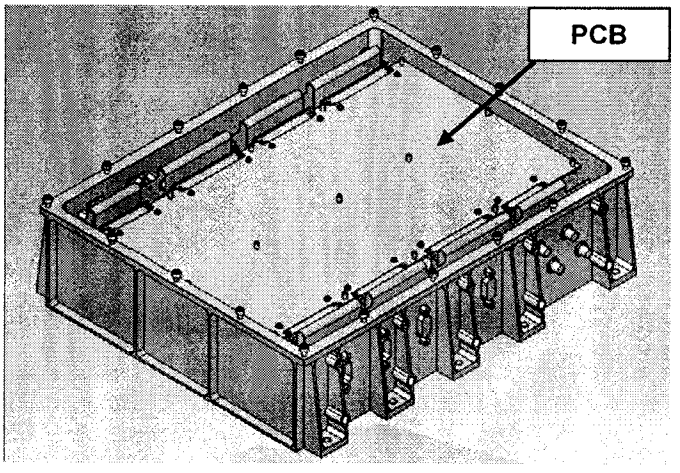

Figure 7: Example of electronic box assembly: C&DH (Cover not shown)

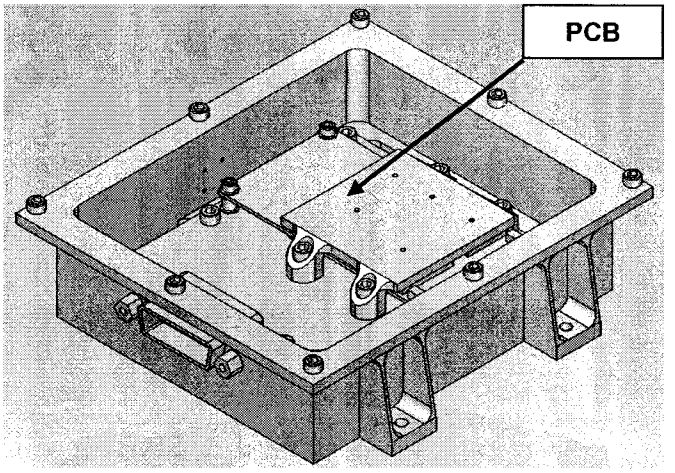

Figure 8: Example of electronic box assembly: CPU Box (Cover not shown)

3.2.1.2 Design Steps regarding the Test Item

The first important step is to design the exterior of the test item. The overall shape is a rectangular box of 192 x 88 x 40 mm on which attachments points and stiffening ribs are added as shown in Figure 9. The external design needs to incorporate some variability over the number of attachment points. For this, the test item has 4 attachment points located at its corner and can also have 2 extra attachment points at the middle of its sidewalls.

The design of the features of the exterior of the test item can be summarized into the following steps according to Figure 9:

- Attachment points: Protrusions on the side walls incorporating holes for M6 bolts.
- Flange of the cover: Protrusion on the top of the test item to sit the cover. It incorporates M2.5 threads to attach the cover.

- Cover: A rectangular plate fixed along its edges onto the cover flange.
- Flanges of the attachment points: Connect the attachment points to the main box from the bottom to the cover's flange.
- Stiffening ribs of the endwalls: Stiffen the endwalls and add support to the cover.

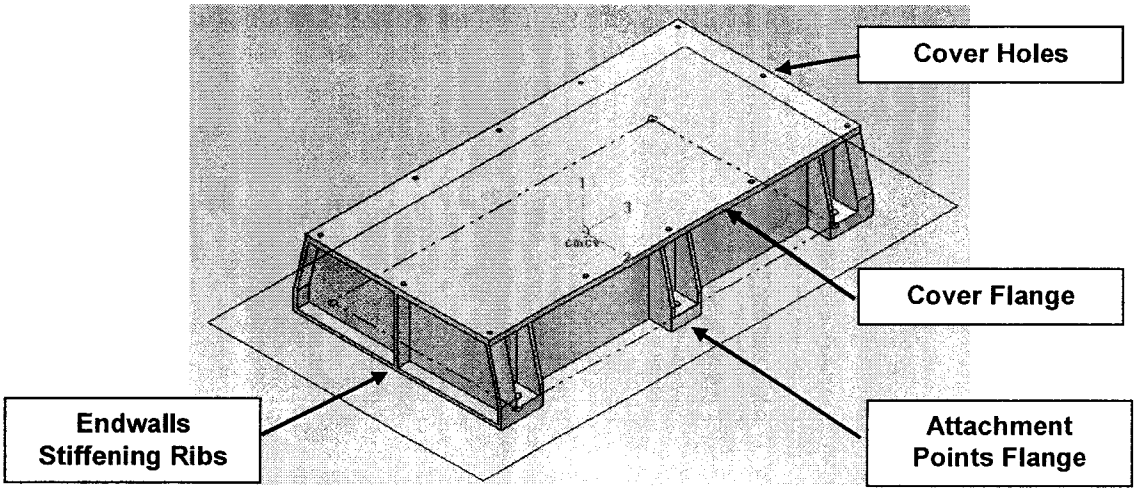

Figure 9: Isometric view of the exterior of the test item

The next important design step is to design the interior of the test item shown in Figure 10. The design of the interior of the test item has to account for many parameters to be used in the sensitivity study. The next section presents these parameters and a strategy to meet them.

It is important to provide enough space for the board, the components, connecting devices (bolts) and ultimately, accelerometers within the test item. Considering this, the total height of the test item is set to 40 mm.

Moreover, the test articles have been designed in a way to avoid contact between parts. It should be noted that contact between parts results in non-linear phenomenon, which has not been considered in the FE analysis. Avoiding inter-parts contact increases the fidelity of the numerical model and thus reduces the possible discrepancies between analytical and experimental results.

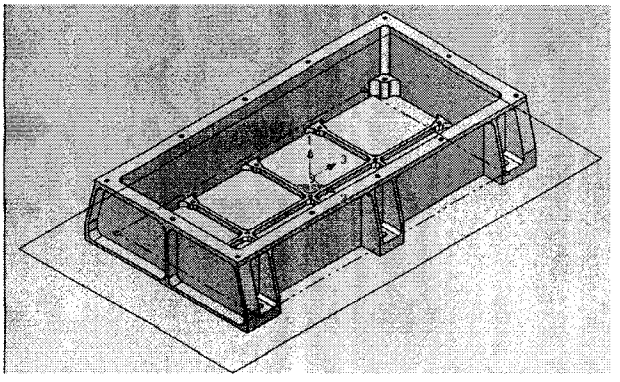

Figure 10: Isometric view of the designed test item box

PCBs are commonly made of aluminium and woven glass-epoxy laminate (FR4). However, it is more convenient for fabrication purposes to carry out the experiment with the aluminium prototype instead of FR4. To ensure that the board is representative, a method described by Steinberg [52] is applied. It is basically based on the bending inertia to obtain the equivalent aluminium thickness of the board. The thickness of the aluminium board is 1.5 mm and thickness of its equivalent FR4 counterpart board is 2.25 mm.

The prime function of the attachment points of the board is to transfer the load from the components to the test item box. To increase the variability of the

dynamics characteristic, the location of the attachments points should allow producing symmetric and anti-symmetric flexural mode of the board. This has a significant impact on the effective mass, thus influencing the amount of overtesting. Details of the design can be seen in Figure 11. The board is divided in 4 sections along its length and 2 sections along its width to support the board at allowable distance, which is 20 times its thickness [52]. The board maximal free span is thus of 45 mm (20 x 2.25).

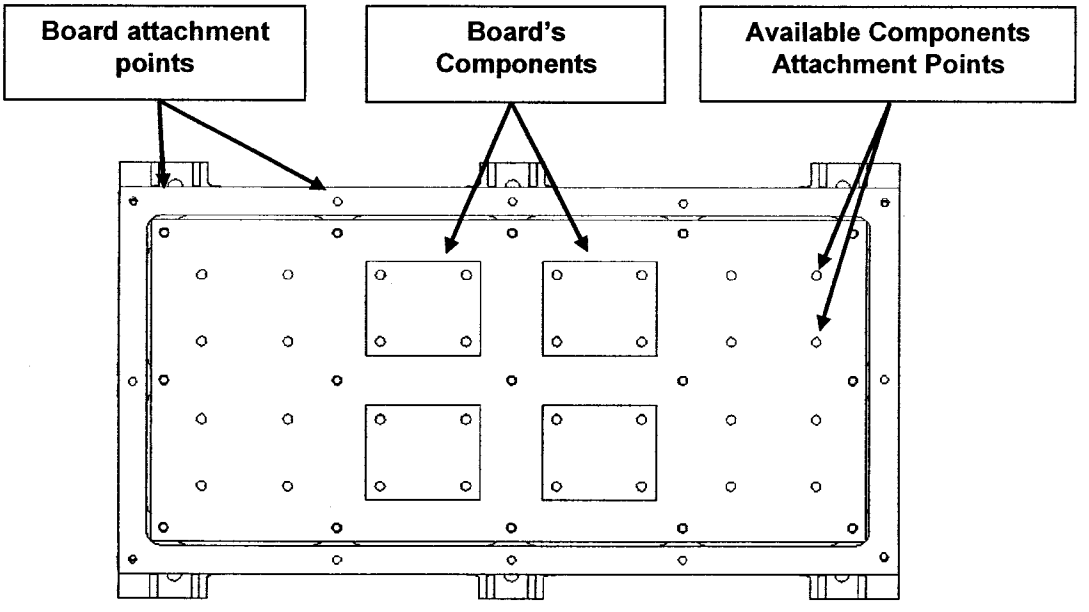

Figure 11: Top view of the board and the components

By taking advantage of the subdivisions created by the board attachment points, it is possible to provide a variety of mass and location for the components mounted on the board. Figure 11 illustrates this design with 4 components. 4 other components could be added at the available attachment points.

The dimensions of the board's components are fixed at 30 x 25 x 2.5 mm. Brass is used to replace the copper of large electric components. The mass of one component is 17g. Many components can be stacked on top of each other to form a heavier mass. The components are fixed to the board through M2.5 bolts and washers.

The main purpose of the ribs as seen in Figure 12, is to support the load of the board. They are also useful because they stiffen the test item with minimal mass and provide a mechanism to modify the stiffness of the test item.

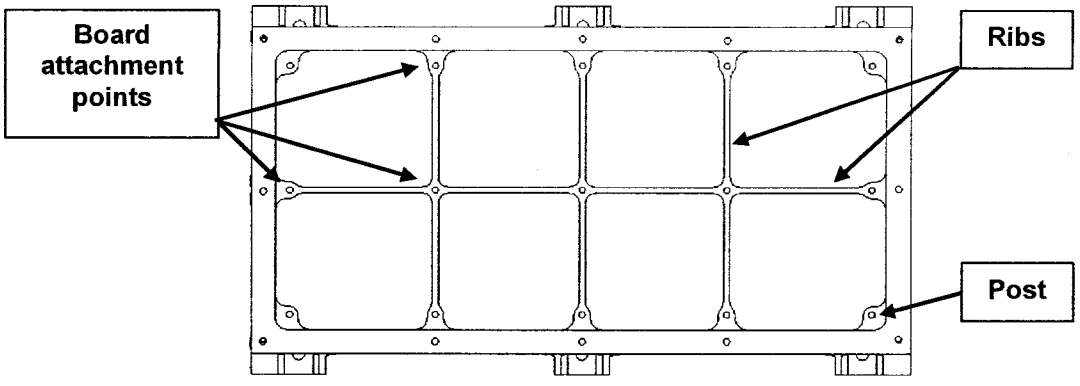

Figure 12: Top view of the test item box

In order to modify the stiffness, the test item can be configured with low and high ribs. The height of the ribs is set so that the first significant frequency of the test item is moderately below the upper frequency range of analysis (1200 Hz). The low-ribs height is chosen to be minimal while still supporting the load. The resulting high-ribs and low-ribs height are 10 mm and 3 mm, respectively. To support the design process, the test item is analysed using FE when configured

as cases 1 and 4. Details of the configuration are explained in section 3.4. Table 6 summarises the investigation of the ribs height.

Table 6: Summary of Rib Height Design Investigation

Configuration	Ribs Height (mm)	Fundamental Mode Frequency (Hz)	Modal Effective Mass Fraction of the Fundamental Mode (%)
Low	3	733	58%
High	10	1008	67%

The mode shape of the fundamental mode is shown in Figure 13 for each low and high-ribs configurations. While both modes correspond to the first bending mode, significant differences can be observed in the deflection of the test item floor around the centerline. Thus adjusting the ribs height shows to be an effective mean of changing the test item's stiffness for the sensitivity analysis.

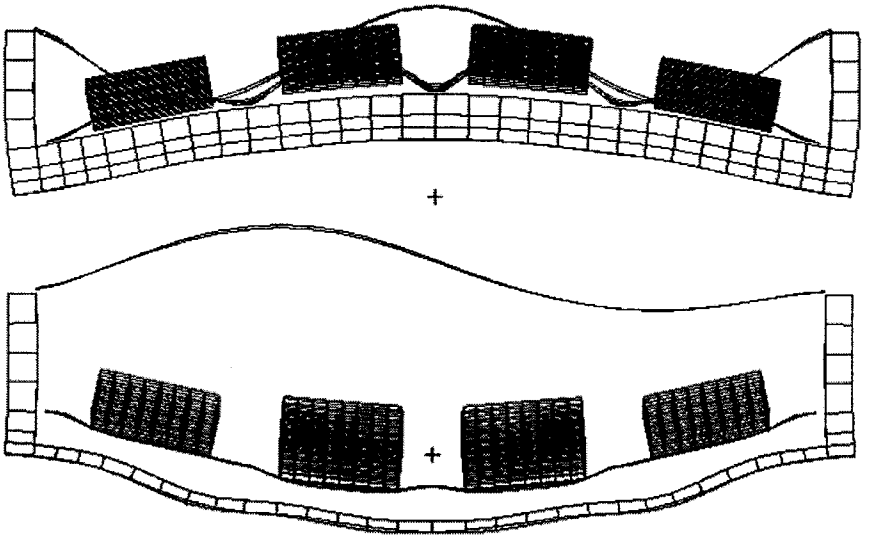

Figure 13: First significant mode shape of the test items: high-ribs (up) and low-ribs (down)

A male-female threaded standoff is used to support the board when the test item is in the low-ribs configuration and it is shown in Figure 14. The length of the standoff is 7 mm. No standoffs are used in the high-ribs configuration.

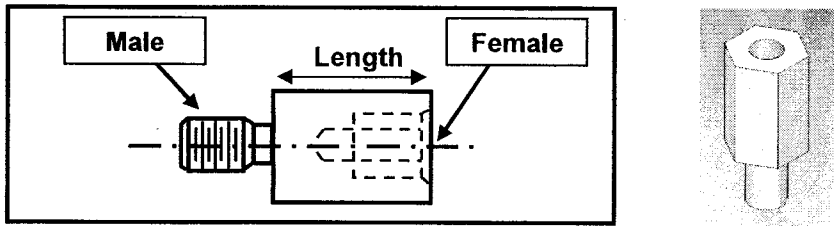

Figure 14: Male-Female Standoff

3.2.2 Mounting Structure Design

Various requirements about the key characteristics of the mounting structure were presented in chapter 2. The mounting structure is not directly replicating any particular structure. It should only be dynamically representative of the structure on which an electronic box, the test item, is mounted. These structures are diverse ranging from simple panels to complex instruments.

Consequently, the mounting structure has to be a very generic structure. The overall view of the designed mounting structure is shown in Figure 15. As for many space structures, the basic geometry of the designed mounting structure is a modified box. The overall dimensions are approximately 300 x 188 x 155 mm and its mass ranges from 2.66 kg to 7.75 kg for different cases. The structure of the mounting structure is made of aluminium while the lumped masses are in brass.

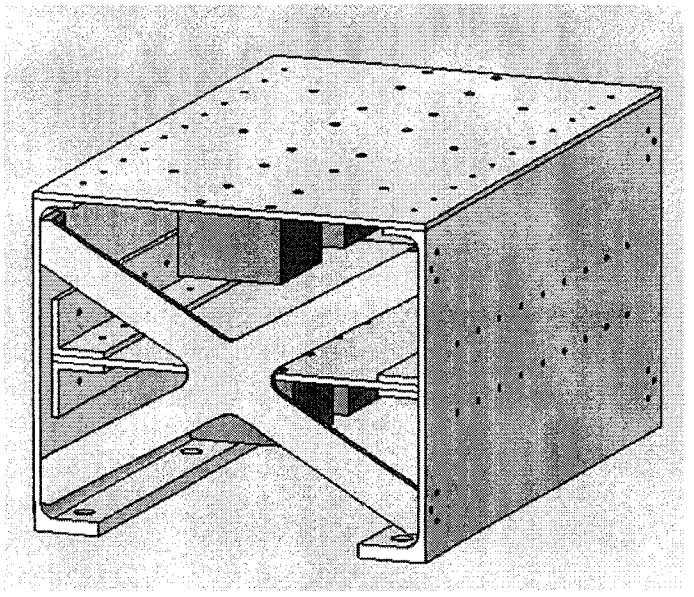

Figure 15: Isometric view of the mounting structure

As seen in Figure 16, the mounting structure consists of an assembly of:

- Top panel: The top panel is where the test item is attached.
- C-shape extrusions: The C-shape extrusions link the top panel to the shaker. It also provides enough room to incorporate masses.
- Mid panel: The mid panel purpose is mainly to allow adding extra mass to the assembly. It also adds dynamics complexity, making the mounting structure more representative of space structure.
- L-shape stiffeners: They connect the mid panel to the C-shape extrusions. They also add stiffness in shear about the in-plane axes.
- X-shape stiffeners: The X-shape stiffeners are considered to add stiffness in shear about the in-plane axes. They connect the corners of the mounting structure together. X-shape stiffeners have the advantage over

full panels as they allow access to the interior of the mounting structure to modify the configuration of the lumped masses.

- Lumped masses: Lumped masses are added to lower the fundamental frequency of the mounting structure. It also ensures that the mounting structure is heavier than the test item, which is coherent with the level of assembly hierarchy. The masses are added to both the mid and top panel in two configurations: 4 masses centered or 8 masses distributed along the length. They are made of brass because of its high density and have thickness of 15 or 30 mm.

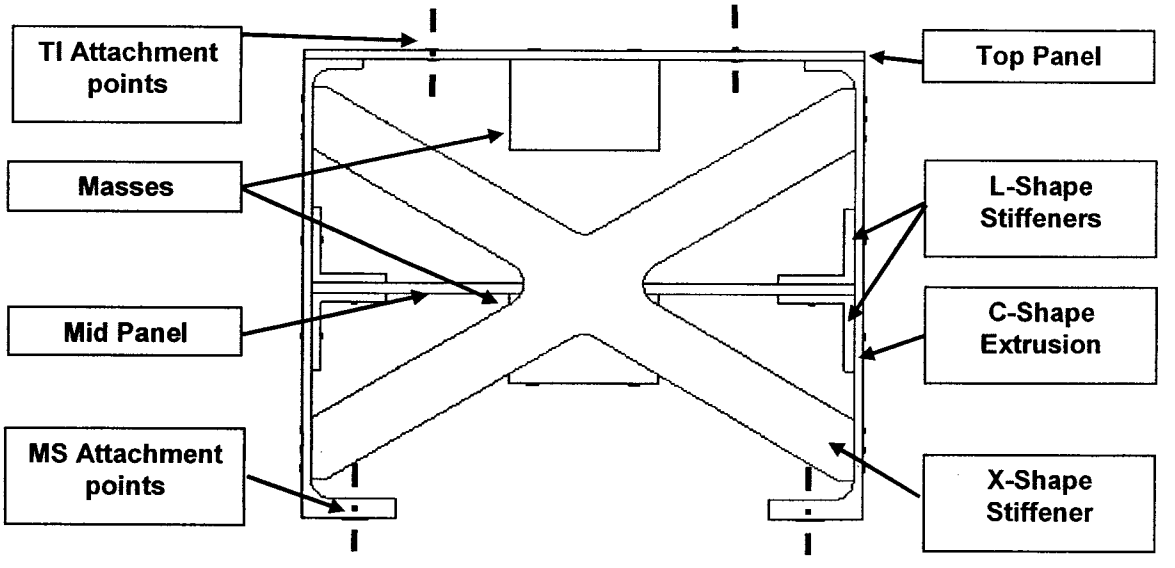

Figure 16: Front view of the mounting structure

The different members are linked together by M2.5 bolts spaced by approximately 25 mm. This mounting method is considered rigid enough to ignore shock attenuation due to mechanical junction [6].

3.3 Test Articles Modelling using Finite Element

The finite element software MSC PATRAN [53] is used to create the FE models of the test item and of the coupled system assembly, as shown in Figure 17 and Figure 18, respectively. The models are then analysed using MSC NASTRAN for all the desired load cases. Modal and random vibration analyses are performed in chapter 4 and transient vibration analyses are performed in chapter 5. Because no FE model can perfectly render the reality, some simplifying assumptions have to be made in order to create the model. Final FE models of test articles have been established through a reasonable tradeoff between model complexity, accuracy and computational time. The upcoming sections of the thesis present an example of FE models of electronic boxes, an investigation of the type of elements, the experimental correlation of the FE models and the modelling practices employed to create the final FE models.

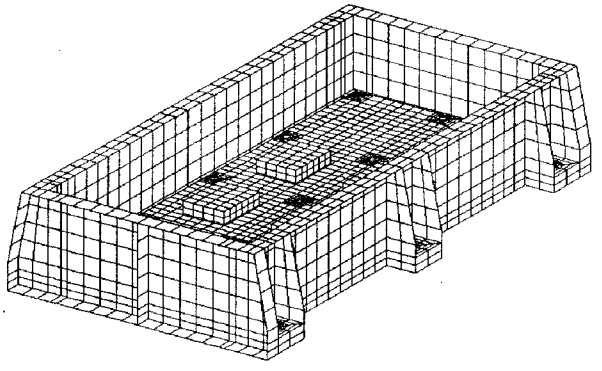

Figure 17: Final FE model of the TI (cover not shown)

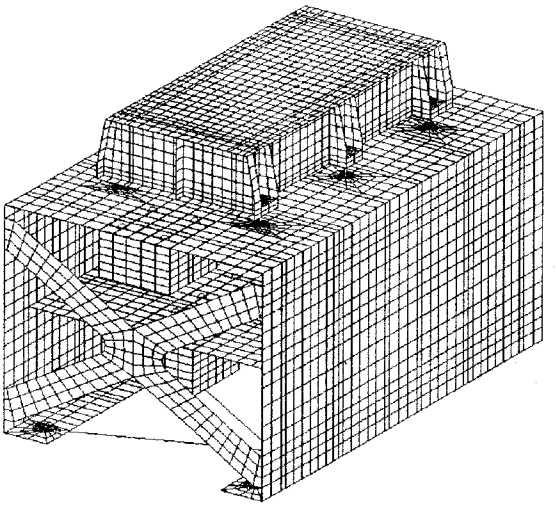

Figure 18: Final FE model of the coupled system assembly

3.3.1 Example of FE Model of an Electronic Box

Figure 19 shows an example of a FE model of an electronic box. The geometry details of the box were presented in Figure 6. The model is a blend of line, shell and solid elements.

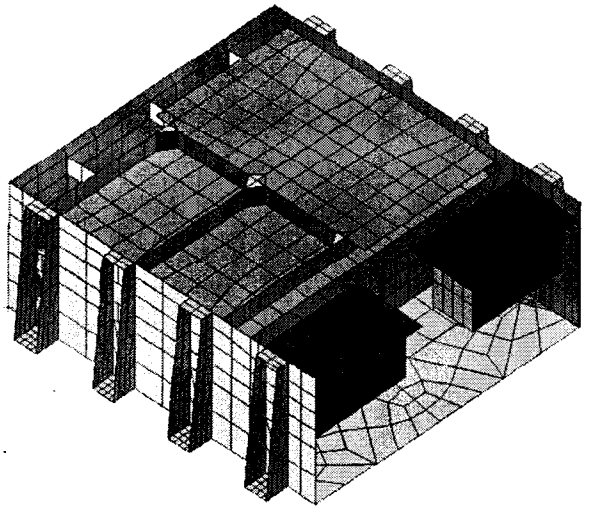

Figure 19: Example of FE model of an electronic box assembly [15]

3.3.2 Investigation of the Type of Elements

This section investigates the type of elements used for the current model. Solid elements and shell elements are effectively used to develop FE models. Mostly based on computational expenses, 4 nodes quadrilateral element (CQUAD4) shell elements are selected to create the final FE model. More modelling practices using shell elements are presented in the section 3.3.4.

3.3.2.1 Solid Element

PATRAN [53] can import an assembly of parts created by a computer-aided design (CAD) software such as Solid Edge and can directly mesh them using solid elements. 10 nodes tetrahedral (TET10) element has been used for this purpose. The developed model is created very rapidly and reflects the original geometry accurately. This is an effective modeling technique for thick parts where accurate rendering of geometry is crucial. However, in thin walled parts like the current design of the test item, elements generally can have a very high skewness ratio, which induces numerical errors. Also, the total number of elements and subsequently the number of degrees of freedom (d.o.f.) is generally very high. It requires about 20000 elements and 112000 computational d.o.f. to properly model the test item box using TET10 elements as shown in Figure 20. These numbers are considered quite high and thus computational cost is prohibitive. Moreover, it can be seen in Figure 20 that the general shape of the mesh is highly unstructured which is undesirable.

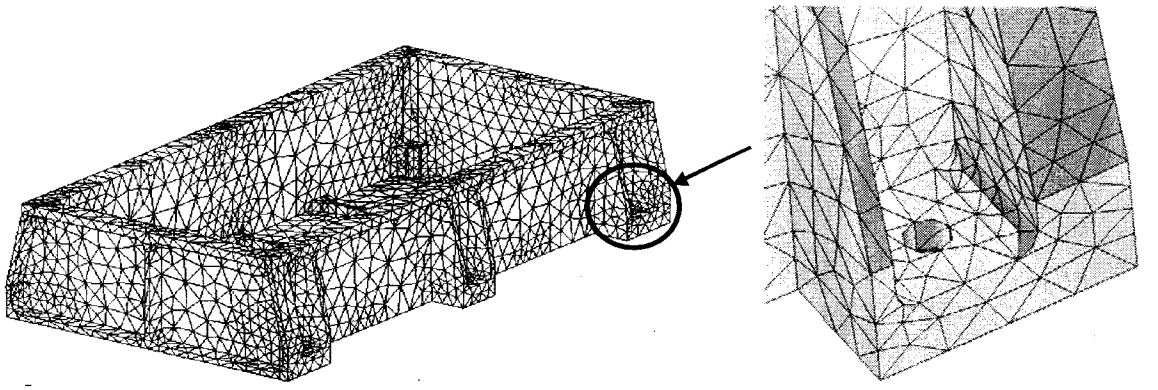

Figure 20: Tentative TI box solid element model

3.3.2.2 Shell Element

A second modeling technique is attempted which consists of building a model using shell elements in thin walled regions. The developed model using shell elements is shown in the Figure 21. This is considered a regular modeling technique in thin walled structures where the length over thickness ratio is over 10. Each wall has to be represented via its mid-thickness surface. The extracted surfaces need to be trimmed to form a coherent representation of the original geometry. 4 nodes quadrilateral element (CQUAD4) is selected over higher order elements based on its simplicity and computational efficiency. More elements are to be used to ensure proper modal representation.

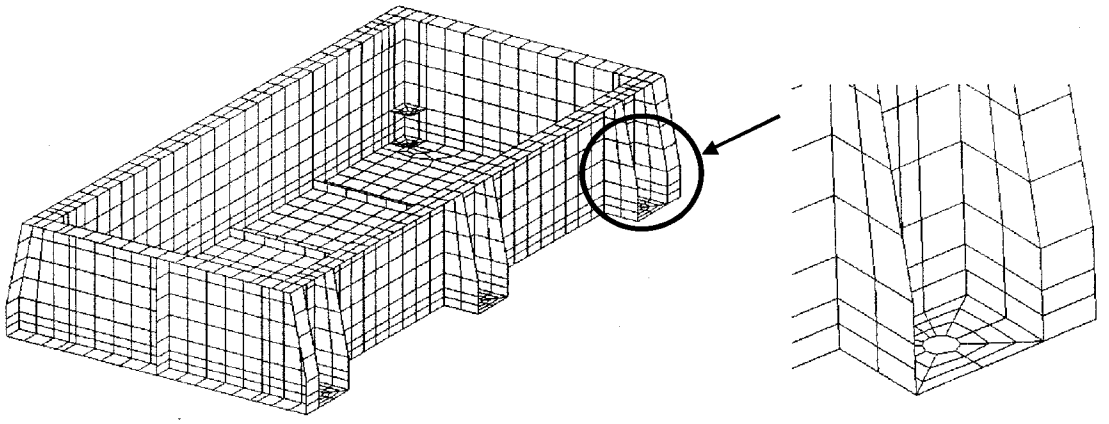

Figure 21: Tentative TI box shell element model

To choose the number of elements, one can directly specify the global edge length, which defines the maximum length of one element. Kiryenko et al. [12] have concluded that the maximum element size required for shock simulation can be obtain by having 4 to 6 elements within the shortest wave length. In thin walled structure, the shortest wavelength is usually associated with flexural mode which its wavelength (λ) can be computed using Eq. (8). For an aluminium panel with 1 mm thick (t), the wavelength associated with flexural mode is 55.5 mm at 3000 Hz, thus requiring a maximum element size of 9 mm [12].

$$\lambda = \left(\frac{2\pi}{f}\right)^{1/2}\left(\frac{Et^2}{12\rho}\right)^{1/4} \qquad \textbf{Eq. (8)}$$

The actual mesh size has been generated to be relatively uniform in all regions of the test item, resulting in a maximum element size of 7 mm. This size is smaller than the required size, thus ensuring to capture the modes accurately.

The developed shell elements model of the test item box shown in Figure 21 contains about 2000 elements and 10000 computational d.o.f.

3.3.3 Experimental Correlation

First, the physical mass of the test item is measured and compared to the mass evaluated using FE model, which respectively are 0.650 kg and 0.673 kg. The FE model generates slightly higher mass which is mainly due to the added rigid bar elements (See corrective actions 2 below). The difference between TI physical mass and that evaluated by FE model is about 3% which is still acceptable. The physical mass of the mounting structure is 5.210 kg which is very close to mass of 5.208 kg evaluated by the developed FE model. The test item and coupled system are set as for case 3 which is defined in the last section of this chapter.

Next, the fundamental frequencies of the test item and coupled system evaluated by FE models are compared with those obtained experimentally. This task was performed within the experiment section which is described in chapter 8. Basically, the test item and the coupled system were fixed to the shaker head of the electrodynamics shaker. The test articles in both configurations were excited at their base by random vibration. The apparent mass of the test item, obtained experimentally and its comparison with FE results, is shown in Figure 22. The acceleration at the interface of the test item is obtained in the coupled system configuration and is shown in Figure 23 along with FE results. Table 7

summarises the comparison of the frequencies of the main modes. All FE results shown are derived from the final FE model analysed in chapter 4.

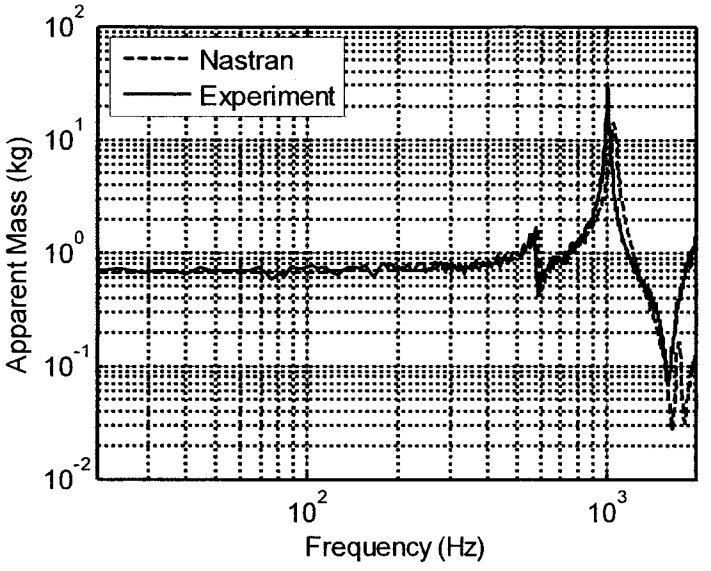

Figure 22: Comparison of the apparent mass of the TI: Experiment vs FE model

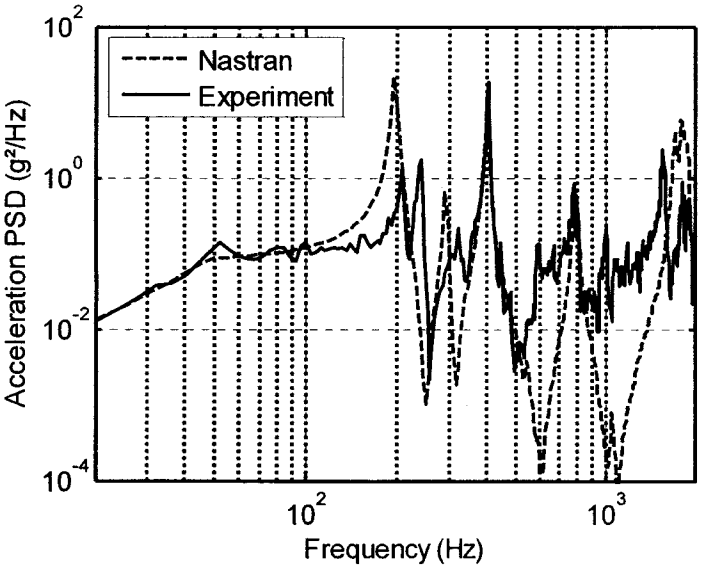

Figure 23: Comparison of the acceleration PSD at TI interface in CS: Experiment vs FE model

As it can be seen, the FE model achieved a high fidelity representation of the reality. It is noted that the error between FE and experimental results for main frequencies is less than 5%. The only mode having a greater mismatch is the mid panel flexural mode. However, this mode is not of special interest for this study. The TI coupled modes are described in section 4.2.3.

Table 7: Summary of the experimental correlation

Configuration	Mode	Frequency (Hz)		Error
		Experiment	Simulation	
TI	Cover	556	585	-5.22%
	Main - Board	1008	1057	-4.86%
CS	Top Panel	208	196	5.77%
	Mid Panel	240	290	-20.83%
	1st TI Coupled	404	398	1.49%
	2nd TI Coupled	780	790	-1.28%

The original developed FE model showed significant differences up to 60% while comparing the frequencies of the fundamental modes of the structure. This level of error appeared unacceptable and its cause was investigated. Most of the errors were attributed to the modelling of the attachment points. In fact, no change was made to the modelling of the structure itself. The implemented corrective actions are listed below and are further illustrated in the next section dealing with the modelling practices.

1. The d.o.f. transmitted by the Multi-Points Constraints (MPC) were changed from constraint in translation and free in rotation to fully constrained.
2. Bar elements were added to the edge of shell elements when a MPC or a standoff connects in-plane with shell elements. This was required to fully transmit in-plane rotational d.o.f. between both elements.
3. The masses on the board of the TI and on the MS were directly extruded from the shell elements beneath them. Originally, the extruded masses were punctually connected at their attachment points instead of being linked at all their lower nodes.

3.3.4 Modelling Practices to Develop Final FE Models

This section presents the main practices employed to create the shell-based FE models of the test item and the mounting structure. Some techniques were acquired from NASTRAN's tutorials [53]; others were defined via comparative studies and correlation with the experimental model. Table 8 summarises the types of element used in the final model.

Table 8: Element types summary

Dimensions	Element type
1D	BAR2
2D	CQUAD4
3D	HEX8
MPC (Rigid)	RBE2

3.3.4.1 Congruent Geometry

One of the advantages of using shell element is its convenience in obtaining a structured mesh. To do so, the Patran's Isomesh capability is exploited: it meshes any 4-sided surfaces in a rectangular and structured fashion. It also requires that adjacent surface's vertices to be placed at the same position as shown in Figure 24: no vertex can be placed on the edge of another surface. This is called congruent geometry in Patran. To do so, one needs to break the original geometry in as many pieces required to obtain the final congruent geometry. All the imported geometry has been broken down into a congruent geometry before meshing any surfaces.

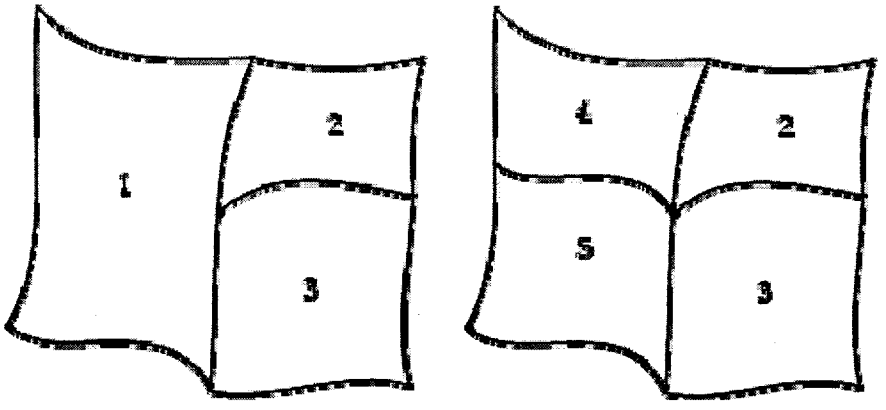

Figure 24: Incongruent and corresponding congruent surfaces [53]

3.3.4.2 Attachment Points Modelling

A surface containing an attachment point needs to be split down in 4-sided surfaces to be meshed in congruent fashion. Once the surfaces are meshed, a multi-points constraint (MPC) is created to link the perimeter nodes to center node as shown in Figure 25. This link is rigid and realised with RBE2 elements.

The center node is then linked to its connecting part. This process is done anywhere a bolt would be placed. All the d.o.f. of the attachments are fully transmitted.

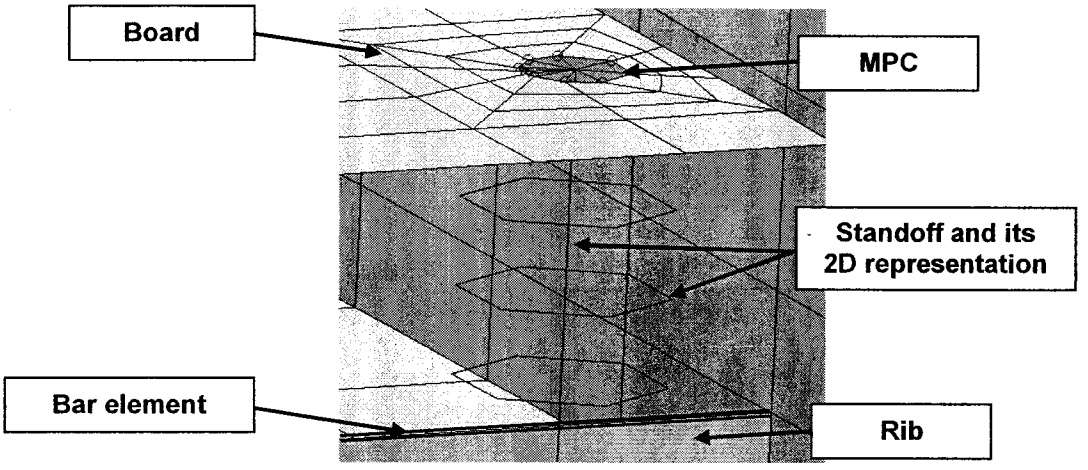

Figure 25: Model of the rib, standoff, board and connection

The standoffs are modeled with 1D bar elements (BAR2) as shown in Figure 25. The lower part of the standoff is directly fixed to the test item ribs. The upper part is available to support the board via its MPC connection as explained above. Bar elements are added on the edge of each shells element where the standoff connects in order to properly transfer the in-plane rotation.

3.3.4.3 Thick Regions Modelling

Some of the features, like the posts and the attachment points of the test item, are difficult to render using only shell elements. Thus, a dedicated solid modeling is undertaken to render their 3D nature. Shell elements are meshed and then extruded to HEX8 solid elements to the right height as shown in Figure 26. This results in a structure solid elements mesh. Since solid elements possess

only translational DOF at their nodes while shell elements possess translational and rotational DOF, a moment-transfer mechanism has to be implemented. This can be done by placing shell elements having a near-zero thickness beneath the solid. With this feature, the shell elements do not contribute to the stiffness or mass and effectively transfer the moment to the solid elements since they have common nodes.

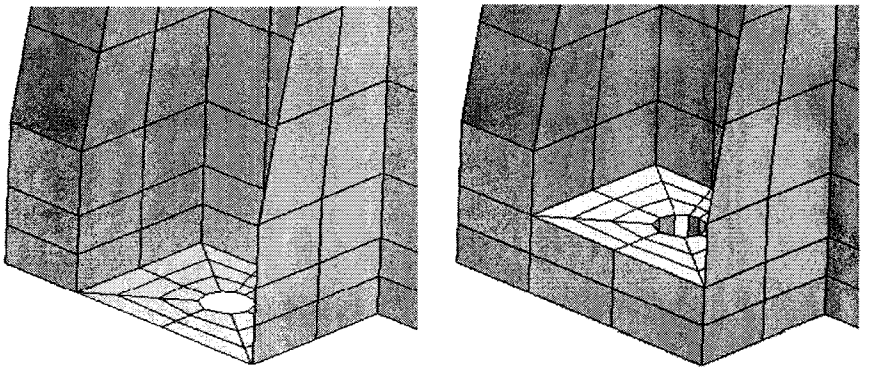

Figure 26: Shell elements and extruded solid elements at TI attachment points

When a hole is located in a solid modelled feature, all the nodes of the inner diameter surface of the hole are constrained with RB2 elements. The master node is located at the center of the hole close to its connecting part.

The components on the board or the masses are modeled using solid elements. They are directly extruded from the 2D elements of their mounting panel to the desired height as seen in Figure 27.

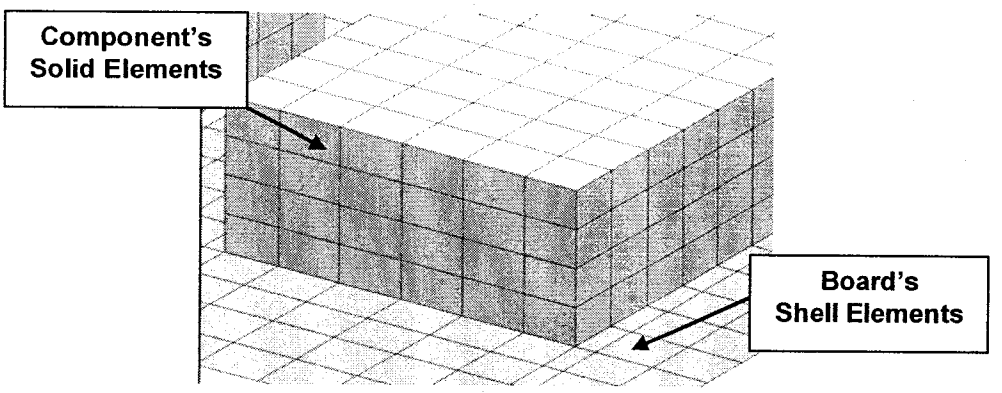

Figure 27: Board and board component

3.4 Sensitivity Study Configurations

Once the design and the FE models of the test item and the mounting structure are finalized, it is possible to create the cases for the sensitivity analysis. These cases consist of different configurations of both the test item and the mounting structure. These cases should result in a broad range of dynamic characteristics allowing performing a significant investigation of the overtesting. The random vibration and shock analyses are performed in chapters 4 and 5.

Table 9 summarizes the cases that are investigated. The first column of the table is the case number, the next 7 columns give information about the test item and the last 4 columns describe the mounting structure.

Table 9: Descriptions of the cases analysed in the sensitivity analysis

Case	Test Item							Mounting Stucture			
ID	Rib Height (mm)	Number of TI Attachment Points	Number of Board Attachment Points	Number of Components	Components Height (mm)	Fundamental Frequency (Hz)	Mass (kg)	Lumped Masses Height (mm)	Number of Lumped Masses	Fundamental Frequency (Hz)	Mass (kg)
1	10	4	15	8	10	1008	0.92	30	4	193	5.21
2	10	4	15	4	10	1057	0.67	15	8	220	5.21
3	10	4	15	4	10	1057	0.67	30	4	193	5.21
4	3	4	15	8	10	733	0.91	15	8	220	5.21
5	3	4	15	8	10	733	0.91	30	8	163	7.69
6	3	4	13	8	10	670	0.91	15	4	255	3.97
7	3	4	13	8	10	670	0.91	30	4	193	5.21
8	3	6	8	8	5	538	0.63	30	8	163	7.69
9	3	6	8	8	5	538	0.63	15	4	255	3.97
10	3	4	5	4	2.5	373	0.42	30	8	163	7.69
11	10	6	13	4	15	811	0.78	15	8	220	5.21
12	10	6	5	8	2.5	495	0.50	30	4	193	5.21
13	3	4	8	8	5	528	0.63	15	4	255	3.97
14	3	4	8	8	5	528	0.63	30	4	193	5.21
15	3	6	13	4	20	471	0.89	15	8	220	5.21
16	3	6	13	4	20	471	0.89	30	8	163	7.69
17	10	6	15	4	15	1034	1.17	15	8	220	5.21
18	10	6	15	4	15	1034	1.17	30	8	163	7.69
19	10	4	13	8	5	1101	0.66	0	0	427	2.73
20	10	6	8	8	15	939	1.17	15	4	255	3.97

For example, the test item of case 1 has ribs of 10 mm and is attached at 4 locations. The board is attached at 15 locations and there are 8 distributed components on the board. The components have a height of 10 mm. The test item has a fundamental frequency of 1008 Hz and a mass of 0.92 kg. It is fixed on a mounting structure having 4 centered masses of 30 mm high. The fundamental frequency of the mounting structure is 193 Hz and its mass is 5.21 kg. The possible locations of the board attachment points are illustrated in Figure 28.

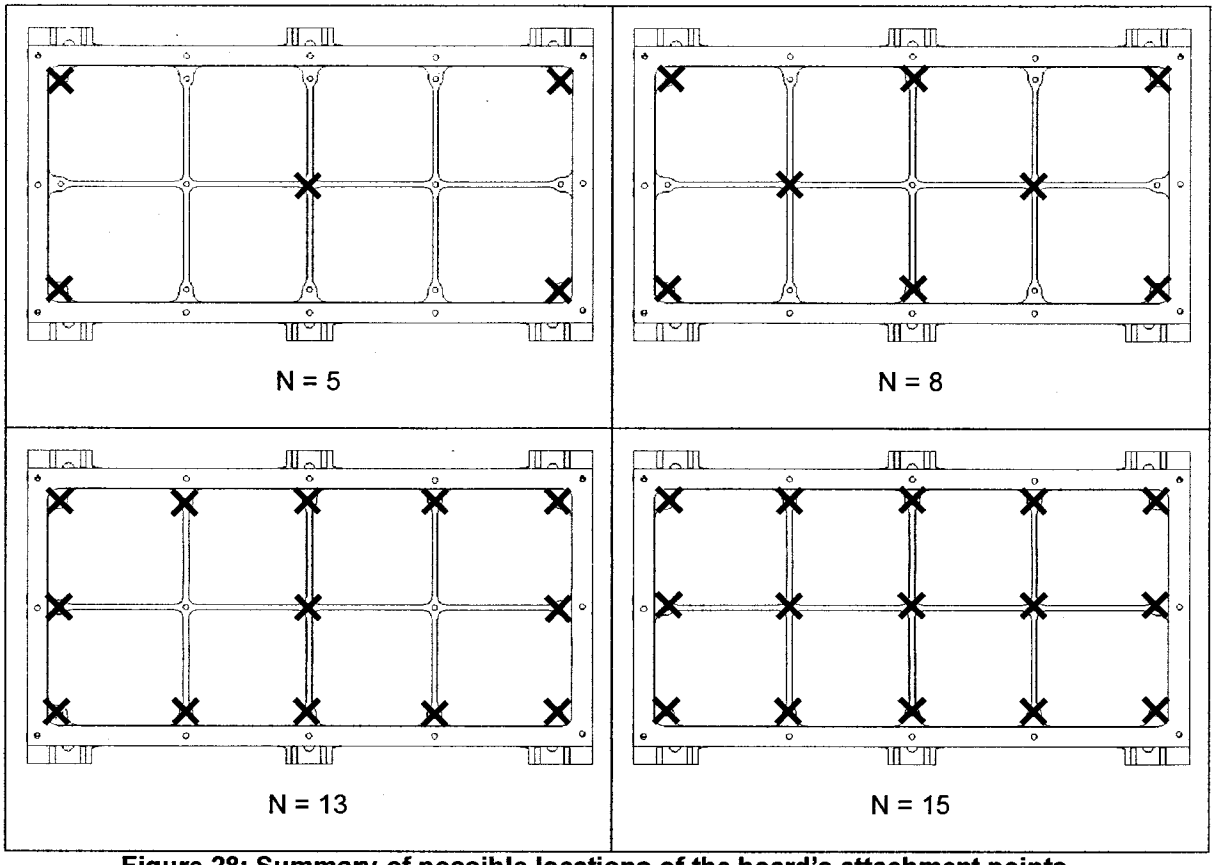

Figure 28: Summary of possible locations of the board's attachment points

3.5 Conclusion

This chapter described the design process of the test item and the mounting structure. This design has been made in agreement with the requirements provided in the chapter 2. To do so, finite element (FE) models of the structures have been developed using MSC NASTRAN. The details of its development are also explained. Finally, different configurations of the structures have been defined and described. These configurations form the cases that are to be analysed in the next chapters.

Chapter 4

Analysis of Overtesting in Random Vibration Testing

4.1 Introduction

This chapter provides all the details regarding the investigation of overtesting occurring in random vibration testing. It makes full use of the methodology develop in force limited vibration (FLV) testing [43]. All the analyses are performed with the FE models created in the chapter 3.

The next section of this chapter explains the analysis steps required to measure the overtesting and provides insights and justifications about the calculation techniques. All the steps are illustrated by an example. The third section provides the results of the investigation along with interpretation of the results.

4.2 Analysis Protocol

This section details the steps to measure the exact overtesting in random vibration. It also contains all the information regarding the calculation parameters. The analysis protocol is demonstrated for case 3 which configuration can be seen in Table 9 of section 3.4. All the analyses are carried in the out-of-plane direction (z).

4.2.1 Test Item Modal Analysis

The first important step is to conduct the modal analysis of the test item mounted on a rigid base. Because a valid response is sought for frequency up to 2000 Hz, it is chosen to include the modes up to 4000 Hz. The modes having a frequency above 4000 Hz are always represented rigidly using the concept of residual mass vectors [44].

For the current case, the fundamental mode is identified from the modal effective mass fraction. Shown in Figure 29, the first flexural mode of the board-floor occurs at a frequency of 1057 Hz and has modal effective mass fraction of 63%. There are a total of 54 modes up to 4000 Hz, which have a cumulative modal effective mass of 84.2%. The modal effective mass of the fundamental mode is therefore very significant.

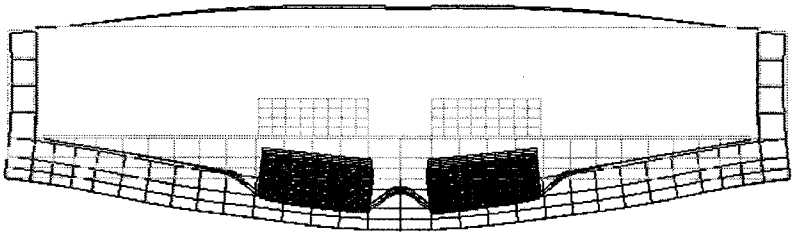

Figure 29: Mode shape of the fundamental mode of the test item

4.2.2 Test Item Random Vibration Analysis

The frequency response analysis of the test item alone is then performed. The calculation technique employed uses a modal formulation. The damping is defined as structural damping of 3% for all the modes. This value is thought to be fairly representative for this level of assembly [12]. The frequency response function is computed for frequencies between 20 and 2000 Hz with a 5 Hz resolution. This resolution is selected because it allows to properly discerning the action of each mode.

The apparent mass frequency response function of the test item is shown in Figure 30 for the current example. For random vibration, the apparent mass squared in the frequency domain can be described as [44]:

$$|M(f)|^2 = \frac{S_{ff}(f)}{S_{aa}(f)} \qquad \text{Eq. (9)}$$

The acceleration spectrum employed is a white-noise. The low-frequency asymptotic value of the apparent mass, M_0, is the physical mass of the structure. In the current example, the low-frequency asymptotic value of the apparent mass is 0.673 kg. The most significant mode of the test item can be observed in Figure 30 at 1057 Hz ($f_{max,m}$) and has an apparent mass of 14.0 kg. This value is used later in the vibration overtesting calculation. This leads to an amplification factor (Q) of 20.8.

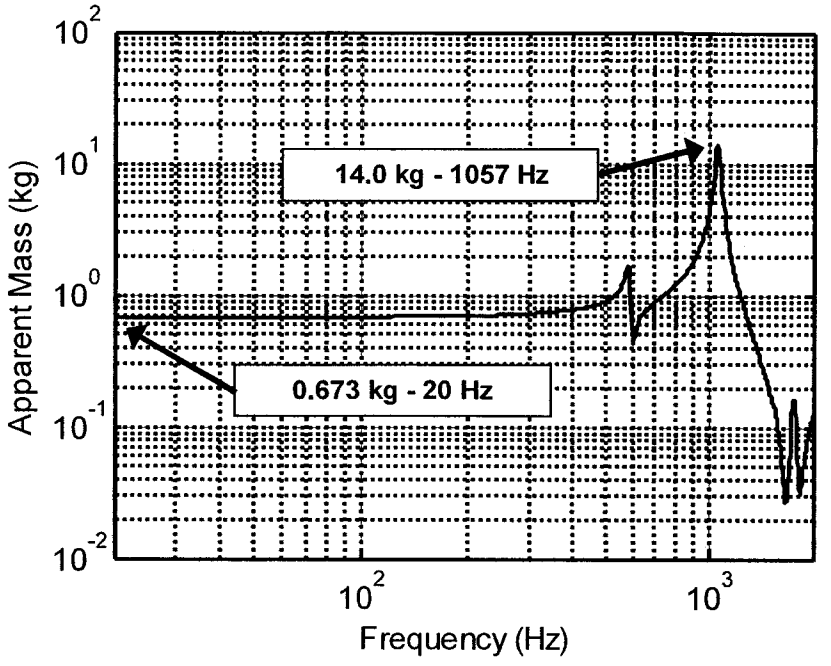

Figure 30: Apparent mass of the test item

4.2.3 Coupled Assembly Level Modal Analysis

A modal analysis of the coupled assembly is performed similarly to the test item modal analysis. It is possible to identify the modes of the coupled assembly which correspond to the TI fundamental mode coupled with the mounting structure. These modes are a direct result of the dynamic absorber effect [43]. They are later referred to as test item coupled modes. They can be determined by examination of the mode shapes of the assembly while seeking the shape that corresponds to the TI fundamental mode. The interface acceleration and force PSDs, which are derived in the next section can help identifying the TI coupled modes. The TI coupled modes should show as peaks on both side of the anti-resonance corresponding to the TI fundamental mode.

The anti-resonance frequency is shifted downward due to the flexibility of the TI boundary conditions at the coupled system level.

In the current case, the TI coupled modes have a frequency of 398 and 790 Hz respectively compared to 1057 Hz for the TI fundamental mode. Both TI coupled mode shapes of the example case are shown in Figure 31 to demonstrate their similitude with the test item fundamental mode shape which is shown in Figure 29. This similitude becomes more evident when closely zoomed.

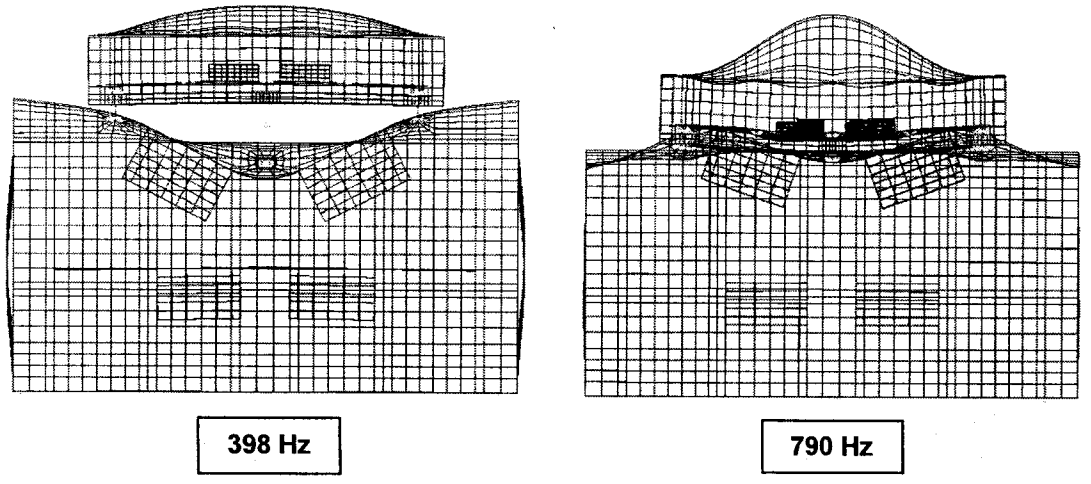

Figure 31: Mode shape of the TI coupled modes of the coupled assembly

4.2.4 Coupled Assembly Level Random Analysis

This section gives details about the random analysis performed at the coupled assembly level. The first part shows the acceleration input chosen for the analysis while the second part shows the analyses performed using the selected specification.

4.2.4.1 Acceleration Input Specification

To perform the random analysis, an acceleration excitation must be applied at the base of the mounting structure in the coupled assembly configuration. This acceleration profile is extracted from NASA GEVS [54] for the acceptance vibration level test performed on structures of 22.7 kg (50 lb) or below. The original GEVS input spectrum has an RMS value of 10.0 g up to 2000 Hz and is shown in Figure 32.

This input spectrum is not convenient for the current study because it is not constant around the expected TI fundamental frequency. It is thus modified to be constant up to 2000 Hz. The modified input spectrum has a RMS value of 12.5 g and is also shown in Figure 32. The modified GEVS spectrum is input to the base of the mounting structure in the coupled assembly configuration.

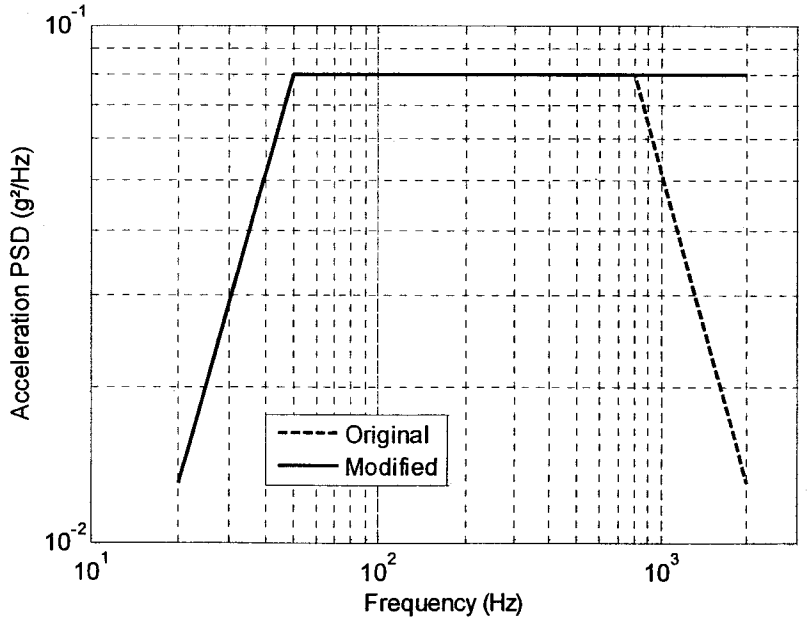

Figure 32: Acceleration input for the coupled system random analysis

4.2.4.2 Random Vibration Analysis

A frequency response analysis is performed on the coupled assembly level system with the same parameters as for the test item. It is used to perform a random vibration analysis of the coupled system under the modified GEVS spectrum. The acceleration (S_{aa}) and force (S_{ff}) PSD at the interface between the mounting structure and the test item are computed and shown in Figure 33 and Figure 34. The acceleration PSD is identical at all the TI attachment points because the structure is symmetric. It is important to identify the TI coupled modes as explained in section 4.2.3. They should show as peaks on both side of the anti-resonance corresponding to the TI fundamental mode. It is interesting to note that this frequency could shift by as much as 40%, although a shift of less than 20% is more commonly observed in this study.

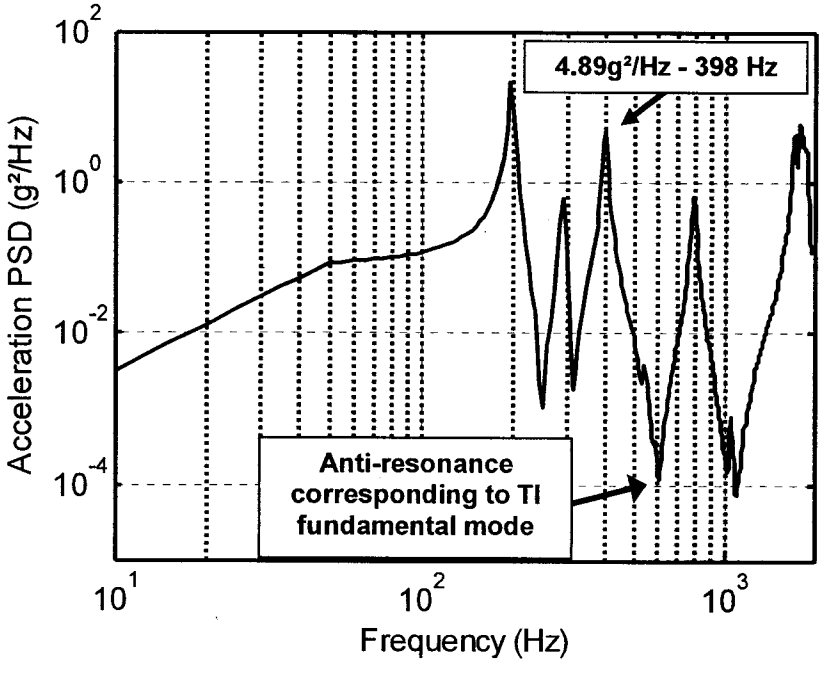

Figure 33: Interface Acceleration PSD

Once the peaks related to these modes are identified, it is possible to envelope the acceleration and force values to the highest value of both peaks. These frequencies are referred to as $f_{max,a}$ and $f_{max,f}$. This forms the reference environment upon which the test item should be qualified. In the current example, the test item coupled modes have a frequency of 398 and 790 Hz. The maximal pertinent interface force and acceleration are respectively 285 N^2/Hz and 4.89 g^2/Hz.

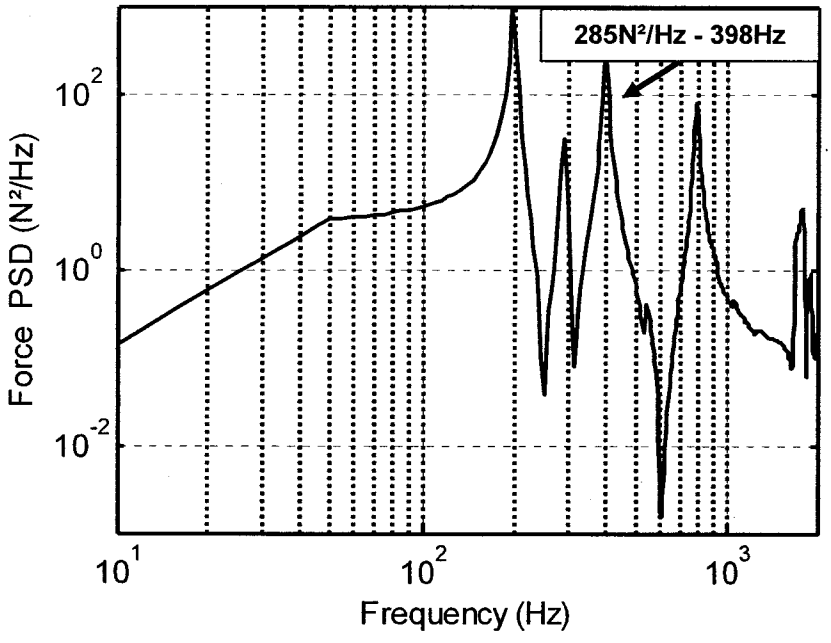

Figure 34: Total interface Force PSD

In order to get the total interface force, the forces at all the attachment points need to be summed. When no other mode has a nearby frequency, it can be done with the square of the sum of the square root [43] as described in Eq. (10). Basically, it relates the force of the i^{th} attachment point, $S_{ff,i}$, to the total

force at the interface of the structure, $S_{ff,total}$. The forces are summed when they are in-phase and subtracted when they are out-of-phase. The phase is determined from the modal analysis.

$$S_{ff,total} = \left[\sum_{i=1}^{N} \sqrt{S_{ff,i}} \right]^2 \qquad \text{Eq. (10)}$$

4.2.5 Investigation of Overtesting in Vibration Test

Once the interface environment is characterized, it is possible to define the level of overtesting occurring in a rigid base test of the test item and to compute the exact C^2 value required by the semi-empirical method [41] which would be used to create the force limit as:

$$C^2 = \frac{s_{ff}(f_{\max,f})}{s_{aa}(f_{\max,a}) \times M_0^2} = \frac{285}{(4.89 \times 9.81^2) \times 0.673^2} = 1.3 \qquad \text{Eq. (11)}$$

To have coherent units, the spectral acceleration S_{aa} needs to be converted from g^2/Hz to $(m/s^2)^2$/Hz. This represents a factor of the gravitational acceleration constant, 9.81 m/s^2, squared.

Next, the amount of overtesting, or inversely the notching, can be determined by comparing the force level at the base of the test item when mounted on a flexible $S_{ff,flexible}$ and on a rigid mounting, $S_{ff,rigid}$ [41]. The so-called

rigid force level can be obtained by multiplication of the maximal apparent mass squared occurring at the TI fundamental frequency by the maximal acceleration of the coupled system. It is equivalent to dividing the amplification factor squared (Q^2) by the C^2 coefficient. The overtesting (N_{Vib}) occurring at assembly-level random vibration testing is [41]:

$$N_{Vib} = 10\log\left(\frac{S_{ff,rigid}}{S_{ff,flexible}}\right) = 10\log\left(\frac{Q^2}{C^2}\right)$$

$$N_{Vib} = 10\log\left(\frac{M^2\left(f_{\max,m}\right)\times S_{aa}\left(f_{\max,a}\right)}{S_{ff}\left(f_{\max,f}\right)}\right) \qquad \text{Eq. (12)}$$

$$N_{Vib} = 10\log\left(\frac{14.0^2\times\left(4.89\times 9.81^2\right)}{285}\right) = 25.1\,dB$$

4.3 Results

All the cases presented in the chapter 3 have been investigated following the same procedure. The results are summarized in Table 10. The second and third columns show the fundamental frequency and the dynamic amplification of the test item. The next two columns show the frequencies of the TI coupled mode at which the acceleration ($f_{max,a}$) and the force ($f_{max,f}$) are maximal which usually are the same frequency for most cases. The last two columns show the C^2 and the vibration overtesting. For most cases, the C^2 values lie between 1 and 3 and the vibration overtesting is between 10 and 20 dB. These C^2 values are lower than the usual reported range of 2 to 5.

Table 10: Vibration overtesting investigation results

Case	Test Item		Coupled System		C^2	N_{Vib}
	Frequency	Amplification	$f_{max,a}$	$f_{max,f}$		
	Hz	-	Hz	Hz	-	dB
1	1008	15.5	375		1.3	22.6
2	1057	20.8	630	555	1.6	24.3
3	1057	20.8	400		1.3	25.1
4	733	19.5	520		3.2	20.7
5	733	19.5	400	660	1.6	23.9
6	670	17.8	450		2.4	21.2
7	670	17.8	370		1.7	22.8
8	538	17.2	270		20.3	11.7
9	538	17.2	255		1.4	23.3
10	373	10.8	245		1.6	18.6
11	811	10.6	745		9.3	10.8
12	495	8.0	215		5.2	10.8
13	528	18.4	710	445	0.8	26.4
14	528	18.4	380		2.7	21.0
15	471	15.0	375		17.6	11.0
16	471	15.0	265		13.4	12.2
17	1034	15.6	780		3.5	18.4
18	1034	15.6	720		2.0	20.9
19	1101	13.0	680		1.4	20.8
20	939	16.2	735		3.4	18.9

The cases 8, 15 and 16 have a C^2 coefficient higher than 10. In the TI coupled modes of these cases, the top plate of the mounting structure is in flexion. Also, the attachment points of the test item lie close to the node of the flexion shape of the top plate. Hence, the acceleration at the test item is small and explains the high C^2 coefficient.

4.4 Conclusion

This chapter investigates the overtesting occurring in vibration testing at assembly-level. It shows that significant overtesting occurs which is due to the vibration absorber effect. This overtesting can be reduced using techniques like force-limiting vibration and its semi-empirical method for which the C^2 coefficient has been calculated.

Chapter 5

Analysis of Overtesting in Shock Testing

5.1 Introduction

This chapter provides all the details regarding the investigation of overtesting due to the dynamics absorber effect during mechanical simulation of pyroshock. The investigation derives a methodology similar to that of FLV testing, explained in the literature review of the chapter 1 and employed in the chapter 4. All the analyses are performed using the FE models described in the chapter 3.

The next section of this chapter explains the shock synthesis technique which is implemented to generate a time-domain acceleration waveform meeting a given standard shock specification in the form of the shock response spectrum (SRS). The third section explains the analysis steps required to measure the overtesting using a SRS specification. The fourth section presents the modification applied to the shock synthesis technique and to the analysis steps to make it applicable to the proposed input energy spectrum (IES) specification. All the steps are illustrated through an example for case 3 as in the previous chapter. The fifth section provides the results of the investigation along with interpretation of the results. The last section concludes on the main findings.

5.2 Shock Synthesis Algorithm

This section presents the shock waveform synthesis technique implemented to perform the shock overtesting analyses. This technique is employed for shock testing using electrodynamics shaker. The first part of this section explains the reasons why this technique is adopted. The second part presents all the details regarding its implementation. The third part presents an example of synthesis applied to the Delta II shock environment, which forms the environment applied at the base of the coupled system.

5.2.1 Justification

In the space community, the standard shock specification is the SRS and it surely represents an effective way of specifying the severity of a transient [3]. Still, the SRS represents an idealization of the shock and information is lost while computing the SRS: the SRS is not reversible. There are basically two methods which can be used to find structural response to a shock envronment: the response spectrum and transient simulation.

Based on the modal analysis, the response spectrum method [55] is accurate to retrieve the SRS and the modal force at other locations in the spacecraft due to an input SRS. In order to obtain the maximum acceleration or force, one important assumption has to be taken regarding the way modes combine in phase, i.e. if they sum or subtract. The most common approach is the square root of the sum squared (SRSS). For most situations, this assumption

leads to good results. Nonetheless, it is not possible to implement it in testing. The response spectrum method is not seen as a good candidate to solve the current problem because a more practical method is sought.

Another method of computing the response of a structure subject to shock is to perform a transient simulation. For this, one would ideally have the actual acceleration waveform that produced the SRS specification. However, this is unrealistic because of the large amount of data involved and unpractical because enveloping or zoning could hardly be done. For this reason, the excitation should be obtained by other means. Once the excitation is known, one can perform the transient simulation and solve for the acceleration and force conditions at the interface of the test item. In addition, those responses can be further post-processed into SRS, IES, PSD and any other desired measurements. Transient simulation is consequently well adapted to solve the current problem and perform the experiment. Finally, the waveform used for the transient simulation can be derived using the state-of-the-art test practices.

The standard shock testing methods are described in the literature review of chapter 1. From this, one sees that there are two methods for shock testing which can be used to tailor a shock to a specification.

These methods can be briefly summarized as:

- Impact table (MIPS): The table is excited by a hammer. A variation of this method uses explosive device as the excitation mean. The excitation is modeled as a force input on the table. The test is tailored by various parameters like the hammer mass and stiffness, the structure under test location, the impact location, etc, so that the input acceleration matches the specification.
- Shaker: A shock synthesis algorithm is employed to generate an acceleration directly matching the specification. A shaker is then controlled according to the waveform to perform the test.

In industry, the impact table method is more common because it can input high acceleration level shock to a test item [3]. Shaker tests are usually limited by their force rating, especially with the high frequency content associated with shock testing. However, the impact table method requires a great deal of case-to-case tuning in order to fit all the parameters to the specification [38]. From this perspective, the shaker method is easier to implement. Also, a low-level test can be performed in order not to have problems with the force rating of the shaker. Based on these facts, it is decided to perform the shock overtesting investigation based on a transient simulation of a structure for an acceleration excitation generated for a shaker test.

5.2.2 Implementation

The implemented algorithm is based on case 5 of Smallwood [39]. It consists of the superposition of several waveforms created by multiplying a relatively arbitrary function by the $\cos^m(x)$ window function. An amplitude coefficient is applied on each waveform to scale its amplitude to the desired level. The general procedure is very similar to that explained in Ref. [36]. However, according to Smallwood [39], the waveform created by the method described in case 5 allows tuning more features of the waveform like the duration and the temporal moments, like skewness, allowing it to be more representative of real shock waveform. To suit shaker testing reality, the overall displacement, velocity and acceleration of the waveform are zero over the total duration. Also, the maximal displacement shall not exceed the maximal shaker stroke.

Smallwood [39] first defines the shaker displacement as:

$$\begin{aligned} d(t) &= A\,y(t)\cos^m(z(t)) && -\frac{z}{2} \le z \le \frac{z}{2} \\ &= 0 && elsewhere \end{aligned} \qquad \text{Eq. (13)}$$

Where A is the amplitude coefficient of the waveform. The other variables are described next.

The velocity and acceleration are simply taken as the proper derivatives as:

$$v = \dot{d} = A\left[\dot{y}\cos^{m}(z) - my\dot{z}\sin(z)\cos^{m-1}(z)\right]$$
$$a = \ddot{d} = A\begin{bmatrix}\left(\ddot{y} - my\dot{z}^{2}\right)\cos^{m}(z) \\ -m(2\dot{y}\dot{z} + y\ddot{z})\sin(z)\cos^{m-1}(z) \\ +m(m-1)y\dot{z}^{2}\sin^{2}(z)\cos^{m-2}(z)\end{bmatrix} \qquad \textbf{Eq. (14)}$$

The $y(t)$ and $z(t)$ functions are defined in the special case 5 as [39]:

$$y(t) = \sin\left(\frac{2\pi f}{T}t\right) \qquad 0 \le t \le 1$$
$$z(t) = \pi\left[\left(\frac{t}{T}\right)^{p} - \frac{1}{2}\right] \qquad 0 \le t \le 1 \qquad \textbf{Eq. (15)}$$

The derivatives of these functions are required and expressed as:

$$\dot{y} = \frac{2\pi f}{T}\cos\left(\frac{2\pi f}{T}t\right) \qquad \ddot{y} = -\left(\frac{2\pi f}{T}\right)^{2}\sin\left(\frac{2\pi f}{T}t\right)$$
$$\dot{z} = \frac{\pi p t^{p-1}}{T^{p}} \qquad \ddot{z} = \frac{\pi p(p-1)t^{p-2}}{T^{p}} \qquad \textbf{Eq. (16)}$$

These expressions can be substituted in the original acceleration expression to create one simple waveform. Many of these single waveforms centered at different frequencies are superposed to create the final synthesis

waveform. The creation process of the final waveform is schematized in Figure 37 and explained in more details after the figure. Several parameters are available to adjust the single waveform shape. Some trial runs have been performed to fully understand the effect of these parameters and to select their value. The effect of the input parameters can be described as:

- f: Control the central frequency of the single waveform where most of the motion is located.
- *P*: Control the temporal shape of the waveform. The "*P*" value is selected at 0.7 to give the waveform a positive skewness like most pyroshock [39]. A positive skewness indicates a rapid rise and a slow decay. The Figure 35 shows an example of two waveforms for values of P of 0.3 and 1.

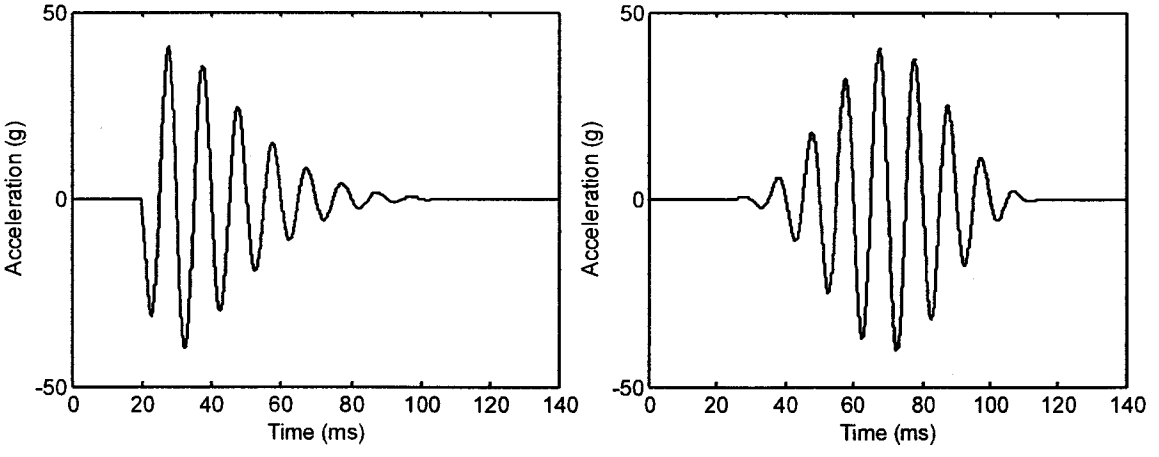

Figure 35: Example of waveform for values of P = 0.3 (left) and P=1 (Right)

- *m*: Exponent of the windows shaping function. It controls the smoothness of the resulting SRS. A high "*m*" value corresponds to a more impulsive

near-field shock and results in rounded SRS peak while a low "*m*" value corresponds to a resonant far-field shock and results in a spikier SRS. Smallwood [39] suggests using value no less than 3. After trials, a medium value of 10 is selected which easily allows reaching the desired shock specification. The Figure 36 shows an example of waveforms and their resulting SRS for value of *m* of 3 and 30.

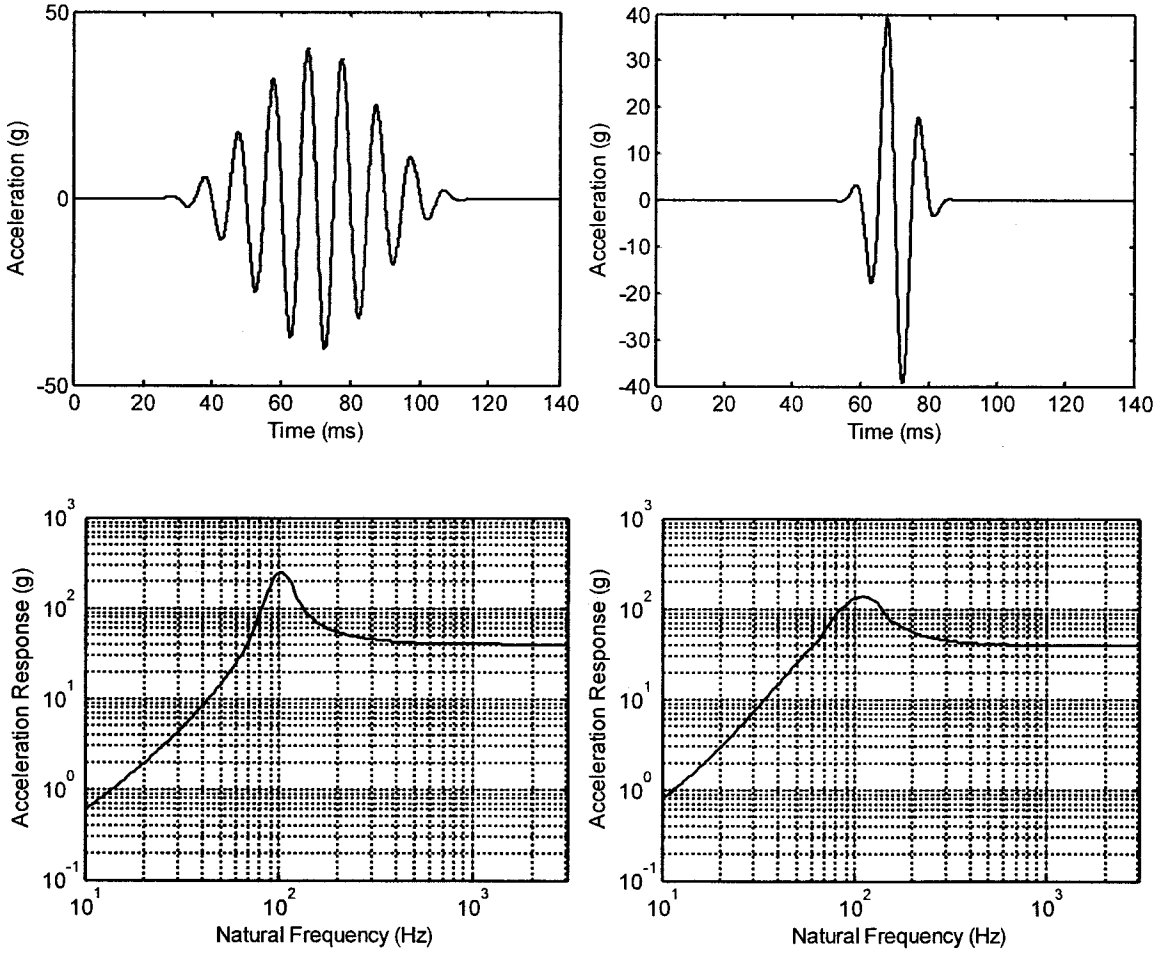

Figure 36: Example of waveform (up) and SRS (down) for value of *m*=3 (left) and m=30 (right)

- *T*: Control the duration. High frequency vibrations are known to damp faster than lower frequencies [36]. The duration of each single waveform is set to be inversely proportional to the square-root of the frequency, as flextural wavelength described in Eq. 8 of section 3.3.2.2. Moreover, because of the positive skewness of the waveform, high frequency content is more present at the beginning of the waveform than at the end. Usually, pyroshocks have most of their energy within 20 ms [3]. The duration of the waveform is tuned using Eq. 17.

The logic of the algorithm is summarized in Figure 37. Basically, it consists of the superposition of many simple waveforms having different frequencies. The waveform frequencies are selected to have a $1/24^{th}$ octave band spacing. Because the amplitude of one waveform at its central frequency affects the SRS value at its neighbouring frequencies, the amplitude coefficients are tuned iteratively. One amplitude coefficient is updated with the ratio of the specification to the synthesis SRS value at the central frequency of the single waveform. The total waveform duration is scaled with the ratio of the specified to the synthezised 10 percent duration. It is important to note that the duration vector is adjusted with this ratio; the inverse proportionality with the square-root of the frequency is preserved.

$$\{A\}_{i+1} = \frac{\{SRS_{(Specification)}\}_i}{\{SRS_{(Synthesis)}\}_i}\{A\}_i \qquad \{T\}_{i+1} = \frac{T10\%_{(Specficication),i}}{T10\%_{(Synthesis),i}}\{T\}_i \qquad \textbf{Eq. (17)}$$

This scheme effectively corrects the amplitude and duration coefficients and allows them to converge quickly within an acceptable tolerance. The shock waveform synthesis algorithm is illustrated in the next section with an example.

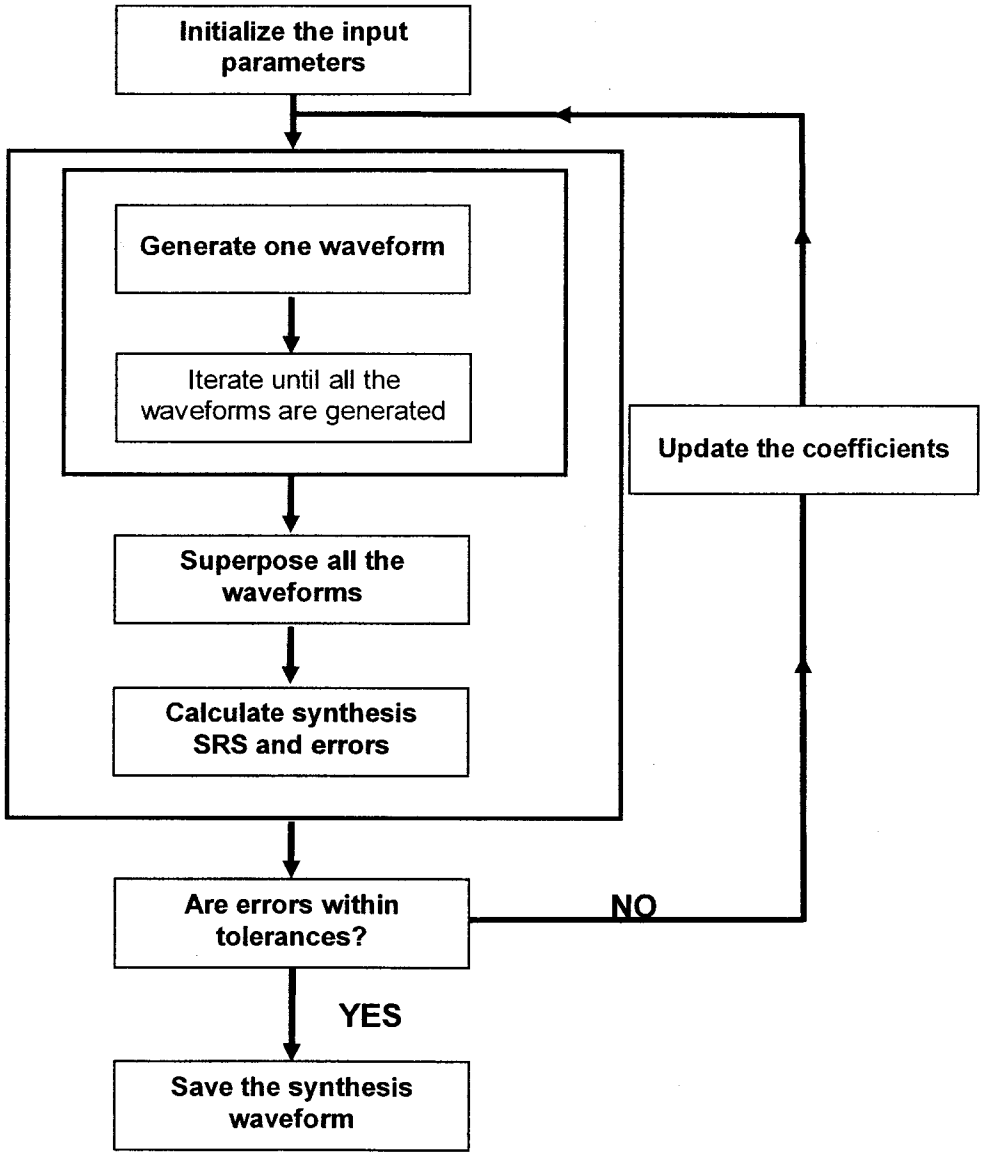

Figure 37: Symbolic representation of the shock synthesis algorithm

5.2.3 Shock Specification

The shock specification is taken from the Delta II planner's guide [56] for "Fig 4.14 - 6019 and 6915 Payload Attach Fitting". This specification has been chosen because it is deemed generic. The specification is reproduced in Figure 38 along with the SRS of the synthesis waveform. Its corresponding generated acceleration waveform is also shown in Figure 38. In this case, the specification was met within a tolerance band of 0.50 dB. It should be noted that the specification extends from 100 to 3000 Hz and that the SRS of the synthesis waveform is shown at lower frequencies for sake of completeness. Although not mentioned in the planner's guide, the shock duration is specified as 15 ms and the actual shock duration is 15.4 ms.

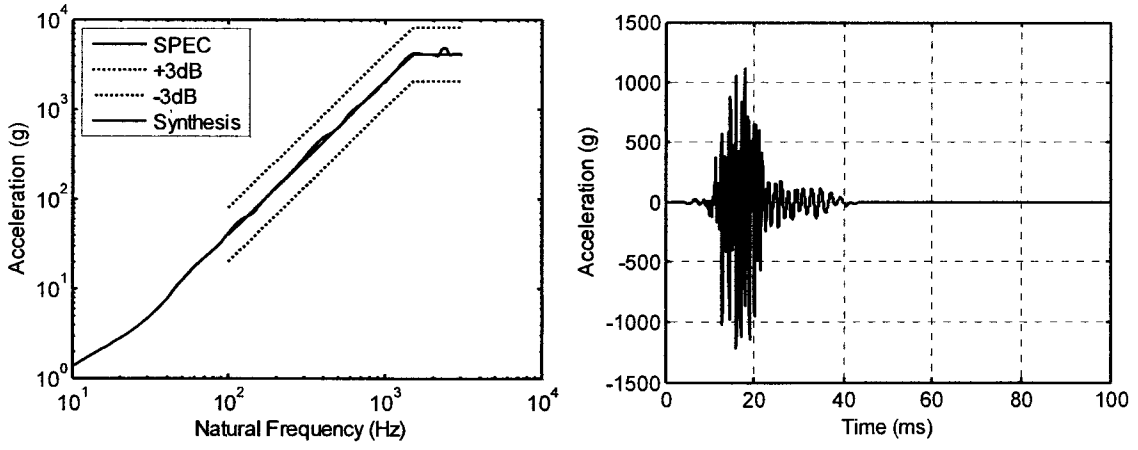

Figure 38: Delta II specification SRS and synthesis SRS (left) and synthesis acceleration waveform (right)

5.3 Shock Analysis using the Response Spectrum

This section details the steps to measure the overtesting in shock testing due to the dynamic absorber effect using the standard SRS specification. It also contains all the information regarding the calculation parameters. As for random vibration in the previous chapter, the analysis protocol is demonstrated for the case 3 configuration. The analyses are carried out in the out-of-plane direction (z).

5.3.1 Coupled Assembly Level Transient Analysis

The first important step is to conduct a modal based transient analysis of the coupled assembly. Because a valid response is sought for frequency up to 3000 Hz, it is decided to include all the modes up to 6000 Hz. As previously, the modes having a frequency above 6000 Hz are to be represented rigidly using the concept of residual mass vectors [44]. The excitation is the time domain acceleration synthesis waveform of the Delta II shock specification shown in Figure 38 and it is input at the base of the mounting structure in the coupled system configuration.

In order to obtain a valid calculation of a SRS up to 3000 Hz, a sampling frequency at least 8 times faster has to be selected [3] which would lead to a time step of 0.041 ms. The analysis time step is actually chosen to be smaller and is 0.03 ms. This time step size requires 5000 samples in order to simulate 150 ms.

It should be noted that most of the excitation is within the first 40 ms and its 10 percent duration is 15 ms as illustrated in Figure 38. The simulation time thus allows capturing almost all, if not all, of the structure response. .

For the current case, the time-domain acceleration and total force at the test item interface is shown in Figure 39 and its resulting SRS is shown in Figure 40. The 10 percent duration of the shock shown is 22.3 ms. Only the most interesting part of the simulation is shown. The SRS shows peaks at the dominant frequencies of the coupled assembly which are physically due to the dynamic amplification occurring at these frequencies.

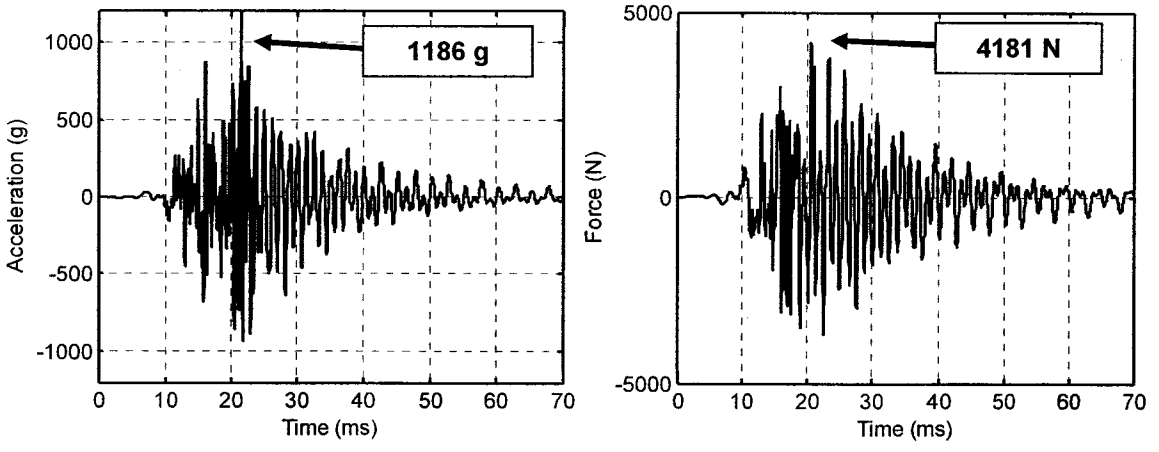

Figure 39: Acceleration (left) and force (right) at TI interface in coupled system

5.3.2 Test Item Shock Environment

In order to create the shock environment of the test item, the maximal TI SRS is computed using the results of the coupled assembly simulation. For each frequency, the maximal SRS value at all the attachment points is taken to form the maximal TI SRS shown in Figure 40. The maximal TI SRS is then enveloped

to create the TI shock environment also shown in Figure 40. This environment serves to shock test the test item on a rigid mounting. In real application, this environment can be derived from various means as described in the literature review in chapter 1. Generally, the maximal SRS is enveloped by a piecewise line approximation. One key principle in developing an envelope is that the system only accepts energy at its modal frequency; therefore the shock input needs to be representative from the lowest modal frequency to the defined high frequency limit of the test [25].

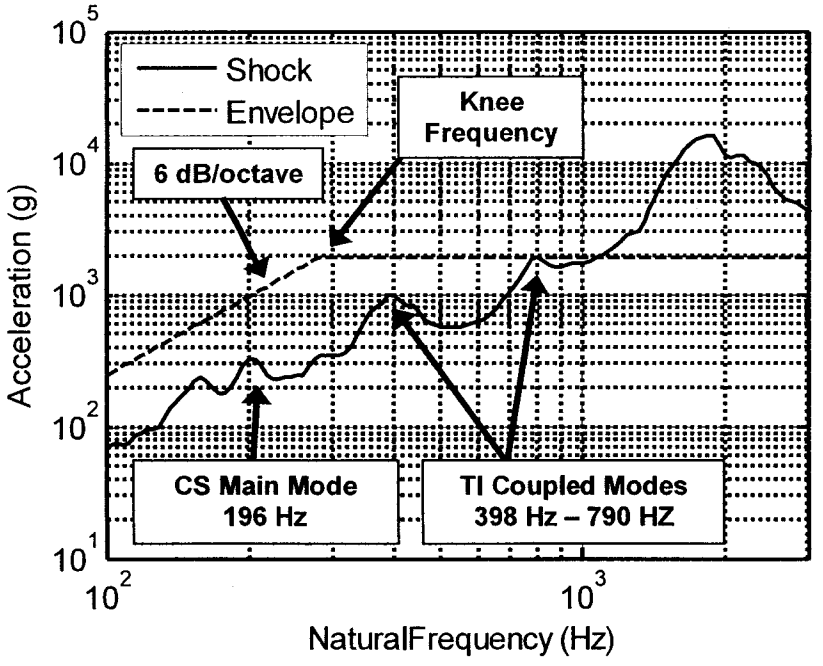

Figure 40: Maximal SRS at TI interface and its envelope

In order to study the effect of the dynamic absorber which causes the overtesting, it is necessary to input the right acceleration level around the fundamental frequency of the test item. As in FLV, this acceleration corresponds to the maximal acceleration level observed at the frequencies of the TI coupled

modes. The knee frequency is placed with a margin of half an octave lower than the first TI coupled mode. A slope of 6 dB per octave is placed at lower frequencies. This slope represents a constant velocity line and is a property of pyrotechnic shock [17, 26]. Peaks at higher frequencies are not enveloped because they could potentially induce a higher acceleration level at the TI fundamental frequency. The SRS envelope is kept flat at higher frequencies. This envelope ensures that the test item is excited with the SRS level than the TI coupled modes.

In some cases, the SRS level at the TI coupled modes frequencies is not due to the TI coupled modes, but to stronger adjacent modes. It is thus not possible to clearly identify the SRS level due to the TI coupled modes. Case 11 configuration in Table 9 is one example of this and its maximal TI SRS can be seen in Figure 41 along with its envelope.

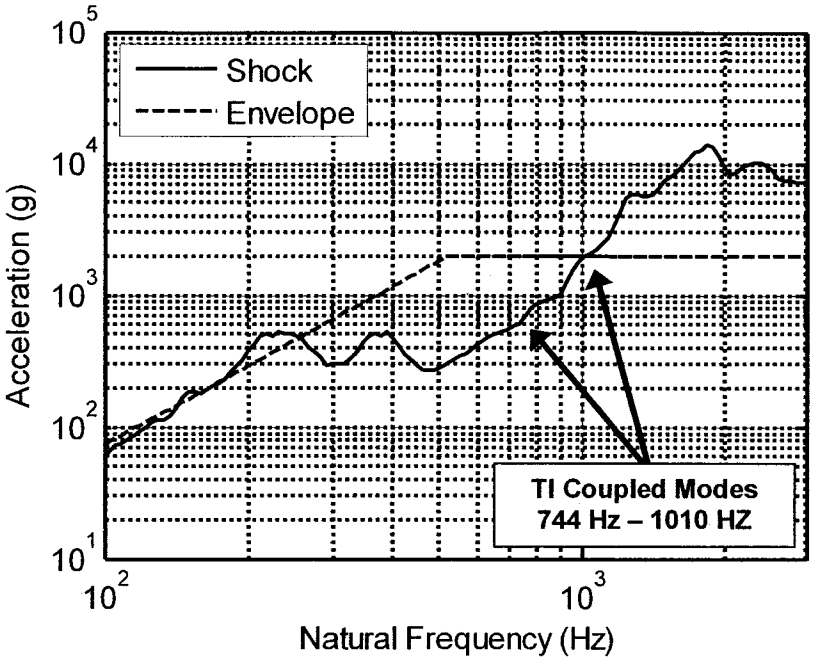

Figure 41: Maximal SRS at TI interface and its envelope for case 11

The envelope level at the knee frequency is taken as the maximal SRS value at the frequencies of the TI coupled modes. This level is higher than the actual acceleration level of the TI coupled mode since it is due to stronger adjacent modes. Hence, the overtesting derived from this envelope gives an upper limit approximation of the exact overtesting. Lower frequencies peaks are not considered since the test item have no mode at those frequencies.

Based on the defined envelope, it is possible to create a synthesis waveform to test the TI on a rigid base. The algorithm described in the section 5.2 is used for this purpose. For all cases, the synthesis SRS fits the TI shock environment envelope within 1dB and the 10 percent duration is matched within 5%. The synthesis waveform for the example case 3 is shown in Figure 42.

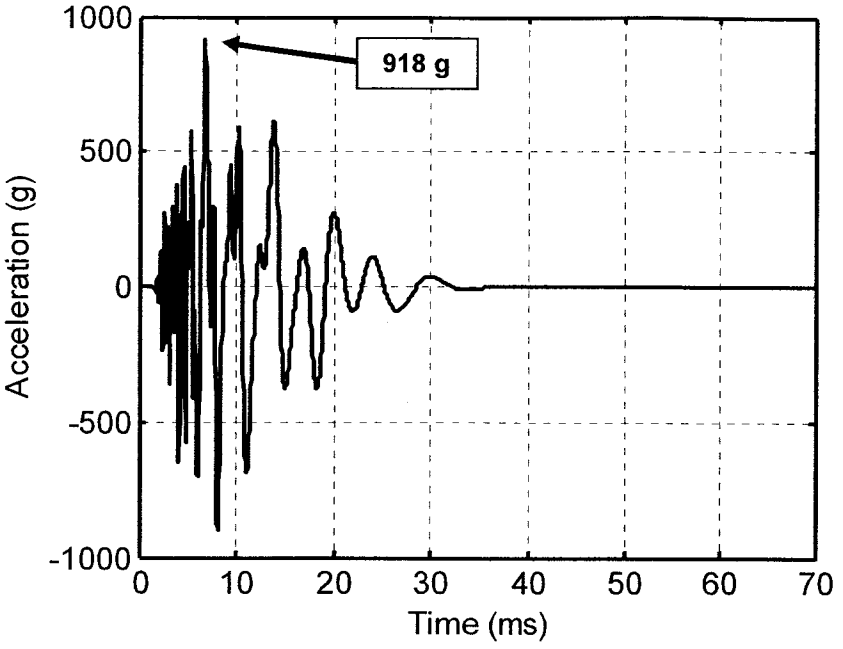

Figure 42: Synthesis acceleration based on the SRS envelope

5.3.3 Test Item Transient Analysis

Now, it is possible to run a modal based transient analysis of the test item mounted on a rigid base. All the analysis parameters are the same as those for the coupled system analysis. The excitation input to the base of the test item is shown in Figure 42. The resulting force at the base of the test item is shown in Figure 43.

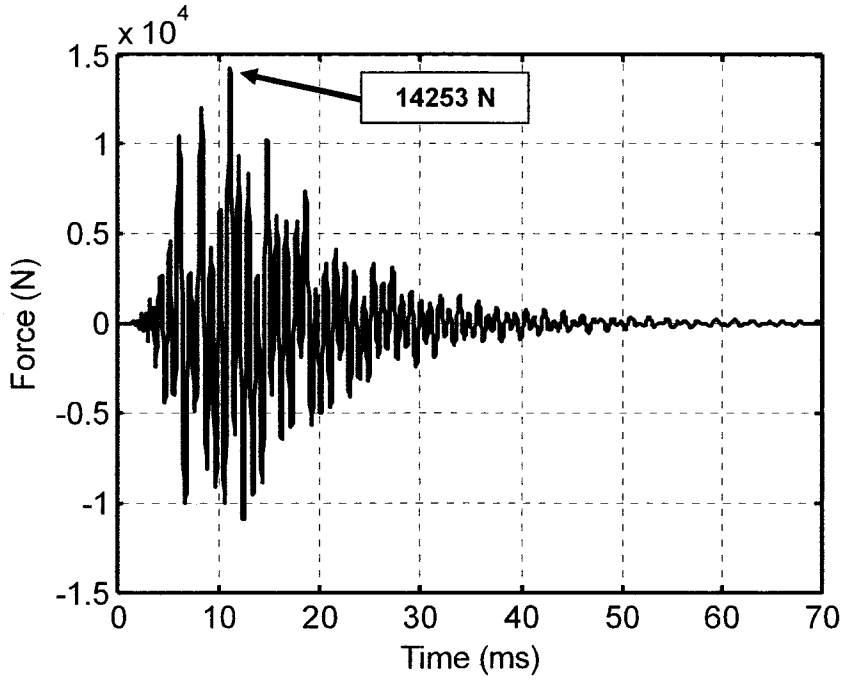

Figure 43: Force at TI interface in rigid configuration using SRS envelope

5.3.4 Investigation of Overtesting

Using the results obtained from the test item transient analysis, it is now possible to investigate the overtesting occurring in shock testing at assembly-level. The first result to compare is the maximal force acting on the test item interface for both mounting configurations. The forces acting at TI interface at the coupled assembly level (flexible) and at the assembly-level (rigid) are shown in Figure 39 and Figure 43 respectively. For the current case, the maximal force ratio in the time-domain is defined as:

$$F_{Max,SRS} = 20\log\left(\left|\frac{F_{\max,rigid}}{F_{\max,flexible}}\right|\right) = 20\log\left(\frac{14253}{4181}\right) = 10.7\ dB \qquad \textbf{Eq. (18)}$$

The compared forces are the result of the contribution of all the modes of the structures and thus are the actual forces acting at the base of the test item. However, they might not properly illustrate the dynamic absorber effect since this interaction occurs close to the TI fundamental frequency. As the overtesting would be more properly quantified in the frequency domain, the power spectral densities (PSD) of the force acting at the TI interface are compared and shown in Figure 44. An exponential decay filter has been used to ensure no spectral leakage is present. Now it is possible to define overtesting considering the same concept in FLV method [43] addressed in the chapter 4. Basically, one should get the force PSD value at the fundamental frequency of the test item for the assembly-level test (rigid). Also, one should get the maximal force PSD value acting at the TI coupled modes in the coupled assembly test (flexible). For the current case where the TI fundamental frequency is 1057 Hz and the maximal occurs at the TI 2nd coupled mode frequency of 790 Hz, one finds the frequency-domain shock overtesting as:

$$N_{SRS} = 10\log\left(\frac{S_{ff,rigid}}{S_{ff,flexible}}\right) = 10\log\left(\frac{8.43e8}{1.26e8}\right) = 8.3\ dB \qquad \textbf{Eq. (19)}$$

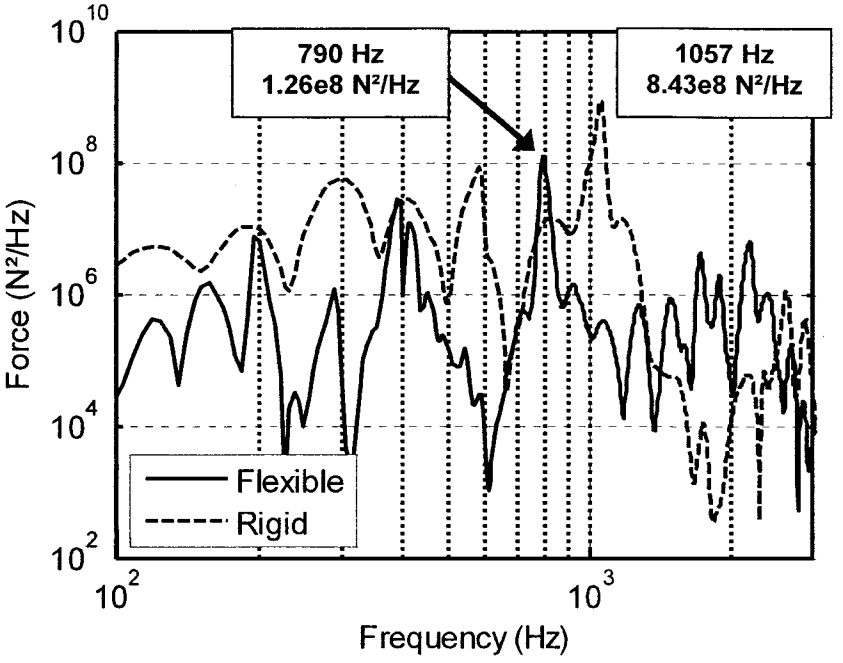

Figure 44: Force PSD at TI interface in coupled system (flexible) and rigid configuration using SRS envelope

5.4 Shock Analysis using the Input Energy Spectrum

This section details the steps to measure the exact overtesting in shock testing using a shock specification in the form of the input energy spectrum (IES). Because the analysis protocols using the SRS and IES are very similar, only the differences between the two are noted in this section. The analysis protocol for IES is also demonstrated for case 3 configuration. The required modifications to the shock synthesis algorithm are also presented.

5.4.1 Coupled Assembly Level Transient Analysis

The same SRS specification from Delta II planner's guide [56] is used at the coupled system level. Since no data is available regarding the IES of the

Delta II shock like for any other launch vehicles, no energy-based synthesis can be done. The coupled assembly level transient simulation is therefore performed with the same excitation shown in Figure 38. In sake of completeness, Figure 45 presents the IES of the synthesis waveform input to the base of the coupled system.

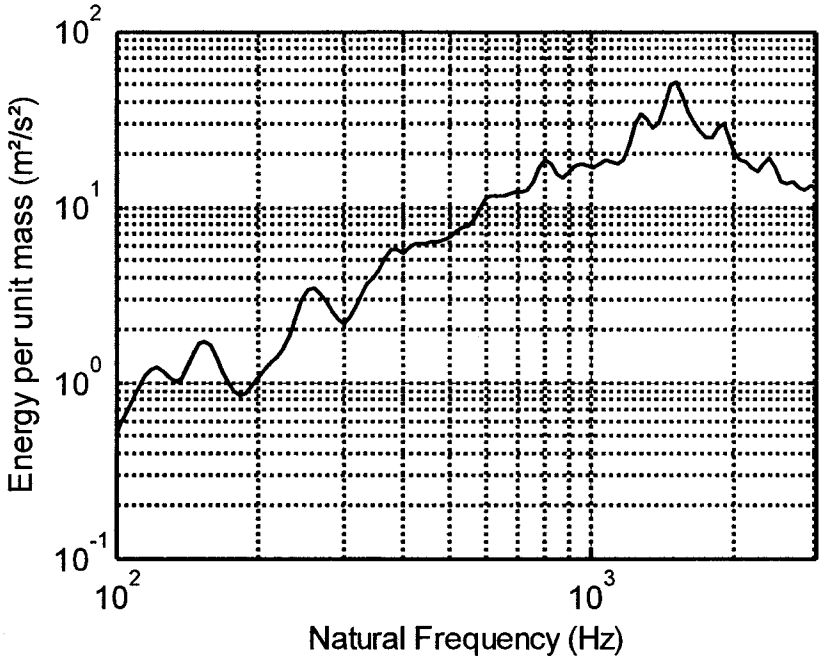

Figure 45: IES of the synthesis acceleration waveform input to the coupled system

5.4.2 Test Item Shock Environment

This section shows the creation of the envelope of the IES at the TI interface of the coupled system and the update to the shock synthesis algorithm.

5.4.2.1 Envelope

The acceleration response at the TI interface of the coupled system simulation is shown in Figure 39. The IES of this acceleration must be enveloped

to create the specification for the assembly-level simulation. Figure 46 presents the maximal TI IES at all the attachment points for each frequency along with its envelope. It is possible to relate each peak with the main modes of the structure.

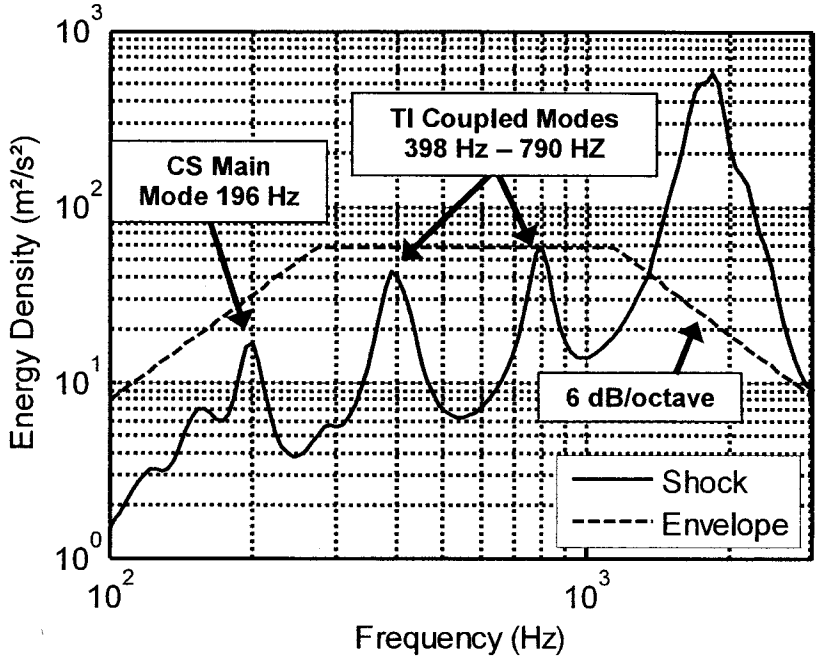

Figure 46: IES at TI interface and its envelope

As for the SRS envelope, it is desirables to envelope the IES using piecewise line approximations. It is important to input the right energy level around the fundamental frequency of the test item to study the dynamic absorber effect. This energy corresponds to the maximal IES level observed at the frequencies of the TI coupled modes. The envelope is constant half an octave around the TI coupled modes. A slope of 6 dB / octave is used at lower and higher frequencies to follow the general trend of the IES.

When it is not possible to identify clearly the IES level due to TI coupled modes, the constant level is taken as the maximal IES value at the frequencies of the TI coupled modes.

5.4.2.2 Shock Waveform Synthesis Algorithm Update

Once the specification for the unit level test is created, it is possible to synthesis an acceleration waveform meeting this specification. For this, a simple update to the shock waveform synthesis algorithm needs to be made. Simply, the waveform amplitude coefficient, *A*, is updated with the IES ratio instead of the SRS ratio according to Eq. 20. Once again, the synthesis IES fits the envelope within 1dB and the 10 percent duration is matched within 5%. The resulting waveform is shown in Figure 47 for the current example.

$$\{A\}_{i+1} = \frac{\{IES_{(Specification)}\}_i}{\{IES_{(Synthesis)}\}_i}\{A\}_i \qquad \{T\}_{i+1} = \frac{T10\%_{(Specficication),i}}{T10\%_{(Synthesis),i}}\{T\}_i \qquad \textbf{Eq. (20)}$$

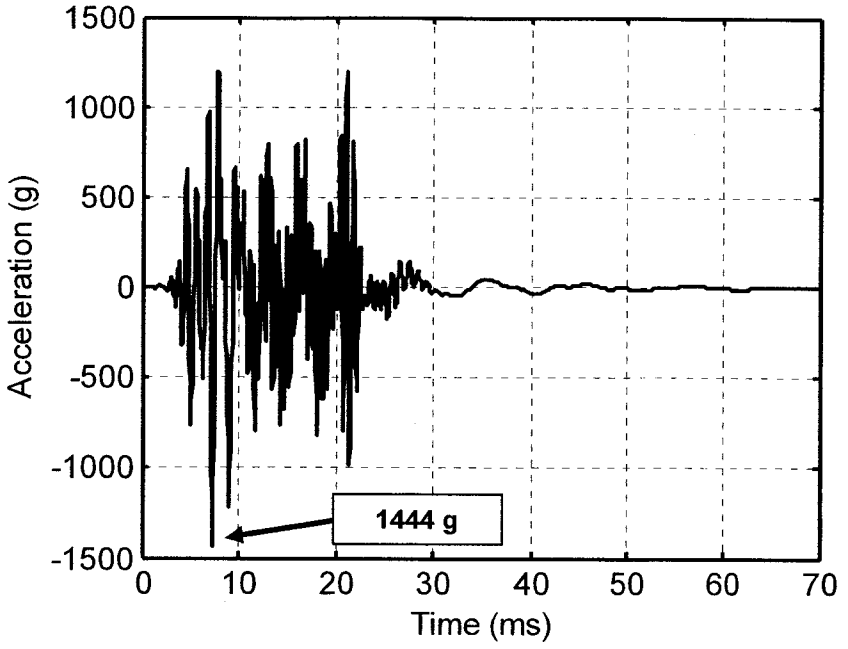

Figure 47: Synthesis acceleration based on the IES envelope

5.4.3 Test Item Transient Analysis

The transient analysis of the test item is performed exactly similarly to the SRS based synthesis. The input acceleration waveform to the base of the test item is shown in Figure 47. The resulting force acting at the base of the test item is shown in Figure 48.

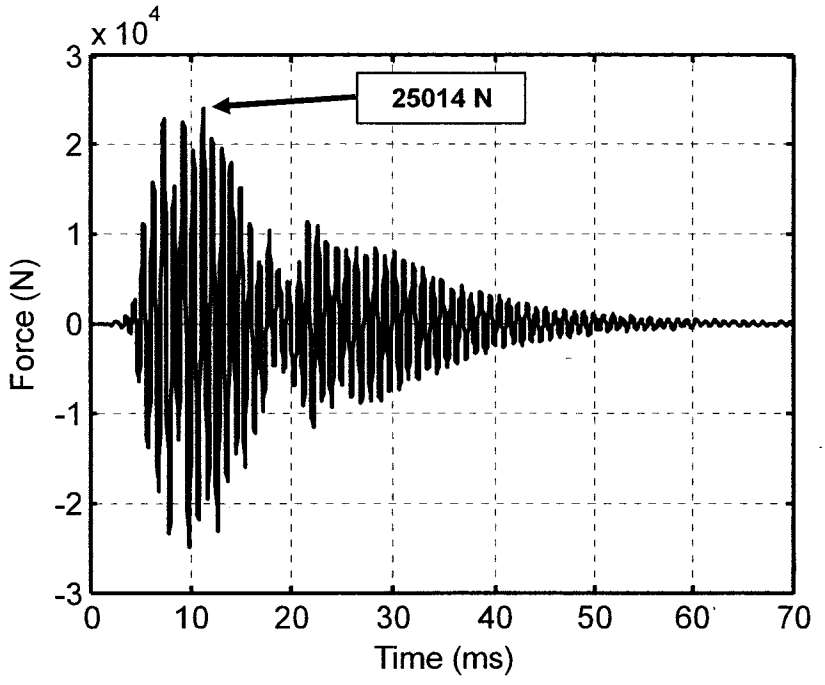

Figure 48: Force at TI interface in rigid configuration using IES envelope

5.4.4 Investigation of Overtesting

It is now possible to investigate the overtesting occurring in shock testing based on energy methods. The overtesting definitions examined are the same as those for the SRS based methods and are explained in details in section 5.3.4. For the current case, the ratio of the maximal time-domain forces is:

$$F_{Max,IES} = 20\log\left(\left|\frac{F_{\max,rigid}}{F_{\max,flexible}}\right|\right) = 20\log\left(\frac{25014}{4181}\right) = 15.5\ dB \qquad \textbf{Eq. (21)}$$

Similarly, the power spectral densities (PSD) of the force acting at the TI interface are compared as shown in Figure 49 and the frequency-domain shock overtesting is computed as:

$$N_{IES} = 10\log\left(\frac{S_{ff,rigid}}{S_{ff,flexible}}\right) = 10\log\left(\frac{6.40e9}{1.25e8}\right) = 17.1\,dB \qquad \textbf{Eq. (22)}$$

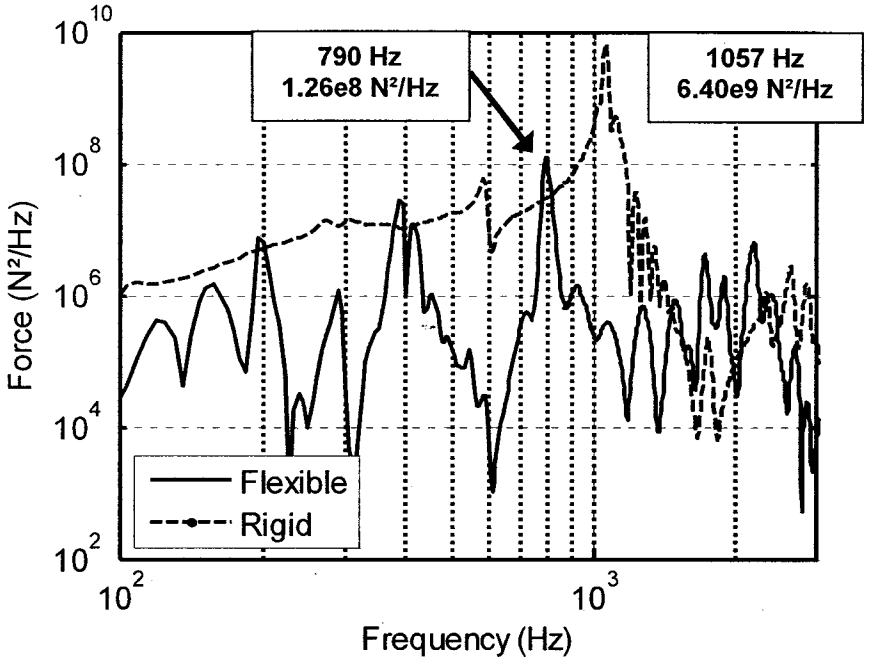

Figure 49: Force PSD at TI interface in coupled system (flexible) and rigid configuration using IES envelope

5.5 Results

The results from the shock overtesting investigation are summarized in the Table 11. This table first shows the shock overtesting defined in the frequency domain (N_{SRS}) and the ratio of the maximal forces ($F_{Max,SRS}$) using the SRS simulations. Computed similarly to the maximal forces ratio, the fourth column, or

$A_{Max,SRS}$, is the ratio of the maximal time-domain accelerations occurring in the rigid and the flexible simulations. The next three columns use the values of the IES simulations to compute the same parameters. The last two columns reproduce data from the vibration overtesting investigation. The cases for which a valid envelope could not be produced are highlighted in grey. It has to be kept in mind that the synthesis algorithm uses a tolerance of 1 dB.

Table 11: Shock overtesting investigation results

Case	SRS			IES			Vibration	
	N_{SRS}	$F_{Max,SRS}$	$A_{Max,SRS}$	N_{IES}	$F_{Max,IES}$	$A_{Max,IES}$	C^2	N_{Vib}
	dB	dB	dB	dB	dB	dB	-	dB
1	4.1	7.5	-3.7	20.4	21.1	7.8	1.3	22.6
2	8.7	1.8	-11.5	21.6	10.9	-4.2	1.6	24.3
3	8.3	10.7	-2.2	17.1	15.5	1.7	1.3	25.1
4	12.9	-8.3	-19.0	17.3	4.0	-12.8	3.2	20.7
5	-0.3	-6.8	-19.1	13.2	6.0	-16.4	1.6	23.9
6	11.3	-7.6	-14.1	15.9	1.2	-13.0	2.4	21.2
7	18.6	7.7	2.3	18.4	8.6	0.8	1.7	22.8
8	12.0	-18.5	-17.3	22.3	-0.9	-6.3	20.3	11.7
9	2.9	-5.8	-3.5	17.3	10.2	6.0	1.4	23.3
10	6.9	-18.4	-28.0	13.7	-7.0	-16.5	1.6	18.6
11	25.4	-1.9	-9.4	21.3	6.0	-10.5	9.3	10.8
12	4.8	-15.1	-19.4	15.4	1.9	-12.9	5.2	10.8
13	25.5	-6.9	-6.3	27.1	2.8	-2.4	0.8	26.4
14	5.3	-7.9	-11.0	14.2	9.8	-0.3	2.7	21.0
15	8.2	-12.3	-18.8	16.0	-0.8	-12.2	17.6	11.0
16	2.4	-8.1	-11.7	17.0	1.9	-7.2	13.4	12.2
17	7.9	1.1	-9.9	14.7	19.0	-5.1	3.5	18.4
18	9.6	4.5	-3.7	17.8	21.1	0.4	2.0	20.9
19	15.3	-2.6	-7.7	18.3	11.4	-5.3	1.4	20.8
20	10.2	-4.7	-14.7	19.0	13.8	-8.5	3.4	18.9

For the cases with a valid envelope, it can be seen that the SRS based overtesting is usually below 10 dB whereas the cases without a correct envelope generally have a larger overtesting. The IES based overtesting is around 15 to 20

dB for most of the cases. One first important observation is that there is no undertesting for any cases. That is, there is no case for which the assembly-level force is less than the coupled system force.

For both the SRS and IES simulations, the ratios of the accelerations, A_{Max}, show that the maximal acceleration at the TI interface is less in the assembly-level simulation than in the coupled system. The observed overtesting is therefore not simply caused by an increased excitation that could have been produced by the shock synthesis algorithm. The maximal time-domain force is lower at the assembly level for the SRS simulations and higher for the IES simulations compared with the coupled system force. Any relation with the overtesting computed in the frequency-domain is therefore not trivial. Considering this, the ratio of the time-domain forces does not appear to be a good indicator of the shock overtesting.

When comparing the vibration overtesting with the SRS overtesting, it can be realized that the SRS overtesting does not exceed the vibration overtesting except for the case 11. Because the SRS does not have a suitable envelope for case 11, the overtesting computed for this case is higher than the actual overtesting. On the other side, the IES overtesting only exceeds the vibration overtesting when the C^2 is relatively large. Otherwise, it is comparable or lower than the vibration overtesting.

5.6 Conclusion

This chapter investigates the overtesting occurring in shock testing at assembly-level. It uses modal based transient simulation with acceleration excitation generated through a synthesis algorithm for shaker testing. The environment at the interface of the test item of the coupled system simulation was enveloped. Later, the forces acting at the base of the test item in both configurations are compared using power spectral densities to create a definition of overtesting similar to that of vibration.

Chapter 6

Shock Overtesting Estimation

6.1 Introduction

This chapter aims to establish relationships leading to the estimation of the shock overtesting. Specially, the relationship between the overtesting evaluated in random vibration testing and shock testing is investigated. Simple linear regressions between independent and dependent variables are studied to highlight these relationships.

The next section justifies the use of a simple linear regression over more sophisticated tools. The third and fourth sections respectively present the independent and the dependent variables employed. The fifth section presents the coefficient of determination found for all combinations of variables.

6.2 Rational

The goal of the linear regression is to show any correlation between independent and dependent variables that would lead to physically sound explanations of the shock overtesting. The goal is not to create a predictive model that perfectly renders the results obtained in the present study, but to facilitate depicting more general trends. Moreover, linear regression with only

one independent variable is used to reduce the number of parameters required to generate one estimate. The simple linear regression model is described as [57]:

$$y_i = b_0 + b_1 x_i + \varepsilon$$
$$\hat{y}_0 = b_0 + b_1 x_0 \qquad \text{Eq. (23)}$$

Where x_i and y_i are a set of values of the independent and dependent variables and ε is the error of the regression. x_0 and $\hat{y}_0$ are an observation and its related predicted value, respectively. Using a least square of the error fit, the parameters b_0 and b_1 are selected to minimise the sum square of the error as:

$$SS_{Error} = \sum_{i=1}^{n} \varepsilon_i^2 = \sum_{i=1}^{n} (y_i - \hat{y}_i)^2 = \sum_{i=1}^{n} (y_i - (b_0 + b_1 x_i))^2$$

$$b_1 = \frac{n\sum_{i=1}^{n} x_i y_i - \sum_{i=1}^{n} x_i \sum_{i=1}^{n} y_i}{n\sum_{i=1}^{n} x_i^2 - \left(\sum_{i=1}^{n} x_i\right)^2} \qquad \text{Eq. (24)}$$
$$b_0 = \bar{y} - b_1 \bar{x}$$

Where $\bar{x}$ and $\bar{y}$ are the mean of the values of the independent and dependent variables, respectively. The coefficient of determination is defined as:

$$R^2 = 1 - \frac{SS_{Error}}{SS_{Total}} = 1 - \frac{\sum_{i=1}^{n} (y_i - \hat{y}_i)^2}{\sum_{i=1}^{n} (y_i - \bar{y})^2} \qquad \text{Eq. (25)}$$

The coefficient of determination helps assessing the goodness of the fit and is the square of the correlation between two variables.

6.3 Independent Variables

The independent or predictive variables are variables allowing to estimate the shock overtesting. These values should be either provided with the shock specification or available after FLV testing.

First, it is desirable to investigate the variables related to the vibration testing such as the vibration overtesting, the C^2 coefficient and the amplification factor, Q. It is also interesting to investigate relationships based on undimensional variables related to shock. For this purpose, the ratio of the shock duration to the fundamental period of the test item ($SRS(f_{TI}) / A_{max}$) and also the ratio of the SRS value at the TI fundamental frequency to the maximal input acceleration (T10%/ TI Period) have been used. Both the shock duration and the maximal acceleration values are taken from the coupled assembly shock and are often provided with the specification. All these variables are presented in the Table 12. The last two columns in Table 12 state if the SRS and IES envelope represents the TI coupled modes correctly as explained in the chapter 5. It should be noted that the regression is performed for the correct cases only. The same independent variables are used to study the IES based shock overtesting. Since there is no equivalent to the SRS to maximal acceleration ratio, this variable is not employed for the IES investigation.

Table 12: Independent variables of the regression

Case	N_{Vib}	C^2	Q	T10% / TI Period	SRS(f_{TI}) / A_{Max}	Valid SRS Envelope	Valid IES Envelope
	dB	-	-	-	-		
1	22.6	1.32	15.5	24.3	1.46	Y	Y
2	24.3	1.60	20.8	22.8	0.63	N	Y
3	25.1	1.33	20.8	23.6	1.62	Y	Y
4	20.7	3.24	19.5	19.2	0.23	N	N
5	23.9	1.56	19.5	20.1	0.23	N	Y
6	21.2	2.38	17.8	19.6	0.49	Y	N
7	22.8	1.66	17.8	18.8	2.25	N	N
8	11.7	20.32	17.2	14.0	0.30	N	Y
9	23.3	1.40	17.2	15.0	1.34	Y	Y
10	18.6	1.61	10.8	9.7	0.09	Y	Y
11	10.8	9.34	10.6	19.3	0.75	N	N
12	10.8	5.24	8.0	13.8	0.19	N	Y
13	26.4	0.78	18.4	13.3	1.09	Y	Y
14	21.0	2.71	18.4	11.6	0.66	Y	Y
15	11.0	17.58	15.0	11.2	0.25	Y	Y
16	12.2	13.40	15.0	12.1	0.28	Y	Y
17	18.4	3.50	15.6	24.5	0.89	Y	Y
18	20.9	2.00	15.6	19.8	1.19	Y	Y
19	20.8	1.38	13.0	47.3	1.27	Y	Y
20	18.9	3.36	16.2	16.7	0.48	Y	Y

6.4 Dependent Variables

The dependent or response variables are variables that need to be predicted. They directly lead to estimate the shock overtesting.

Table 13 provides SRS and IES based dependent variables. The second column in Table 13 is the shock overtesting as calculated in chapter 5. The third column is the difference between the shock overtesting and the vibration overtesting. The fourth column is the ratio of these two values. The same parameters are reproduced in the last 3 columns using the values obtained for the IES based shock investigation. Values for all cases are reproduced although

the regressions are only made when the TI coupled modes are enveloped correctly. Again, the cases where a valid envelope could not be produced are highlighted in grey.

Table 13: Dependent variables of the regression

Case	SRS			IES		
	N_{SRS}	$N_{SRS} - N_{Vib}$	N_{SRS} / N_{Vib}	N_{IES}	$N_{IES} - N_{Vib}$	N_{IES} / N_{Vib}
	dB	dB	-	dB	dB	-
1	4.1	-18.5	0.18	20.4	-2.2	0.90
2	8.7	-15.6	0.36	21.6	-2.7	0.89
3	8.3	-16.9	0.33	17.1	-8.1	0.68
4	12.9	-7.8	0.62	17.3	-3.4	0.83
5	-0.3	-24.2	-0.01	13.2	-10.6	0.55
6	11.3	-10.0	0.53	15.9	-5.3	0.7
7	18.6	-4.1	0.82	18.4	-4.4	0.8
8	12.0	0.4	1.03	22.3	10.7	1.91
9	2.9	-20.3	0.13	17.3	-5.9	0.75
10	6.9	-11.7	0.37	13.7	-4.9	0.74
11	25.4	14.6	2.35	21.3	10.5	2.0
12	4.8	-6.0	0.44	15.4	4.6	1.42
13	25.5	-0.8	0.97	27.1	0.7	1.03
14	5.3	-15.6	0.25	14.2	-6.8	0.68
15	8.2	-2.9	0.74	16.0	4.9	1.45
16	2.4	-9.9	0.19	17.0	4.8	1.39
17	7.9	-10.5	0.43	14.7	-3.7	0.80
18	9.6	-11.3	0.46	17.8	-3.0	0.85
19	15.3	-5.5	0.73	18.3	-2.5	0.88
20	10.2	-8.7	0.54	19.0	0.1	1.00

6.5 Results from Linear Regressions

A simple linear regression investigation is performed using all the possible combinations of independent and dependent variables presented. The data is first linearized back from decibel in order to create the regressions. Only the

cases correctly enveloped are used for the regression. Table 14 provides the coefficient of determination, R^2, for all combinations using the values of the SRS and IES based simulations.

Table 14: Correlation between the independent and the dependent variables

Variables		R^2	
Independent	Dependent	SRS	IES
N_{Vib}	N_{Shock}	**0.46**	**0.51**
	$N_{Shock} - N_{Vib}$	0.10	0.04
	N_{Shock} / N_{Vib}	0.02	0.01
C^2	N_{Shock}	0.04	0.20
	$N_{Shock} - N_{Vib}$	0.07	0.00
	N_{Shock} / N_{Vib}	0.02	0.00
Q	N_{Shock}	0.04	0.05
	$N_{Shock} - N_{Vib}$	0.00	0.02
	N_{Shock} / N_{Vib}	0.03	0.04
T10% / TI Period	N_{Shock}	0.01	0.02
	$N_{Shock} - N_{Vib}$	0.01	0.00
	N_{Shock} / N_{Vib}	0.02	0.02
$SRS(f_{TI}) / A_{Max}$	N_{Shock}	0.03	
	$N_{Shock} - N_{Vib}$	0.00	
	N_{Shock} / N_{Vib}	0.00	

Figure 50 also shows the linear regressions and the 95% confidence bands. It can be seen that the vibration overtesting has a larger dispersion than that of the shock overtesting. Moreover, the shock overtesting of the case 13 is much larger than that for the other cases. Removing this case from the regression decreases the R^2 coefficient at 0.01 and 0.10 for the SRS and IES

based regressions. While doing so, the correlation between any other combinations of variables is not increased considerably. Thus it can be concluded that the correlation between the vibration and the shock overtesting is weak.

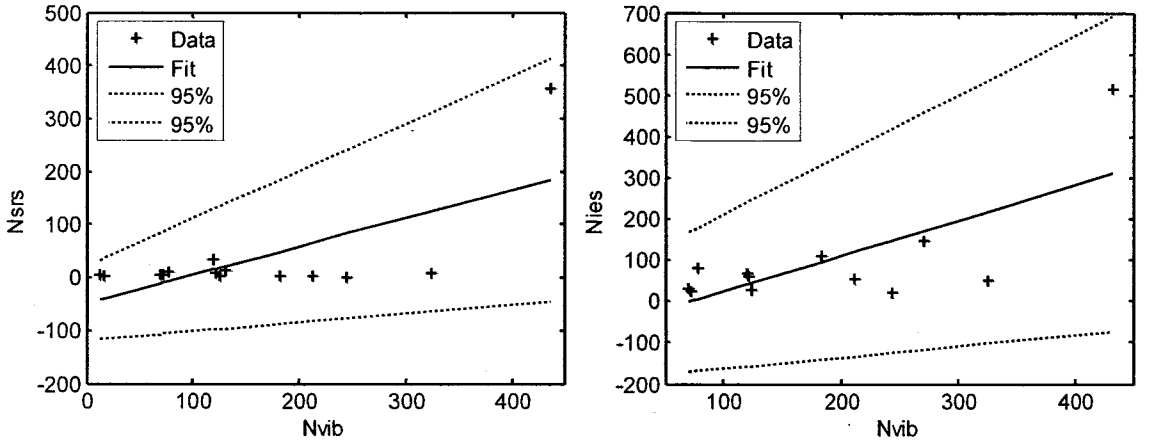

Figure 50: Vibration versus shock overtesting: SRS (left) and IES (right)

6.6 Conclusion

This chapter investigates the relationship between variables allowing to estimate the shock overtesting. Simple linear regression is used for this purpose. No strong correlation is found linking the shock overtesting to the vibration overtesting or any other variable.

Chapter 7

Shock Overtesting Reduction

7.1 Introduction

The objective of this chapter is to provide a mechanism to reduce the shock overtesting in assembly-level test. For this, the results from the previous chapters are used to introduce a notch into the existing shock specification. The notch reduces the force of the assembly-level shock to a level comparable to the coupled system shock. Finally, the shock synthesis algorithm is employed to generate the excitation and to validate the process.

The next section explains the main principles behind the modification of the shock specification with a notch function. The third section demonstrates the creation of a notch function for both the SRS and the IES specification and its application. The fourth section presents the results of the simulations performed using the synthesis waveforms generated for the notched shock specifications. Yet, the shock synthesis algorithm employed is found to have limited capacity to conduct this task.

7.2 Rational

The Force-limited vibration technique adjusts the input acceleration spectrum during a test so that the interface force does not excess the determined

force limit. Due to the nature of shock testing, it is impossible to adjust the test in real time because of practical considerations like the duration of the test. Also, the tests are often conducted with equipment that simply does not allow modifying the test, i.e. impact table. Therefore, it is necessary to pre-modify the input acceleration so that the TI interface force does not excess the force limit.

In FLV testing, Fitzpatrik and McNeill [45] pre-modified the input acceleration spectrum in order not to exceed the force limit. As explained in the literature review, their notching method introduced a groove in the input acceleration spectrum centered around the main frequencies of the test item and having a depth of the estimated overtesting. The introduced notch had a width of 0.2 octave and a slope of 65 dB per octave.

Here, a notch function is proposed to modify the input specification of the assembly-level shock test. In fact, the concept is analog to a bandstop filter used in signal processing. An overview of the method is presented below and its implementation is made for the SRS and IES specifications in the next sections.

1. Estimate the overtesting: For the current study, the evaluated overtesting, presented in Table 11, is employed as the estimate in order to validate the notching method. However, it would clearly be impossible to do so in practice. Thus, the overtesting should be estimated by other means.

2. Generate the notch function: The notch function consists of a groove with the depth of the overtesting centered around the TI fundamental frequency and it should be one everywhere else.
3. Notch the original shock specification: The original specification is derived in section 5.3.2 for the SRS and section 5.4.2 for the IES. It should be adjusted with the notch function to produce the notched shock specification.
4. Test using the notched specification: In this study, the notched specification is used to synthesize an input acceleration.

7.3 Shock Notch Functions

The input level at the fundamental frequency of the TI resulted in a larger than required in-test force and thus, an overtesting. It is thus logical to reduce the in-test force by reducing the input level at the fundamental frequency of the TI. In order to enable using the technique of force-limited vibration in a similar way proposed by Fitzpatrik and McNeill [45], it is desirable to relate the specification to the Fourier amplitude spectrum of the input acceleration. In the following, the procedure to generate the notch function is explained for the SRS and then for the IES together with results for case 3 configuration.

7.3.1 SRS Notch Function

The Random Response Spectrum (RRS) gives the equivalent SRS of a input Fourier amplitude spectrum, $A(\omega)$ and can be compute from the input

Fourier amplitude spectrum, $A(\omega)$, and the transfer function, H_A, relating the ground acceleration to the relative acceleration, as [36]:

$$RRS(\omega_n) = 3\sqrt{\int_0^\infty |H_A|^2 A(\omega) d\omega}$$

$$where\ H_A(\omega;\omega_n,\zeta) = \frac{1+2i\zeta\dfrac{\omega}{\omega_n}}{1-\left(\dfrac{\omega}{\omega_n}\right)^2+2i\zeta\dfrac{\omega}{\omega_n}} \qquad \textbf{Eq. (26)}$$

This relationship is not exact and holds only for certain assumptions, namely, that the maximal SDOF response is 3 times the RMS value of the SDOF response. The Miles formula represents a simplification of this relationship.

The Fourier amplitude spectrum, $A(\omega)$, is tailored to include a notch of the depth of the estimated overtesting around the fundamental frequency of the test item. The Fourier amplitude spectrum is set to one at every other frequencies. The width of the notch is 1/6th of an octave and its slopes have a width of 1/3rd of an octave. The relatively wide notch leads to gentle slopes in the notch function and helps the shock synthesis algorithm converging. Finally, the notch function is normalised to one. The notched Fourier amplitude spectrum and its corresponding SRS notch function can be seen in Figure 51. The depth of the SRS notch function corresponds to the shock overtesting

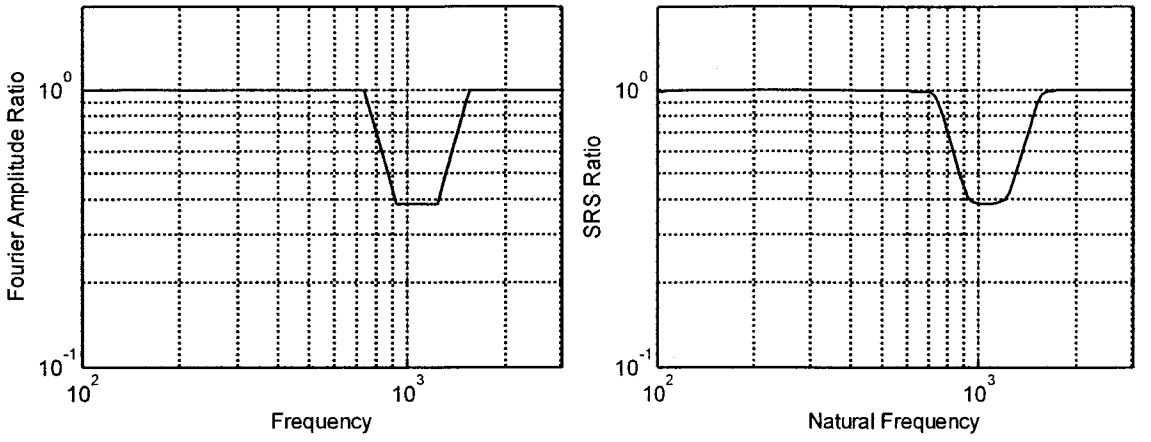

Figure 51: Fourier amplitude ratio (left) and resulting SRS notch function (right)

It is now possible to apply the normalised SRS notch function to the original specification to obtain the notched specification. Figure 52 compares the original and notched specification.

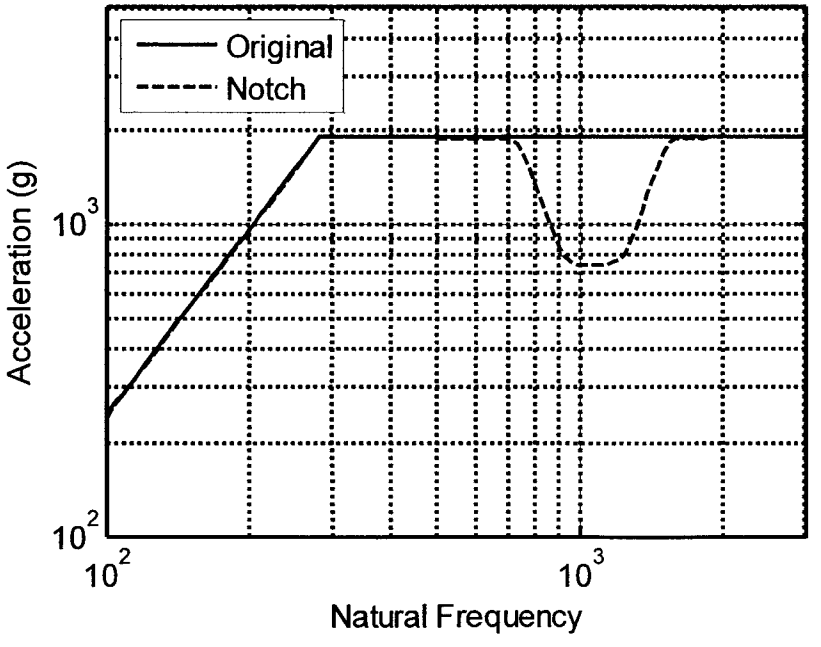

Figure 52: Original and notched SRS specifications

7.3.2 IES Notch Function

Smallwood and Edwards [27] suggested using the input energy spectrum to introduce force limiting techniques in shock testing. Because the IES can be computed from Fourier amplitude spectrum, it readily allows using the methodology developed for force-limited vibration (FLV) [43]. Rewritten for the sake of clarity, Eq.27 relates the Fourier amplitude spectrum to the IES as [30]:

$$E_I(\omega,\zeta) = -\frac{1}{\pi}\int_0^{\infty} |A(\omega)|^2 \,\mathrm{Re}\left[H_V(\omega;\omega_n,\zeta)\right] d\omega$$

$$\text{where } H_V(\omega;\omega_n,\zeta) = -\frac{2\zeta\omega_n\omega^2}{\left(\omega_n^2-\omega^2\right)^2+\left(2\zeta\omega_n\omega^2\right)^2} \qquad \textbf{Eq. (27)}$$

Using the overtesting estimated from the IES simulations, the notched Fourier amplitude spectrum, $A(\omega)$, is obtained similarly to that for the SRS. The notched Fourier amplitude spectrum and its corresponding IES notch function can be seen in Figure 53. The IES notch function is also normalised to one.

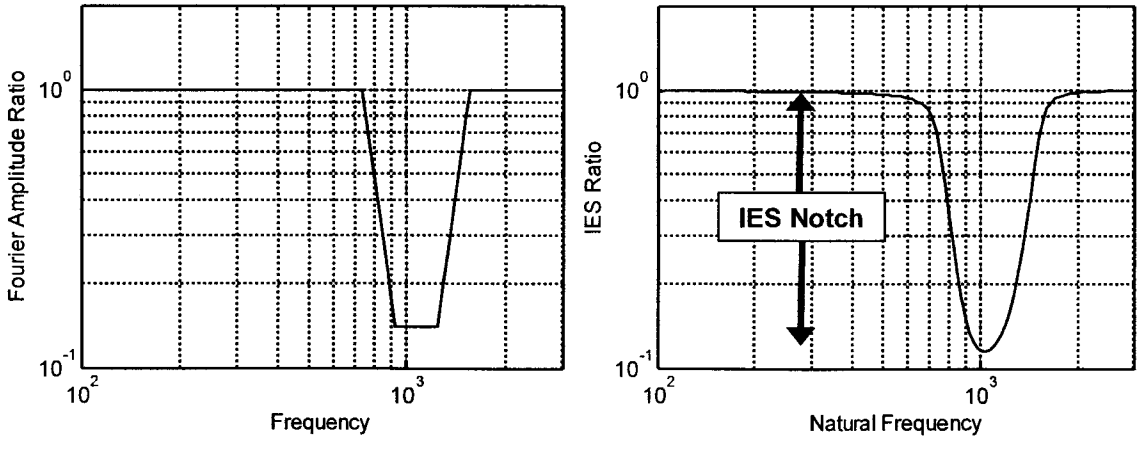

Figure 53: Fourier amplitude spectrum (left) and IES notch function (right)

It is now possible to apply the normalised IES notch function to the original specification to obtain the notched specification. Figure 54 compares the original and notched specification.

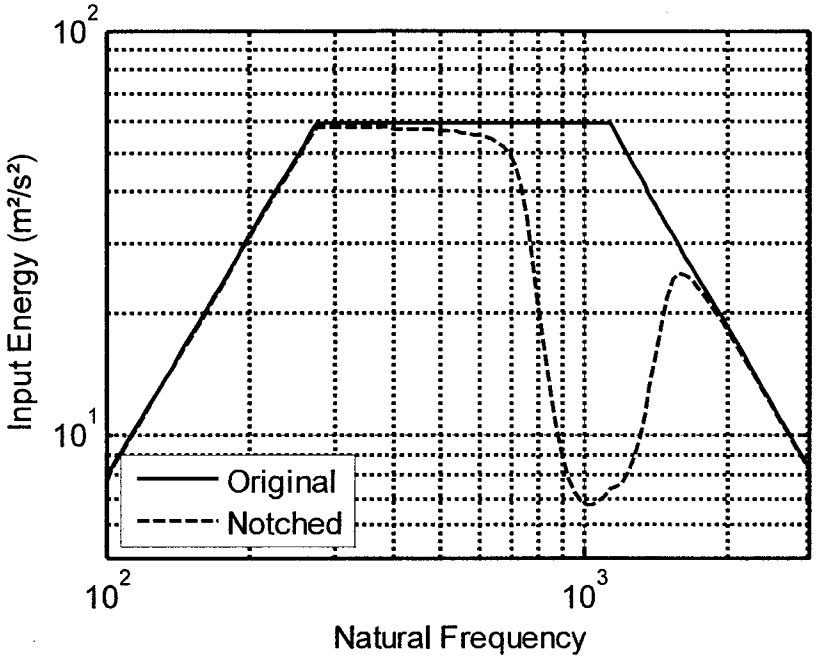

Figure 54: Original and notched IES specifications

7.4 Results

The procedure of the previous section is repeated for all cases. The SRS and IES notched specifications are shown in Figure 52 and Figure 54 for the example case 3. Having the SRS and IES notched specifications, synthesis acceleration waveforms are then generated using the algorithm described in Chapter 5. Based on these simulations, the environment at the interface of the TI is studied as discussed in the chapter 5.

7.4.1 Simulations for notched SRS

For most cases, the synthesis algorithm is not able to properly generate one excitation waveform to perform the simulations using the notched SRS specifications. This is mainly due to the existence of deep notch (12 dB or more) in some case configurations such as case 13 shown in Figure 55. For these cases the shock synthesis algorithm could not converge to a waveform that meet the specification within an acceptable tolerance.

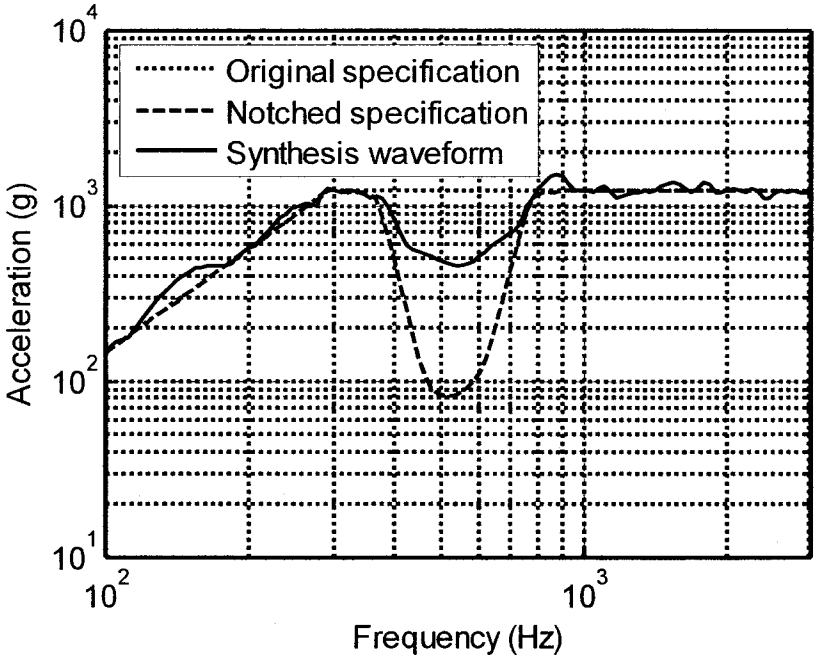

Figure 55: Original and notched specification and synthesis waveform of case 13

For the other cases, the synthesis algorithm could generate a waveform meeting the specification within the 1 dB tolerance. To accomplish this, many more iterations than usual were performed in which the amplitudes of the simple waveforms around the TI fundamental frequency were constantly decreased. As

shown in Figure 56 for case 3, the acceleration PSD around the notch frequencies is greatly reduced compared to the original waveform. Also, the force at the TI fundamental frequency of the notched simulation is many orders of magnitude lower than that of the original simulation. In fact, undertesting as high as 20 dB may be induced. This problem illustrates one drawback of the SRS and the limitations of the current shock synthesis algorithm, which is misadapted for generating waveforms matching notched specifications.

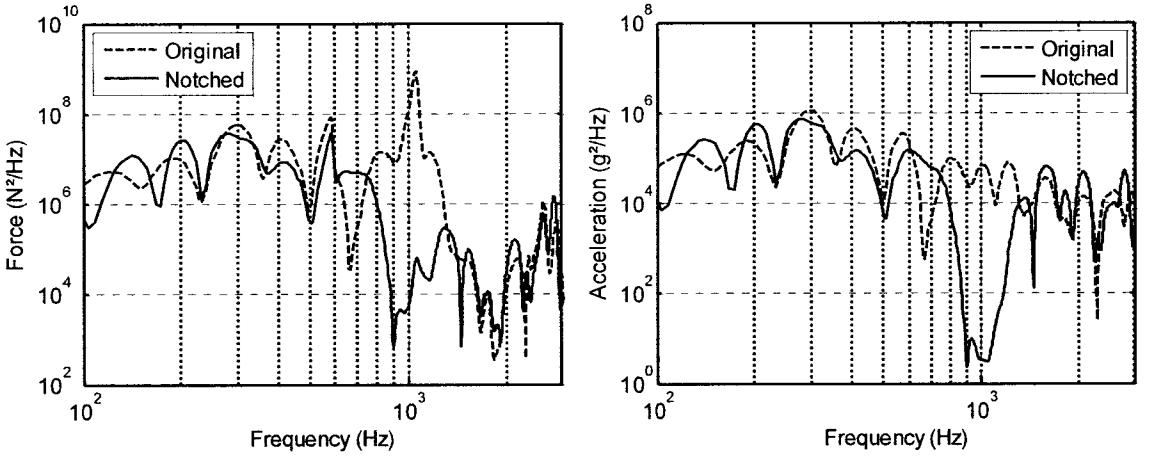

Figure 56: Force (left) and acceleration (right) PSD at TI interface for notched SRS simulations of case 3

Nonetheless, satisfactory waveforms could be generated for the cases 1, 2 and 9. Table 15 summarizes the results obtained for these cases using the notched SRS specifications. The second and third columns of the table show the overtesting for the original assembly-level (rigid) specification discussed in chapter 5 and the notched specification of the current chapter. The next three columns show the reduction of overtesting, maximal force ratio and maximal

acceleration ratio compared with the original assembly-level simulations. As it can be realized the notch introduced in the SRS specification effectively reduced the overtesting and brings back the force of the assembly-level simulations to the coupled system simulations.

Table 15: Reduction of the shock overtesting using the SRS

Case	Overtesting		Reduction		
	Original	Notched	N_{SRS}	$F_{Max,SRS}$	$A_{Max,SRS}$
	dB	dB	dB	dB	dB
1	4.1	-0.9	5.0	1.5	-3.2
2	8.7	-0.1	8.8	4.8	-11.5
9	2.9	0.5	2.5	-3.5	-4.6

7.4.2 Simulations for notched IES

Figure 57 compares the force PSDs at the interface of the test item resulting from the original assembly-level (rigid) IES specification presented in Chapter 5 and the notched specification of the current chapter for case 3. It is possible to see that the notch greatly reduced the amount of overtesting occurring at the TI fundamental frequency. Also, the effect of the notch is limited to the frequencies for which the notch is introduced; the force level outside the notch is unmodified. For example, the force level associated with the flextural mode of the TI cover at 585 Hz is unmodified.

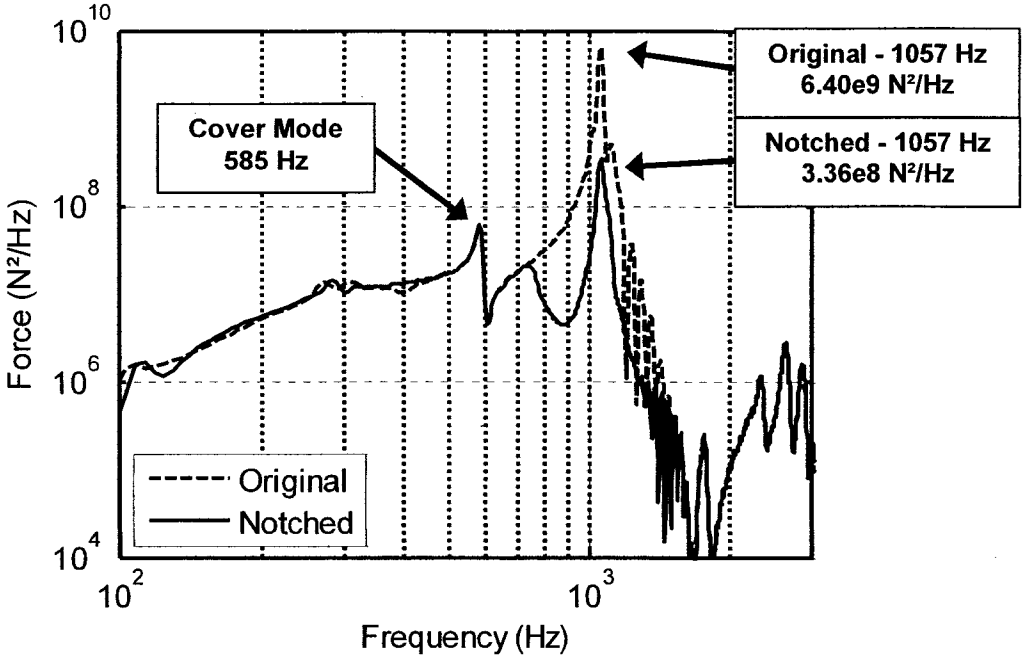

Figure 57: Force PSD at TI interface for the original and notched IES simulations

Table 16 summarizes the results obtained from the simulations using the notched IES specifications. The second and third columns of the table show the overtesting from the original assembly-level (rigid) specification addressed in chapter 5 and from the notched specification of the current chapter. The fourth column measures the depth of the IES notch function shown in Figure 53 (right). The last three columns show the reduction of overtesting, maximal force and maximal acceleration compared with the original assembly-level simulations

As it can be seen, the overtesting is greatly reduced. The reduction of overtesting is around 10 to 14 dB for most of the cases. Also, the IES notch is fairly constant around 9-10 dB, independently of the notch introduced in the Fourier amplitude spectrum. More investigations showed that the IES notch is

limited to a certain value for a given width. However, the width required to introduce a notch of 20 dB would decrease the level over most of the frequency range of the specification, i.e. from 500 to 2500 Hz, which is undesirable.

Finally, the results show that the maximal force has been reduced, which is an advantage for testing on shaker. One interesting features of the shock overtesting reduction method using the IES is that the overtesting reduction is very constant and predictable. This is a vital characteristic of any technique used to qualify space equipment.

Table 16: Reduction of shock overtesting using the IES

Case	Overtesting		IES Notch	Reduction		
	Original	Notched		N_{IES}	$F_{Max,IES}$	$A_{Max,IES}$
	dB	dB	dB	dB	dB	dB
1	20.4	7.8	9.9	12.5	13.4	5.3
2	21.6	8.5	10.0	13.1	9.0	-1.5
3	17.1	4.3	9.4	12.8	9.2	1.1
4	17.3	3.8	9.4	13.5	6.1	-5.4
5	13.2	2.9	8.4	10.4	6.2	-7.6
6	15.9	3.0	9.1	12.9	4.9	-5.6
7	18.4	3.9	9.6	14.4	7.7	0.0
8	22.3	8.2	10.1	14.1	3.9	-3.0
9	17.3	4.6	9.4	12.8	8.5	1.8
10	13.7	3.2	8.5	10.5	-1.3	-8.2
11	21.3	7.1	10.0	14.2	5.0	-5.3
12	15.4	3.4	9.0	12.0	5.0	-6.0
13	27.1	10.6	10.3	16.5	5.9	-1.3
14	14.2	1.2	8.7	12.9	9.5	-0.2
15	16.0	3.2	9.2	12.7	1.1	-5.7
16	17.0	2.9	9.4	14.2	3.1	-2.7
17	14.7	4.1	8.9	10.7	13.7	-1.8
18	17.8	4.8	9.5	13.1	15.6	1.0
19	18.3	5.9	9.6	12.4	10.1	-3.3
20	19.0	6.2	9.7	12.8	11.5	-5.1

7.5 Conclusions

This chapter establishes a strategy to reduce the overtesting occurring in assembly-level shock testing. It introduces a notch into the original specification which is computed using a relationship between the Fourier amplitude spectrum and the shock indicator, i.e. SRS or IES.

Limitations of the shock synthesis algorithm have prevented to perform all the simulations correctly using the SRS specifications. First, the algorithm could not generate waveforms matching the specification when the overtesting is large. Second, because the specification is hard to match, the amplitude of the simple waveforms around the notch frequencies could be excessively reduced, leading to an important undertesting. Inspecting the acceleration PSD can help evaluating this problem. Simulations were performed for 3 case for which the overtesting was reduced successfully.

The shock overtesting produced with the IES specification could be reduced by 10-14 dB, which is significant. The technique implemented does not remove all the overtesting because the depth of the notch is limited by the width of the notch of the Fourier amplitude spectrum. However, the technique provides consistent results for all the cases.

Chapter 8

Experimental Validation

8.1 Introduction

This chapter presents the experimental validation of the investigation performed in the previous chapters. First, the experiment is used as a tool to correlate the FE model developed in chapter 3. Then, it will be used to validate the results of the vibration and shock overtesting occurring in assembly-level testing.

The next section of this chapter present the setup established during the experiments. The third and the fourth sections provide the measurement of the vibration and shock overtesting as discussed in chapters 4 and 5, respectively.

8.2 Experimental Setup

The tests are performed in the facility of the David Florida Laboratory (DFL) of the Canadian Space Agency (CSA), Ottawa, Ontario. Specifically, this facility includes a 89 kN (40 klbf.) electrodynamics shaker which was used to perform all the experiments. The setup used to test the test item and the coupled system can be seen in Figure 58 and Figure 59. Figure 58 shows the test item mounted on the fixture through the force sensors and bolts. The fixture itself is bolted to the electrodynamics shaker head at all available locations. The shaker

is controlled using a feedback loop through an accelerometer mounted on the fixture next to the test item to reduce effects of the fixture flexibility on the input spectrum. More accelerometers are mounted on the TI cover and on the board. All the accelerometers are glued. It has not been required to add any compensation factor to the output of the force sensor since they accurately reflected the mass of the structures.

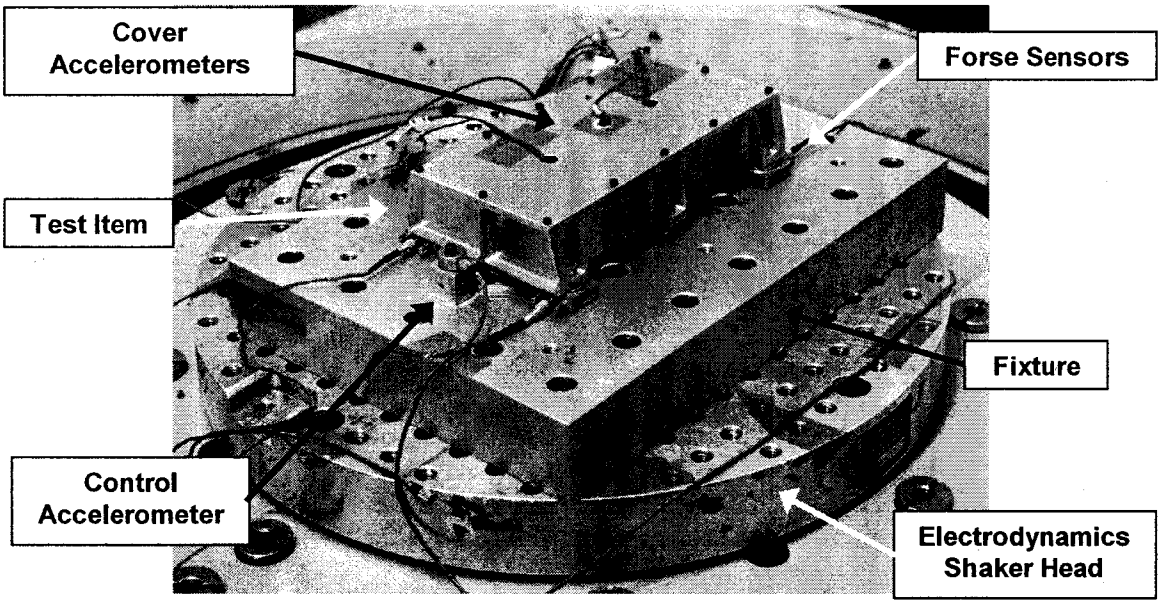

Figure 58: Experimental setup of the test item

Figure 59 shows the test item installed on the mounting structure in the coupled system configuration. The mounting structure is bolted to the fixture. The force sensors are installed between the test item and the mounting structure. Accelerometers are installed next to the TI attachment points to measurement the response at the TI interface. More accelerometers are mounted on the mounting structure top and mid panels.

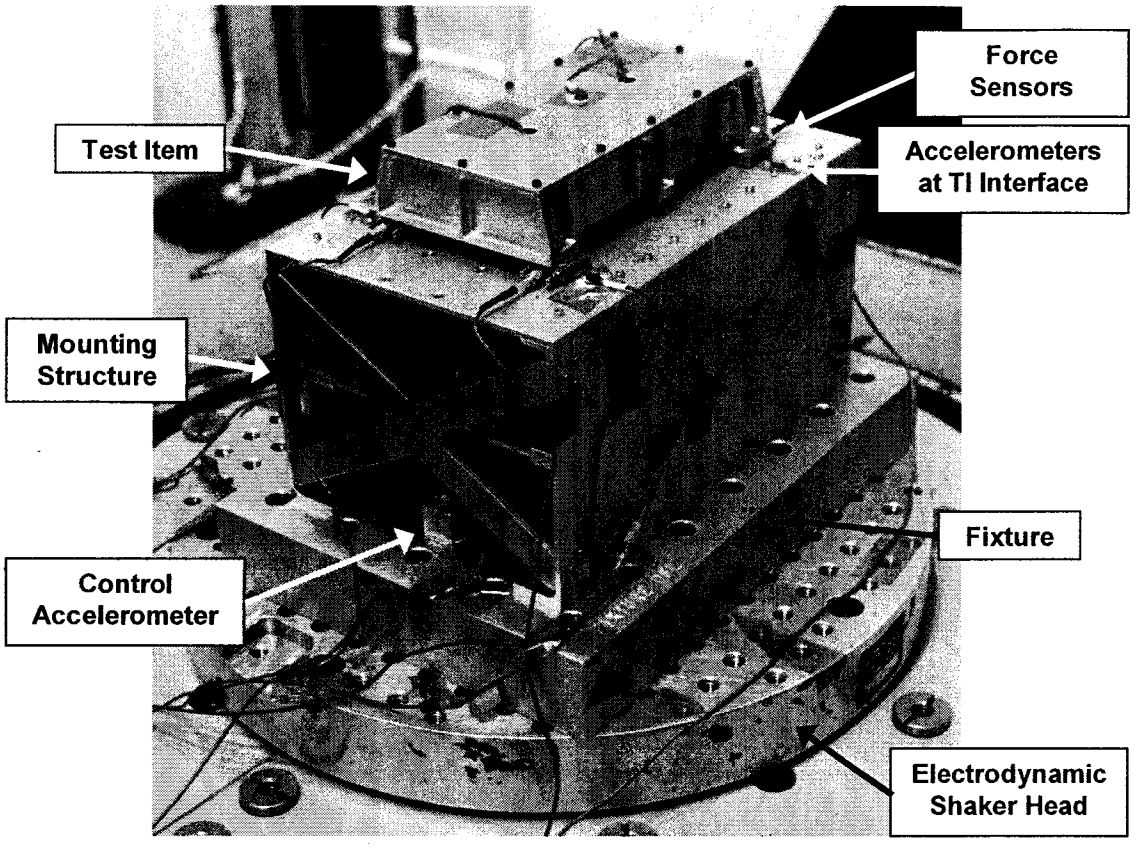

Figure 59: Experimental setup of the coupled system

In order to test the structure on the shaker head, it was necessary to design a fixture which interfaces the shaker head with the mounting or the test item. The fixture is an aluminium block 50 mm thick and is best seen in Figure 58. The appropriate bolts patterns, i.e. shaker head, mounting structure and test item attachment points, are added to the fixture. The rigidity of the fixture is investigated through a sine-survey up to 2000 Hz. This test did not revealed any appreciable deformation of the fixture within the frequency range of interest. The fixture is considered rigid enough to prevent any dynamic interactions with the test articles.

8.3 Random Vibration Testing

Using the setup shown in the previous section, the value of the C^2 coefficient and the vibration overtesting is investigated experimentally. A complete walkthrough of the investigation is performed in chapter 4 using results from FE analysis. The comparison of the apparent mass, the TI interface acceleration and force PSD obtained by the experiment and the FE analysis for the case 3 can be found in Figure 22, Figure 23 and

Figure 60, respectively.

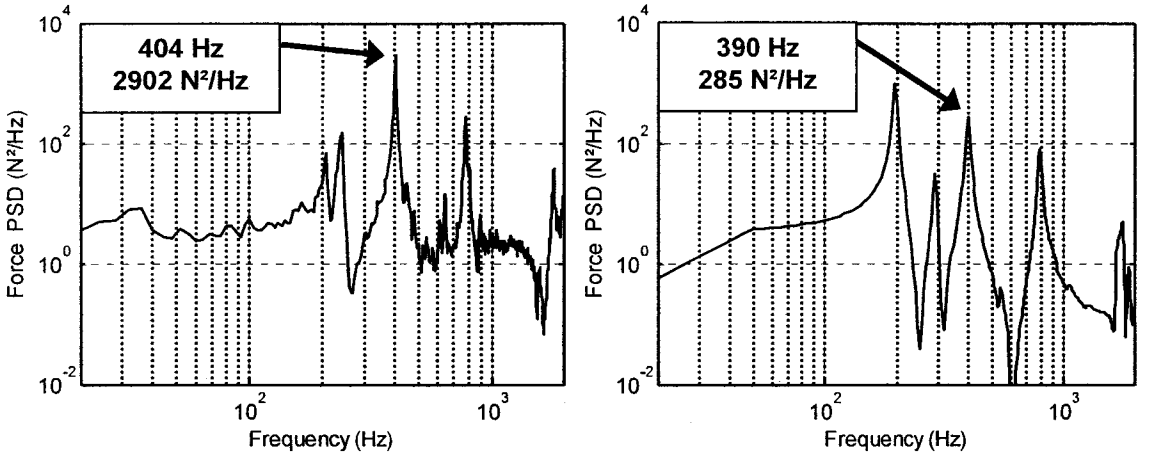

Figure 60: Force PSD at TI interface in coupled system with vibration excitation: Experiment (left) vs Simulation (right)

Table 17 compares the results from experiment and FE analysis for vibration. As it can be seen, the vibration overtesting and particularly the C^2 coefficient observed experimentally are always larger than those evaluated by FE analysis. However, the objective of this study is to evaluate the overtesting

occurring in assembly-level testing. This section shows that the vibration overtesting is reasonably well predicted using the FE models. Yet, these models would need more refinements in order to correctly predict the C^2 coefficient. The differences between the analysis and the experiment are due to an underestimation in the analysis of the impedance, or the force to acceleration ratio, of the coupled system interface. It has been verified that the differences are not due to a mismatch in damping or in the frequency resolution used to extract the data.

Table 17: Results from experiment and FE analysis for vibration

Parameters	Unit	1		2		3	
		Test	FE	Test	FE	Test	FE
Frequency	Hz	380	378	528	555	404	398
Force PSD	N^2/Hz	5564	1357	216	7.44	2902	285
Frequency	Hz	380	378	528	630	404	398
Acceleration PSD	g^2/Hz	20.49	12.37	0.87	0.11	18.63	4.89
Frequency	Hz	964	1008	1008	1057	1008	1057
Physical Mass	kg	0.904	0.923	0.650	0.673	0.650	0.673
Apparent Mass	kg	43.43	14.34	31	14.01	31	14.01
C^2	-	3.5	1.3	6.1	1.6	3.8	1.3
N_{Vib}	dB	28.2	22.6	25.7	24.3	27.7	25.1

As shown in

Figure 60, the force level of the 2nd TI coupled are less underestimated by the analysis: the force obtained experimentally is 278 N^2/Hz while that of the simulation is 80 N^2/Hz for case 3. Also, the range of C^2 values measured experimentally is more in-line than the simulation with the usual range of 2 to 5 reported in the literature.

8.4 Shock Testing

This section investigates the shock overtesting using the SRS specification. The first part presents the results from the coupled system tests while the second part present the results from the assembly-level tests using the SRS specification. No assembly-level tests using the IES specification are performed because DFL equipment does not support this indicator.

8.4.1 Coupled System Tests

The test structures are setup in the coupled system configuration and excited with the synthesis waveform shown in Figure 38. However, the input is scaled down by 18dB in order to ensure that the force sensors stay fully compressed while not exceeding the force limits of the threads linking the test item to the fixture in the assembly-level tests. Figure 61 presents the SRS at TI interface for the coupled system of case 3 obtained from the experiment and the simulation. The simulation predicts with reasonable accuracy the overall shape of the SRS at the TI interface. Especially, the level corresponding with the TI coupled modes are well predicted. As for the random vibration test, the 1st TI coupled mode is slightly more underestimated than the 2nd TI coupled mode.

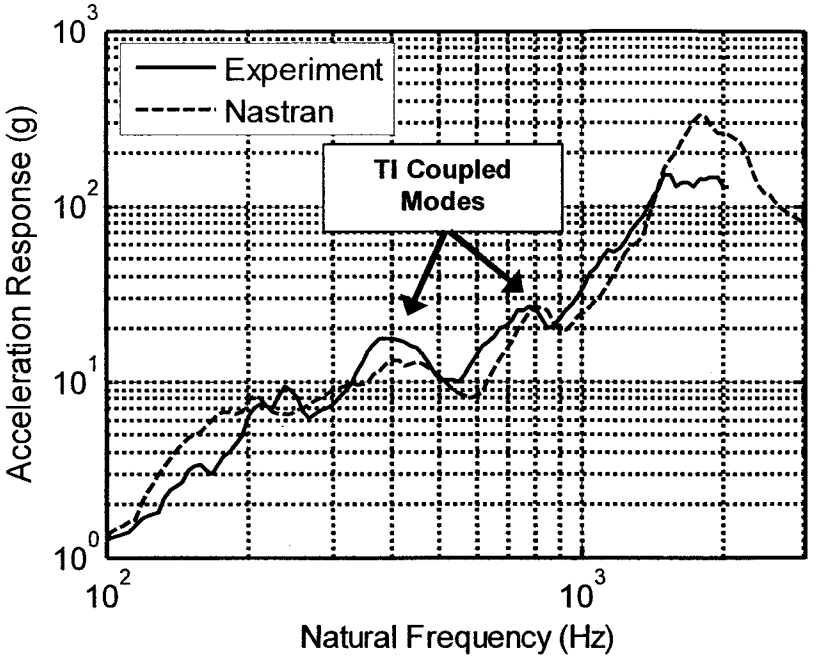

Figure 61: SRS at TI interface in coupled system

The experimental sampling frequency only allowed the SRS to be computed up to 1000 Hz with the required 8 samples per cycle. However, the SRS calculation is extended up to 2000 Hz, where it is computed with only 4 samples per cycle. Thus SRS experimental results well above 1000 Hz are for visual interpretation only. The calculation of PSD is not affected and stays valid up to 2000 Hz.

Figure 62 compares the maximal IES at the TI interface of the coupled system obtained experimentally and by simulation for case 3. The differences between the simulation and the experiment are larger than for the SRS, especially for the 1st TI coupled mode. This is just presented for the sake of comparison although no synthesis for the IES environment is performed.

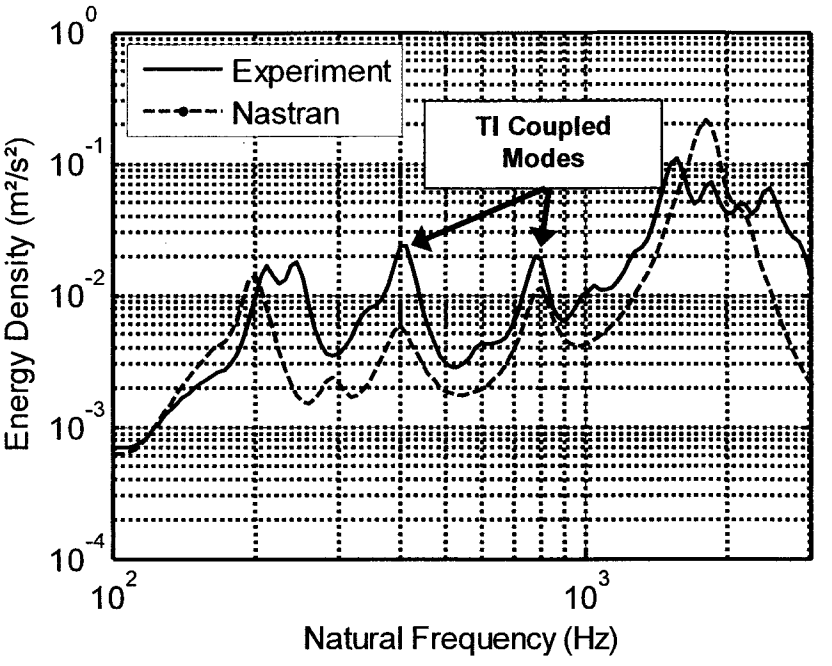

Figure 62: IES at TI interface in coupled system

Figure 63 compares the force PSDs at the TI interface of the coupled system obtained from the experiment and the simulation. The force acting at the 2nd TI coupled mode, which is the maximal and is taken as the reference, is reasonably well predicted. However, the simulation underestimates much the force acting at the 1st TI coupled mode. It is also possible to observe the anti-resonance corresponding to the TI fundamental mode.

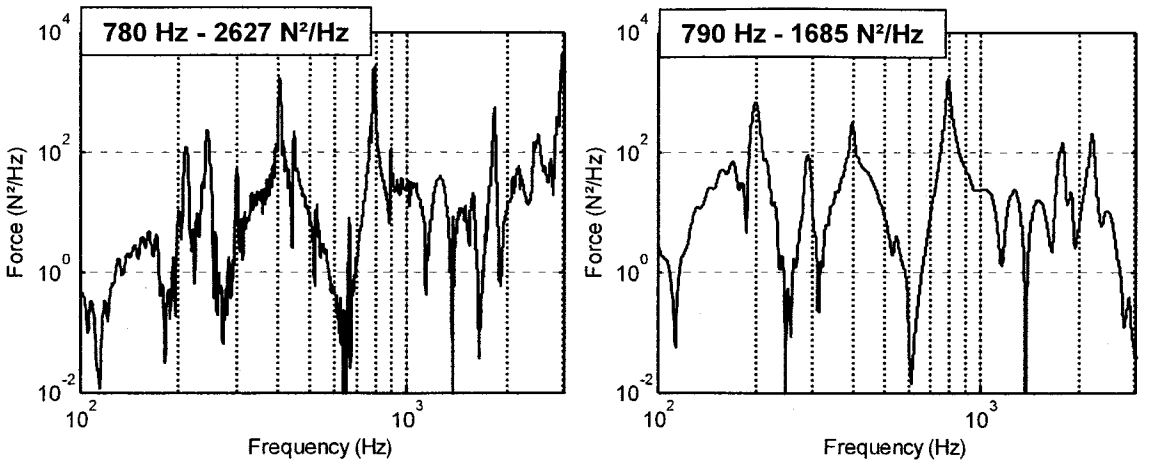

Figure 63: Force PSD at TI interface for coupled system with shock excitation: Experiment (left) vs Simulation (right)

8.4.2 Assembly-Level Tests

It is now possible to envelope the observed environment at the TI interface of the coupled system to create the assembly-level test specification. The envelopes can be seen in Figure 64.

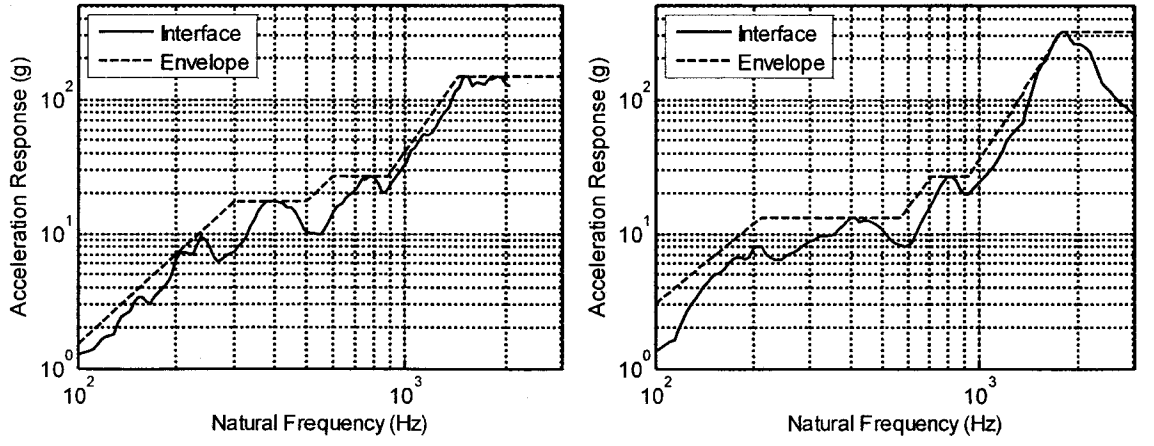

Figure 64: TI interface SRS and envelope for experiment (left) and simulation (right)

This time, the SRS is enveloped to match the environment at all frequencies in contrast to the envelope used in chapter 5 which matched the SRS level of the TI coupled modes. Basically, the experiment envelope is more representative of actual test envelope and produces a more realistic evaluation of the shock overtesting. The envelope of chapter 5 produces an evaluation of the shock overtesting closely related with the lack of absorber effect and compares better with the vibration overtesting.

The envelopes are used to create the synthesis accelerations for the assembly-level tests which are shown in Figure 65. First, an acceleration waveform is synthesised using the method described in Chapter 5. In addition, another waveform synthesis is performed using regular practices employed by DFL software. This allows primarily to verify the results for a variety of synthesis algorithms. Also, it ensures that the procedure is applicable using standard test laboratory equipment. This synthesis is labelled "DFL" while the synthesis using the method employed in this study is called "Current". The prime difference between both syntheses is the duration: the 10% duration of the laboratory synthesis shock is around 5 ms and it uses 6 simple waveforms per octave. In comparison, the current study uses 24 simple waveforms per octave.

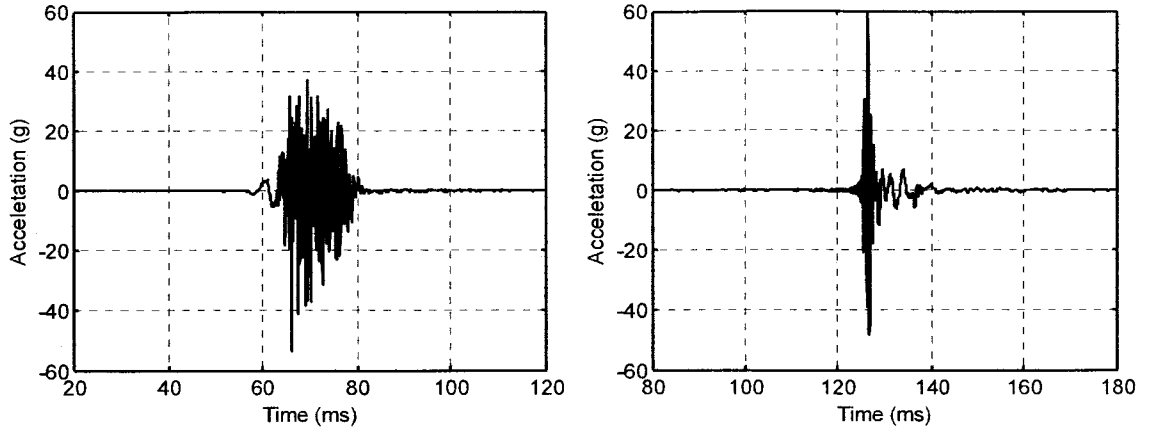

Figure 65: SRS based synthesis acceleration: Current (left) and DFL (right)

Figure 66 compares the force PSDs obtained for the assembly-level tests using both syntheses. These force PSDs can be compared with the coupled system force PSD of the Figure 63 to compute the shock overtesting.

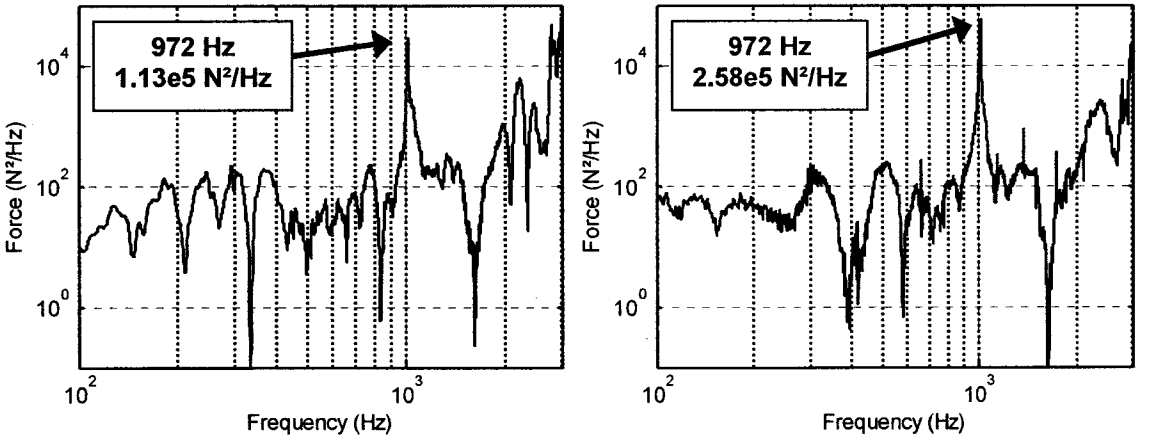

Figure 66: Force PSD at TI base in assembly-level tests: Current (left) and DFL (right)

Table 18 summarises the results from the shock overtesting experiment. As it can be realized the FE simulation successfully predicts the shock overtesting. For cases 2 and 3, the simulation results are between the values

obtained for both experimental syntheses. Considerable differences between the overtesting computed for the Current and the DFL syntheses exist, although they match the same SRS. However, the SRS is computed using a standard amplification of 10 although the structures have a higher amplification. For a structure having an amplification higher than 10, a longer excitation can lead to a higher response even though the SRS (Q=10) are equivalent [36]. In its turn, a higher response leads to a larger force at the assembly-level. This interpretation is coherent with the results for the force ratio and for the shock overtesting for cases 1 and 2, but not 3. Finally, the small number of cases studied refrains from making further conclusion regarding the effect of the duration on the shock overtesting.

Table 18: Summary of the SRS shock overtesting experiment

Case	Synthesis	N_{SRS}	$F_{Max,SRS}$	$A_{Max,SRS}$
		dB	dB	dB
1	DLF	12.3	6.6	2.2
	Current	15.9	7.9	0.5
	Simulation	11.2	5.9	5.1
2	DLF	18.2	9.4	1.4
	Current	27.4	14.6	4.3
	Simulation	22.7	6.8	6.4
3	DLF	13.5	7.3	1.9
	Current	10.1	11.7	-0.2
	Simulation	13.6	5.7	6.0

Additionally, the results show that the shock overtesting can be significantly modified by the envelope used. Using the envelope of the chapter 5 which were set at the acceleration level of the TI coupled mode, the overtestings

were calculated at 4.4, 8.7 and 8.3 dB for cases 1, 2 and 3, respectively. The overtesting found using the experiment's envelopes, which are closer to the actual envelopes used for qualification of hardwares, is significantly more. The larger overtestings can be attributed to the larger SRS values occurring at the fundamental frequencies of the TI.

8.5 Conclusion

This chapter presents the experiments conducted to confirm the FE simulation. It performs measurements for the structure in both coupled system and assembly-level configurations for the cases 1 to 3. First, the C^2 coefficient and the overtesting found in vibration testing at assembly-level are measured. The values predicted by the FE simulation underestimated mostly C^2 coefficient. Then, the overtesting occurring in assembly-level shock testing using the SRS specification is measured. It is shown that different excitations can lead to different overtestings even though the excitations correspond to the same SRS. Having in mind that dispersion, the FE simulations predict reasonably well the shock overtesting.

Chapter 9

Summary, Conclusions and Recommendations

9.1 Summary

In the past, several failures were observed and attributed to pyrotechnics induced shocks in space missions. Today, qualifying equipment against pyroshock environment is now regarded as critical for mission success. Assembly-level structures are usually tested using mechanical devices generating an acceleration input meeting a shock response spectrum (SRS) specification. However, assembly-level tests are suspected to be the cause of several failures that would not have happened in flight. A similar problematic has been encountered while qualifying hardware for vibration environment. Furthermore, the overtesting in vibration testing was shown to be caused by the absence of dynamics absorber effect in the test configuration. In other words, the near infinite impedance of the test apparatus induces a higher force than the flexible flight structure. The Force-Limited Vibration technique has been developed by JPL in order to reduce the overtesting. Although no precise measurements of the shock overtesting can be found in the literature, a similar dynamics is suggested to be occurring in assembly-level shock testing.

The first objective of this thesis is to confirm the presence of the shock overtesting caused by the lack of dynamics absorber effect. For this, a test item

and a mounting structure have been carefully designed to be representative of space hardware and to allow modifying their principal dynamics characteristics easily. Using dedicated finite element models, modal-based transient simulations have been performed on the structure in flight-like and test configuration. A shock synthesis algorithm was implemented which allows generating acceleration waveforms corresponding to a shock specification. Using this tool, it has been possible to compare the forces occurring at the interface for the test item of the flight-like and the test configurations. Finally, the shock overtesting has been evaluated while enveloping the shock response spectrum (SRS) or the input energy spectrum (IES) environment occurring in the flight-like configuration.

The second objective of this thesis is to attempt to discover any relationship with the overtesting occurring in vibration testing. Hence, the overtesting occurring in assembly-level random vibration testing has been evaluated along with the C^2 coefficient of the semi-empirical. Simple linear regressions were carried to highlight any correlations.

The third objective of this thesis is to implement a method to reduce the shock overtesting. Relationships linking the Fourier amplitude spectrum to the shock indictor, i.e. SRS or IES, have been identified which allow notching the specification similarly to the Force-Limited Vibration technique. In turns, the notched specification is used to generate a synthesis waveform to test the equipment with a force level comparable to the coupled system test.

Finally, experiments have been conducted to demonstrate the validity of the current study. First, it has been used to correlate the finite element model. Also, the C^2 coefficient and the vibration overtesting have been measured experimentally with some disagreements with the simulations. At last, the shock overtesting has also been measured experimentally using the SRS envelope. Two different syntheses were employed in the experiment and compared with the simulation.

9.2 Conclusions

The following conclusions can be drawn from the analytical and experimental sensitivity studies undertaken in this thesis. Major conclusions on the proposed techniques to estimate and to reduce the shock overtesting can also be drawn. The major conclusions of this research project are:

1. Vibration Overtesting: The range of value taken by the C^2 coefficient was found analytically between 1 and 3. After the experiment, the range of 2 to 5, as previously reported in the literature, is found to be more realistic.
2. Shock Overtesting: Using the SRS, the shock overtesting does not exceed the vibration overtesting. It only exceeds the vibration overtesting for large C^2 value while using the IES. The shock overtesting associated with the lack of dynamics absorber effect is usually below 10 dB when enveloping the SRS and usually between 15 and 20 dB when enveloping the IES.

3. Shock Overtesting Estimate: Other than the stated limits, no relation could be established between the shock and the vibration overtesting.
4. Shock Overtesting Reduction: It is possible to reduce the shock overtesting by introducing a notch in the shock specification around the fundamental frequencies of the test item. Great care should be taken in order not to introduce an excessive notch.

9.3 Recommendations for Future Work

This thesis has taken an important first step toward the comprehension of the shock overtesting phenomena. Much effort can still be done to complement the work presented in this thesis. In addition, this thesis has identified many new areas of interest for research. These thoughts of future efforts can be summarised in two main categories.

Evaluation and Estimation of the Shock Overtesting

1. Incorporate variations in the shock duration and in the damping of the structure in the sensitivity study. The variations should be introduced for both the coupled system and the assembly-level tests.
2. Investigate more cases with different structures to gain additional knowledge on the range of value taken by the shock overtesting and to find parameters explaining the overtesting.

3. Measure the shock overtesting when enveloping completely the environment at the interface of the test item. The overtesting resulting from this envelope will be more representative of overtesting occurring in actual test. Also, it will allow extending the study to all the modes of the structure. Moreover, any relationship with the vibration overtesting is not expected anymore.

Reduction of the Shock Overtesting

4. Develop a shock synthesis algorithm capable of generating waveforms meeting notched specifications. Both the shock specification, in the form of the SRS or the IES, and the acceleration power density (PSD) should be examined.
5. Investigate the feasibility of implementing the proposed shock overtesting reduction technique using the Mechanical Impact Pyroshock Simulator (MIPS) table.

REFERENCES

1 Moening C.J., "Pyrotechnic shock flight failures", IES Pyrotechnic Shock Tutorial Program, 31st ATM, Institute of Environmental Sciences, April-May 1985

2 Freeman M. T., Spacecraft on-orbit deployment anomalies: What can be done?, IEEE, April 1993

3 Anonymous, "Pyroshock Test Criteria", NASA Technical Handbook, NASA-STD-7003, 1999

4 Kiryenko S., Parquet J. L., Grzeskowiak H., "Susceptibility of equipments to pyroshocks: Return of experience from ESA programmes", Oct. 2005

5 Anonymous, "Shock Handbook - Introduction", ESA Contract Report No 20503/06/NL/SFe, Issue 1, December 2008

6 Bement L.J., Schimmel M.L., " A Manual for Pyrotechnic Design, Development and Qualification ", NASA Technical Memorandum 110172, 1995

7 Chang, Kurng Y., "V-Band Separation Shock Characteristics", 75th Shock and Vibration Symposium, Virginia Beach, VA, October 17, 2004

8 Chang, Kurng Y., "Pyrotechnic Devices, Shock Levels and Their Applications", Pyroshock Seminar, ICSV9, July 8-11, 2002

9 Luhrs, H.N., "Pyrotechnic Shock Workshop: Designing electronics for pyrotechnic shock", 56th Shock and Vibration Symposium, 1985

10 Anonymous, "Shock Handbook – Part3: Shock Damage Risk Assessment", ESA Contract Report No 20503/06/NL/SFe, Issue 1, December 2008

11 Anonymous, "Environmental test methods and engineering guidelines", USA Department of Defence military standard, MIL-STD-810E, 1989

12 Kiryenko S., Kasper J., Ngan I., "Shock prediction for aerospace applications – Return of experience from ESA programmes", Oct. 2005

13 Smith J.L., "Effects of Variables upon Pyrotechnically Induced Shock Response Spectrum", NASA technical paper 2872, 1988

14 Butler T.A., Hemez F.M., Schultze J., Sohn H., Doebling S.W., "Model Validation for a Complex Jointed Structure", IMAC XIX, 2001

15 De Benedetti M., Garofalo G., Zumpano M., Barboni R., "On the damping effect due to bolted junctions in space structures subjected to pyro-shock", Acta Astronautica, 2007

16 Biot M.A. "Transient Oscillations in Elastic System", Ph.D. Thesis, No. 259, Calif. Inst. of Tech., Pasadena, , U.S.A., 1932

17 Irvine T., "An introduction to the shock response spectrum", Revision P, May 24 2002

18 Matsuzaki, Y, "A Review of Shock Response Spectrum", The Shock and Vibration Digest, 1977

19 Thompson W.T., Dahleh M.D., " Theory of Vibration with Applications", 5th edition, Prentice-Hall, 1998

20 Filippi E., "Development of the Alcatel ETCA Pyroshock Test Facility", ESA SP-428, 1999

21 Smallwood, D.O., "An Improved Recursive Formula for Calculating Shock Response Spectra", Shock and Vibration Bull., N° 51, Pt2, pp 211-217, May 1981

22 Hunt F.V., "Stress and Strain Limits on the Attainable Velocity in Mechanical Vibration", The Journal of the Acoustical Society of America, Vol. 32, No. 9, 1960

23 Gaberson H.A., Chalmers R.H., "Modal Velocity as a criterion of shock severity", Shock and Vibration Bulletin, Naval Research Lab, December 1969

24 Garberson H.A., "Half Sine Shock Tests to Assure Machinery Survival in Explosive Environments", IMAC XXII, 2004

25 Gaberson H.A., "Pseudo Velocity Shock Spectrum Rules For Analysis Of Mechanical Shock", 76th Shock and Vibration Symposium, New Orleans, 2005

26 Kacena W.J., McGrath M.B., Rader W.P., "Final Report – Aerospace Systems Pyrotechnic Shock Design Guidelines Manual", Martin Marietta Corporation, 1970

27 Smallwood D., Edwards T., "Energy Methods for the Characterization and Simulation of Shock and Vibration", Spacecraft and Launch Vehicle Dynamic Environment Workshop, El Segundo, CA, p.25, June 2008

28 Zahrah T.F., Hall W.J., "Earthquake Energy Absorption in SDOF Structures", J. of Structural Engr., Vol. 110, No. 8, Aug. 1984, p.1757-1770

29 Hall W.J., McCabe S.L., "Current Design Spectra: Background and Limitations", Annals New York Academy of Science, p.222-233, 1989

30 Ordaz M., Huerta B., Reinoso E., "Exact computation of input-energy spectra from Fourier amplitude spectra", Earthquake Engng Struct. Dyn, 2003, p.597-605

31 Anonymous, "Dynamic Environmental Criteria", NASA Technical Handbook, NASA-HDBK-7005, 2001

32 Anonymous, "Shock Handbook – Part 1: Shock Input Derivation to Subsystems", ESA Contract Report No 20503/06/NL/SFe, Issue 1, December 2008

33 Kiryenko S., Parquet J.L., "Shock environment in spacecraft from early definition to final verification", ESA/ESTEC, Dec. 2002

34 Barboni R., Galluccio G., Collini L., De Benedetti M., "On the use of FEM for pyro-shock propagation in space strutures", 53rd International Astronautical Congress, Houston, 2002

35 Barboni R., Galluccio G., Sciandra E., De Benedetti M., "On the experimental validation of FEM for pyro-shock propagation in space structures", AIDAA XVII Congresso Nazionale, Rome, 2003

36 Anonymous, "Shock Handbook – Part 2: Shock Verification Approach", ESA Contract Report No 20503/06/NL/SFe, Issue 1, December 2008

37 Doejaaren F., Wijker J., "Pyroshock tests on a solar array holdown and release system", Proceedings of the European Conference on Spacecraft Structures, Materials and Mechanical Testing, Noordwijk, The Netherlands, ESA SP-468, 2001

38 Kiryenko S., Piret G., Kasper J., "ESA/ESTEC Shock Bench Presentation", Proceedings of the European Conference on Spacecraft Structure, Materials and Mechanical Testing, 2005

39 Smallwood D.O., "A Family of Transient Suitable for Reproduction on a Shaker Based on the cosm(x) Window", Journal of the IEST, Volume 45, p. 178-184, 2002

40 Foss R., Rossi S., Greene J., " Practical Guidelines to Evaluate Shock Duration Over-Test Severity", Proceedings of the 20th Aerospace Testing Seminar, 2002

41 Scharton T.D., "Force Limited Vibration Testing", NASA Technical Handbook, NASA-HDBK-7004, 20 p., 2000.

42 Soucy Y., Dharanipathi V., Sedaghati R., "Comparison of Methods for Force Limited Vibration Testing", IMAC XXIII, 2005

43 Soucy Y., Dharanipathi V., Sedaghati R., "Investigation of Force-Limited Vibration for the Reduction of Overtesting", Journal of Spacecraft and Rockets, Vol.43, No.4, p. 866-876., 2006

44 Sedaghati R., Soucy Y., Etienne N., "Efficient Estimation of Effective Mass for Complex Structure under Base Excitations", Canadian Aeronautics and Space Journal, Vol. 49, No. 3, 2003

45 Fitzpatrik K., McNeill S., "Methods to Specify Random Vibration Acceleration Environments That Comply with Force Limit Specifications", IMAX XXV, Orlando, p.12, 2005

46 Bement L.J., Schimmel M.L., "A Manual for Pyrotechnic Design Development and Qualification", NASA Technical Memorandum 110172, p.76, 1995

47 Luhrs H., "Designing Electronics for Pyrotechnic Shock," Pyrotechnic Shock Workshop, Shock and Vibration Bulletin 57, Naval Research Laboratory, Washington D.C., p. 2, 1987, p.2

48 Luhrs, H., "Equipment Sensitivity to Pyrotechnic Shock", Proceedings of the 22nd ATM, Institute of Environmental Sciences, p. 3-4, April 1976, p.2

49 Ferebee R., Clayton J., Alldredge D., Irvine T., "An Alternative Method of Specifying Shock Test Criteria", Spacecraft and Launch Vehicle Dynamic Environment Workshop, El Segundo, CA, p.18, June 2008

50 Larue L., Carval S., Mary S., "Equipment susceptibility to shock (SEC-CI)". Workshop on Spacraft Shock Environment and Verification, Noordwijk, Netherlands, p.16, May 2008

51 Anonymous, "Operating Instructions – Quartz Force Transducer for Three Components Type 9251", Kistler, 14 p.

52 Steinberg D.S., "Vibration analysis for electronic equipment", 3rd Ed, John Wiley & Sons Inc, p. 440 , 2000

53 Anonymous, "Patran Users Guide – Patran 2005 r3", MSC Software, p. 184, 2005

54 Anonymous, "General Environmental Verification Specification for STS & LEV Payloads, Subsystems, and Components", NASA GEVS-SE Rev A, 1996

55 Wijker J., "Mechanical Vibrations in Spacecraft Design", 1st Ed., Springer, p. 431 , 2003

56 Anonynuous, "Delta II planner's guide", McDonnel Douglas Aerospace, MDC H3224D, April 1996

57 Bowerman B.L., O'Connel R.T., Dickey D.A., "Linear Statistical Models: An applied approach", 1st Ed., Duxbudy Press, p. 690, 1986

Appendix A

Engineering Drawings

DO NOT SCALE DRAWING

NOTES:

1. REMOVE ALL BURRS AND BREAK SHARP EDGES
2. MATERIAL: AL 6061-T6

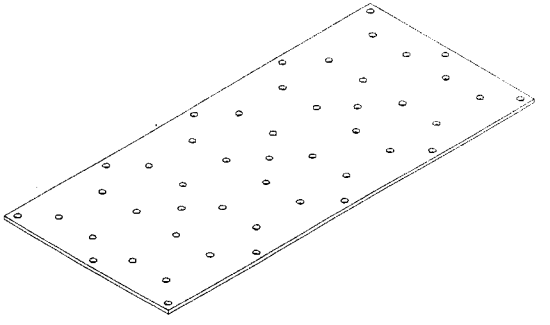

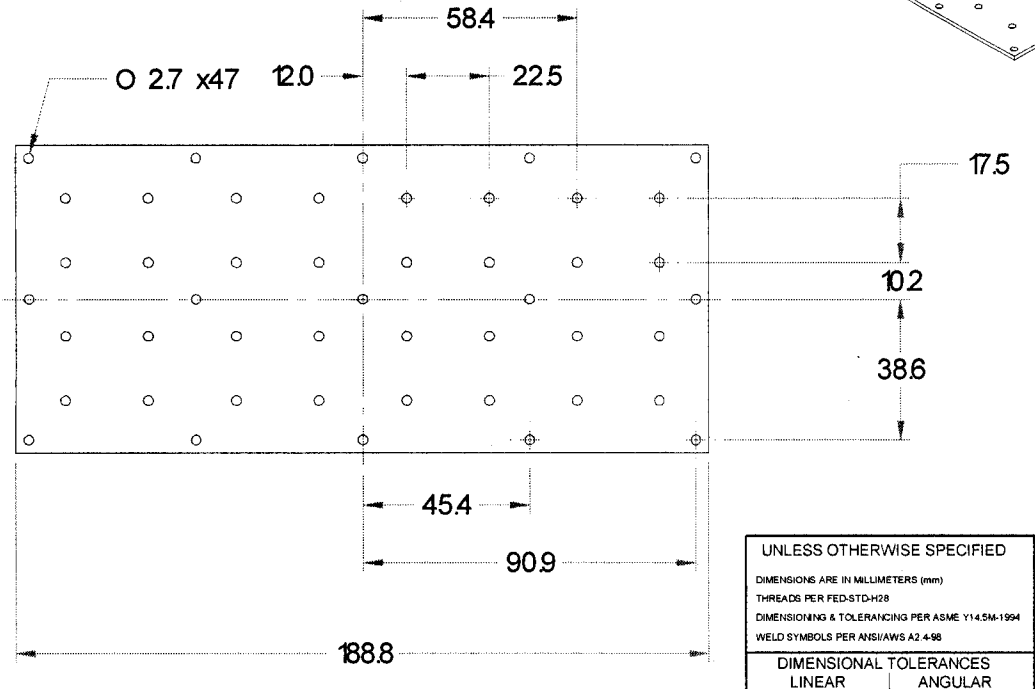

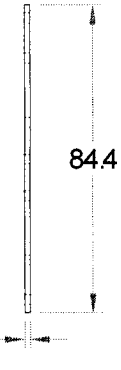

APPROVALS	DATE	SIGNATURES
DRAWING: J-P Deblois	(Y-M-D) 08-04-09	
DESIGN:	08-04-09	

UNLESS OTHERWISE SPECIFIED

DIMENSIONS ARE IN MILLIMETERS (mm)
THREADS PER FED-STD-H28
DIMENSIONING & TOLERANCING PER ASME Y14.5M-1994
WELD SYMBOLS PER ANSI/AWS A2.4-98

DIMENSIONAL TOLERANCES

LINEAR	ANGULAR
.X ± 0.1	X ± 1°
.XX ± 0.05	.X ± .5°
.XXX ± 0.025	.XX ± .25°

[X] NON FLIGHT
[ ] FLIGHT

THIRD ANGLE PROJECTION

Canadian Space Agency / Agence spatiale canadienne
6767 ROUTE DE L'AEROPORT SAINT-HUBERT, QC, CANADA J3Y 8Y9

PROJECT: Shock Overtesting Investigation

TITLE: Board

SIZE	DWG NO.	REV
A	CON-TI-01	P1

SCALE 1 : 1 | WEIGHT | SHEET 1 OF 1

DO NOT SCALE DRAWING

NOTES:

1. REMOVE ALL BURRS AND BREAK SHARP EDGES
2. MATERIAL: BRASS
3. QUANTITY: 8

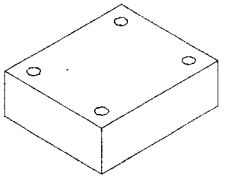

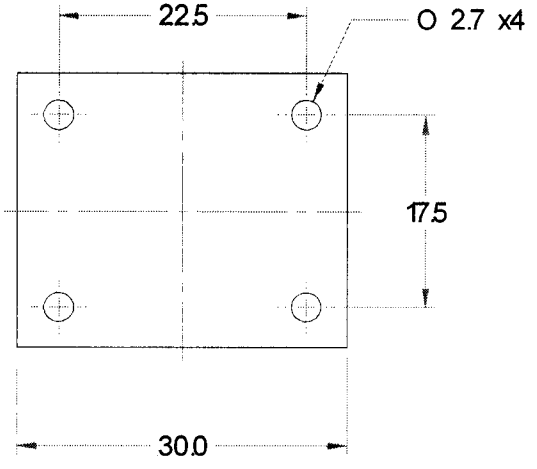

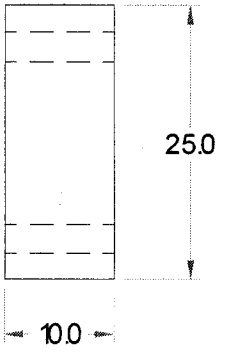

APPROVALS	DATE	SIGNATURES
DRAWING: J-P Deblois	(Y-M-D) 08-04-09	
DESIGN:	08-04-09	

UNLESS OTHERWISE SPECIFIED

DIMENSIONS ARE IN MILLIMETERS (mm)
THREADS PER FED-STD-H28
DIMENSIONING & TOLERANCING PER ASME Y14.5M-1994
WELD SYMBOLS PER ANSI/AWS A2.4-98

DIMENSIONAL TOLERANCES

LINEAR	ANGULAR
.X ± 0.1	X ± 1°
.XX ± 0.05	.X ± .5°
.XXX ± 0.025	.XX ± .25°

[X] NON FLIGHT
[ ] FLIGHT

THIRD ANGLE PROJECTION

Canadian Space Agency / Agence spatiale canadienne
6767 ROUTE DE L'AEROPORT SAINT-HUBERT, QC, CANADA J3Y 8Y9

PROJECT: Shock Overtesting Investigation

TITLE: Component

SIZE	DWG NO.	REV
A	CON-TI-02	P1

SCALE 2 : 1 | WEIGHT | SHEET 1 OF 1

DO NOT SCALE DRAWING

NOTES:

1. REMOVE ALL BURRS AND BREAK SHARP EDGES
2. MATERIAL: AL 6061-T6

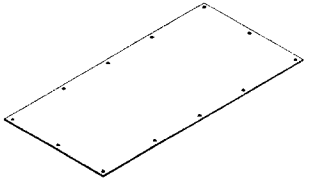

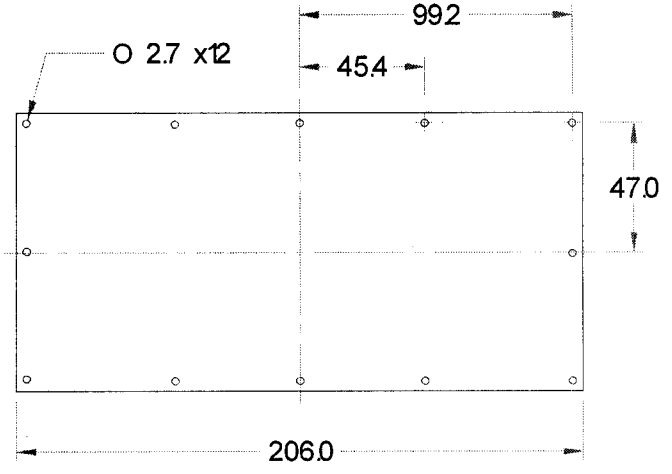

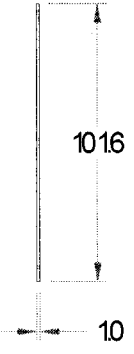

UNLESS OTHERWISE SPECIFIED

DIMENSIONS ARE IN MILLIMETERS (mm)
THREADS PER FED-STD-H28
DIMENSIONING & TOLERANCING PER ASME Y14.5M-1994
WELD SYMBOLS PER ANSI/AWS A2.4-98

DIMENSIONAL TOLERANCES

LINEAR	ANGULAR
.X ± 0.1	X ± 1°
.XX ± 0.05	.X ± .5°
.XXX ± 0.025	.XX ± .25°

[X] NON FLIGHT
[ ] FLIGHT

THIRD ANGLE PROJECTION

APPROVALS	DATE (Y-M-D)	SIGNATURES
DRAWING: J-P Deblois	08-04-09	
DESIGN:	08-04-09	

Canadian Space Agency / Agence spatiale canadienne
6767 ROUTE DE L'AEROPORT SAINT-HUBERT, QC, CANADA J3Y 8Y9

PROJECT: Shock Overtesting Investigation

TITLE: Cover

SIZE	DWG NO.	REV
A	CON-TI-03	P1

SCALE 1 : 2 | WEIGHT | SHEET 1 OF 1

DO NOT SCALE DRAWING

NOTES:

1. REMOVE ALL BURRS AND BREAK SHARP EDGES
2. MATERIAL: AL 6061-T6

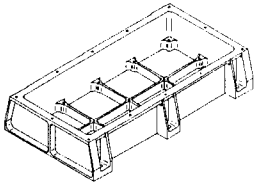

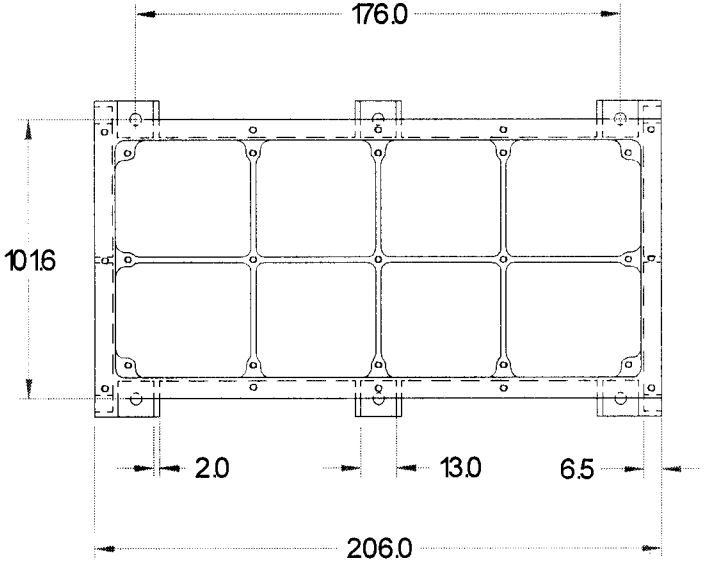

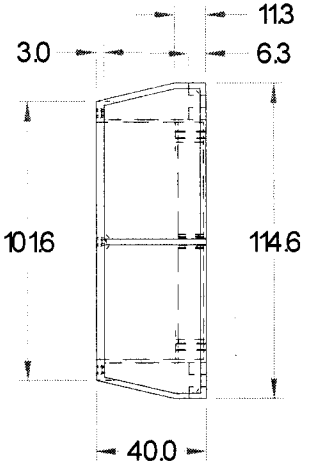

APPROVALS	DATE	SIGNATURES
DRAWING: J-P Deblois	(Y-M-D) 08-04-09	
DESIGN:	08-04-09	

UNLESS OTHERWISE SPECIFIED

DIMENSIONS ARE IN MILLIMETERS (mm)
THREADS PER FED-STD-H28
DIMENSIONING & TOLERANCING PER ASME Y14.5M-1994
WELD SYMBOLS PER ANSI/AWS A2.4-98

DIMENSIONAL TOLERANCES

LINEAR	ANGULAR
.X ± 0.1	X ± 1°
.XX ± 0.05	.X ± .5°
.XXX ± 0.025	.XX ± .25°

[X] NON FLIGHT
[ ] FLIGHT

THIRD ANGLE PROJECTION

Canadian Space Agency / Agence spatiale canadienne
6767 ROUTE DE L'AEROPORT SAINT-HUBERT, QC, CANADA J3Y 8Y9

PROJECT: Shock Overtesting Investigation

TITLE: Test Item Box

SIZE	DWG NO.	REV
A	CON-TI-01	P1

SCALE 1 : 2 | WEIGHT | SHEET 1 OF 1

DO NOT SCALE DRAWING

NOTES:

1. REMOVE ALL BURRS AND BREAK SHARP EDGES
2. MATERIAL: AL 6061-T6
3. QUANTITY: 2
4. Basic shape: 1/4 C-shape extrusion 23023

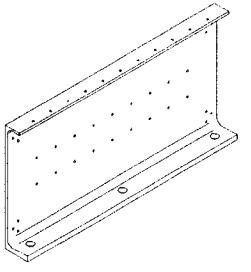

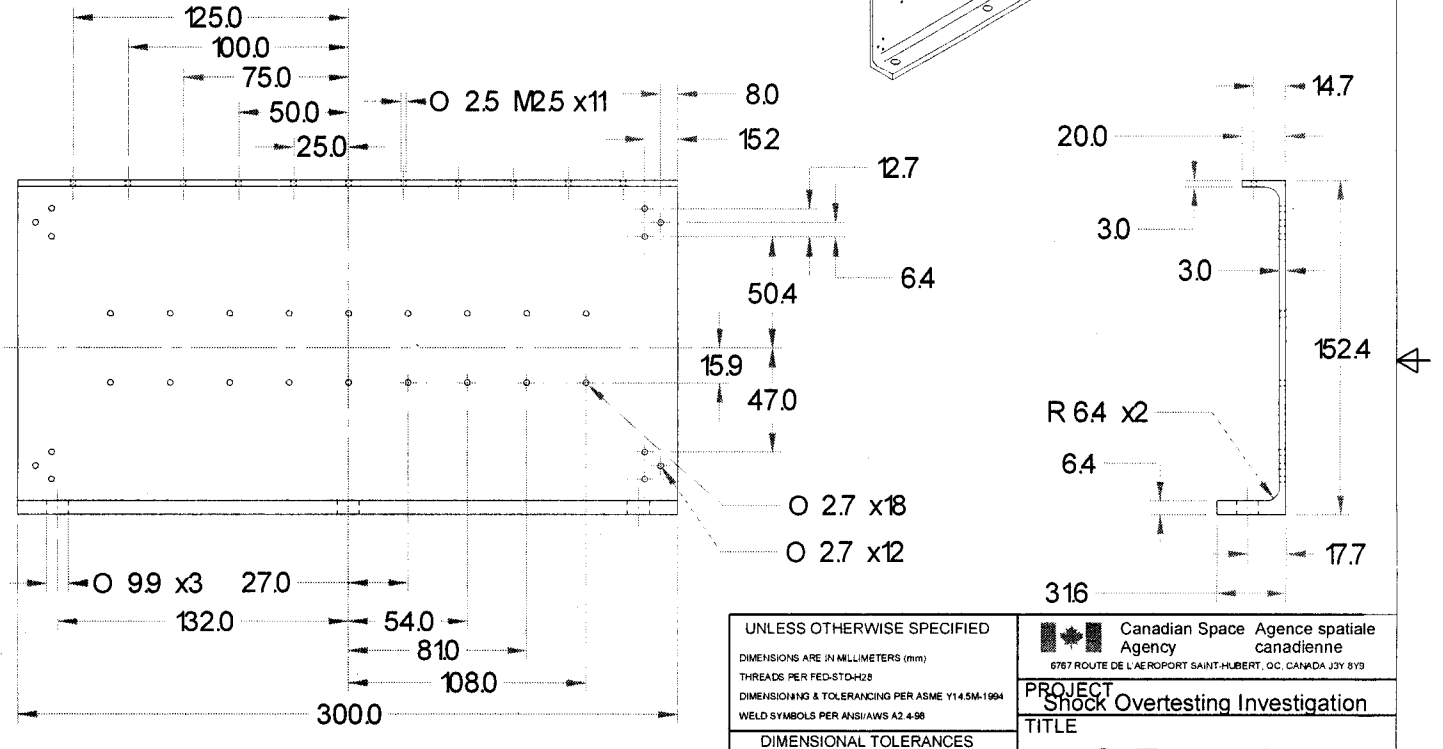

APPROVALS	DATE	SIGNATURES
DRAWING: J-P Deblois	(Y-M-D) 08-04-09	
DESIGN:	08-04-09	

UNLESS OTHERWISE SPECIFIED

DIMENSIONS ARE IN MILLIMETERS (mm)
THREADS PER FED-STD-H28
DIMENSIONING & TOLERANCING PER ASME Y14.5M-1994
WELD SYMBOLS PER ANSI/AWS A2.4-98

DIMENSIONAL TOLERANCES

LINEAR	ANGULAR
.X ± 0.1	X ± 1°
.XX ± 0.05	.X ± .5°
.XXX ± 0.025	.XX ± .25°

[X] NON FLIGHT
[ ] FLIGHT

THIRD ANGLE PROJECTION

Canadian Space Agency / Agence spatiale canadienne
6767 ROUTE DE L'AEROPORT SAINT-HUBERT, QC, CANADA J3Y 8Y9

PROJECT: Shock Overtesting Investigation

TITLE: C Extruxion

SIZE	DWG NO.	REV
A	CON-MS-01	P1

SCALE 1 : 2.5 | WEIGHT | SHEET 1 OF 1

DO NOT SCALE DRAWING

NOTES:

1. REMOVE ALL BURRS AND BREAK SHARP EDGES
2. MATERIAL: AL 6061-T6

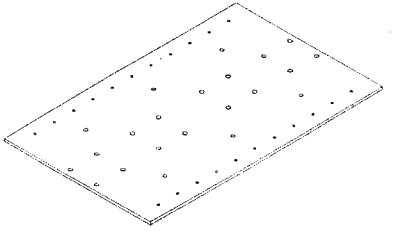

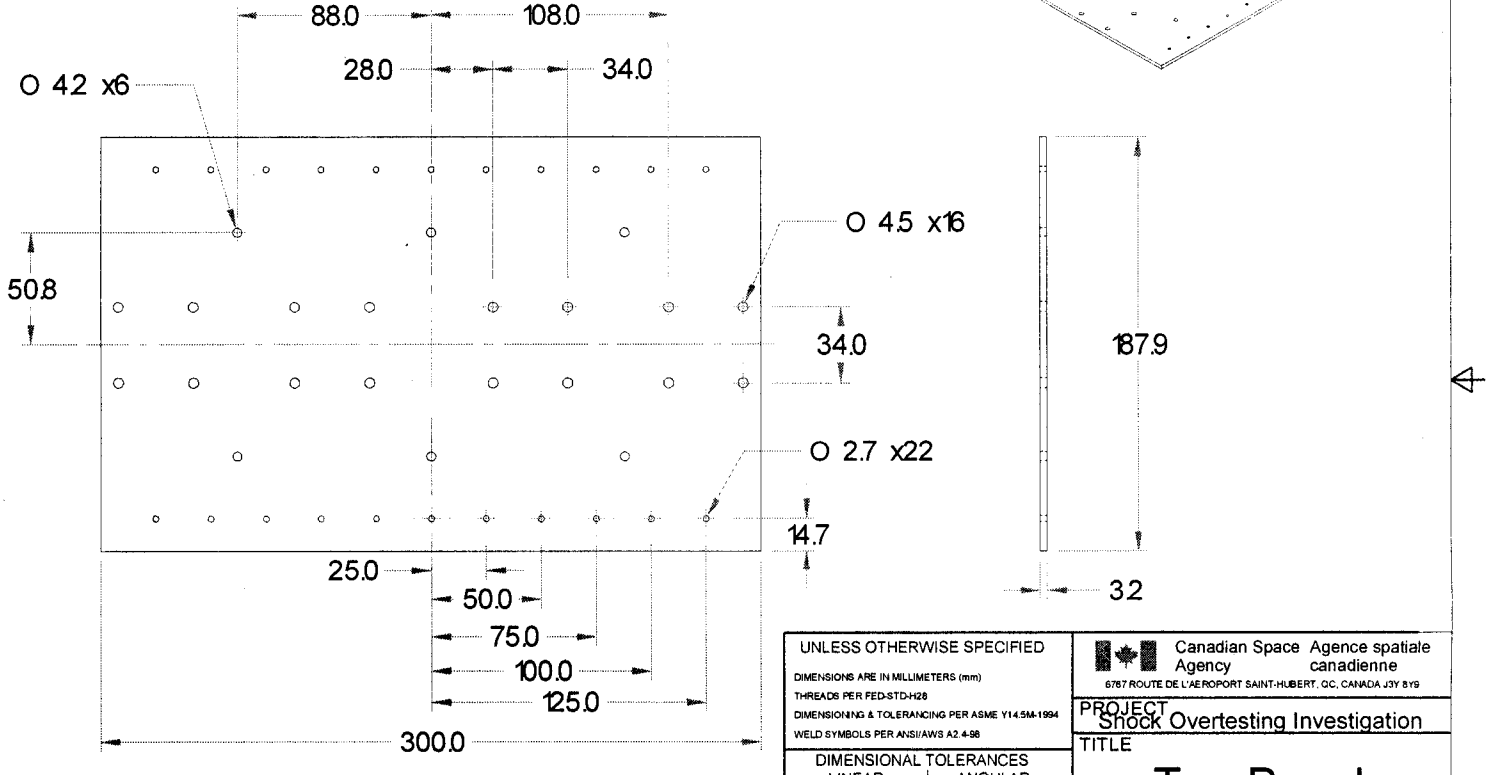

APPROVALS	DATE	SIGNATURES
DRAWING: J-P Deblois	(Y-M-D) 08-04-09	
DESIGN:	08-04-09	

UNLESS OTHERWISE SPECIFIED

DIMENSIONS ARE IN MILLIMETERS (mm)
THREADS PER FED-STD-H28
DIMENSIONING & TOLERANCING PER ASME Y14.5M-1994
WELD SYMBOLS PER ANSI/AWS A2.4-98

DIMENSIONAL TOLERANCES

LINEAR	ANGULAR
.X ± 0.1	X ± 1°
.XX ± 0.05	.X ± .5°
.XXX ± 0.025	.XX ± .25°

[X] NON FLIGHT
[ ] FLIGHT

THIRD ANGLE PROJECTION

Canadian Space Agency / Agence spatiale canadienne
6767 ROUTE DE L'AEROPORT SAINT-HUBERT, QC, CANADA J3Y 8Y9

PROJECT: Shock Overtesting Investigation

TITLE: Top Panel

SIZE	DWG NO.	REV
A	CON-MS-02	P1

SCALE 1 : 2.5 | WEIGHT | SHEET 1 OF 1

DO NOT SCALE DRAWING

NOTES:

1. REMOVE ALL BURRS AND BREAK SHARP EDGES
2. MATERIAL: AL 6061-T6
3. QUANTITY: 4
4. Basic Shape: 1/8 L-Shape extrusion 117010

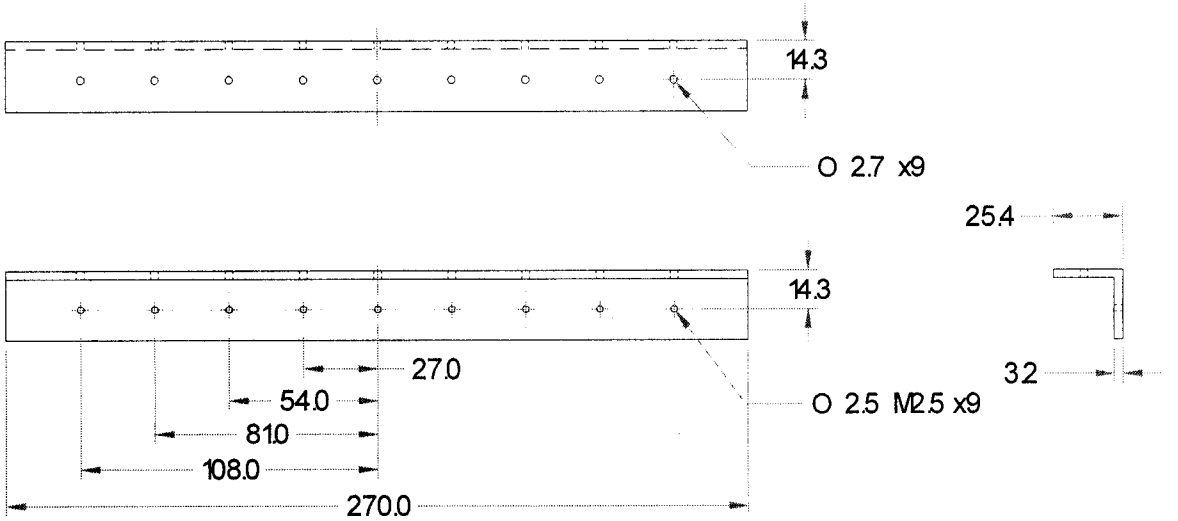

APPROVALS	DATE	SIGNATURES
DRAWING: J-P Deblois	(Y-M-D) 08-04-09	
DESIGN:	08-04-09	

UNLESS OTHERWISE SPECIFIED
DIMENSIONS ARE IN MILLIMETERS (mm)
THREADS PER FED-STD-H28
DIMENSIONING & TOLERANCING PER ASME Y14.5M-1994
WELD SYMBOLS PER ANSI/AWS A2.4-98

DIMENSIONAL TOLERANCES

LINEAR	ANGULAR
.X ± 0.1	X ± 1°
.XX ± 0.05	.X ± .5°
.XXX ± 0.025	.XX ± .25°

[X] NON FLIGHT
[ ] FLIGHT

THIRD ANGLE PROJECTION

Canadian Space Agency / Agence spatiale canadienne
6767 ROUTE DE L'AEROPORT SAINT-HUBERT, QC, CANADA J3Y 8Y9

PROJECT: Shock Overtesting Investigation

TITLE: Holder

SIZE	DWG NO.	REV
A	CON-MS-03	P1

SCALE 1 : 1 | WEIGHT | SHEET 1 OF 1

DO NOT SCALE DRAWING

NOTES:

1. REMOVE ALL BURRS AND BREAK SHARP EDGES
2. MATERIAL: AL 6061-T6

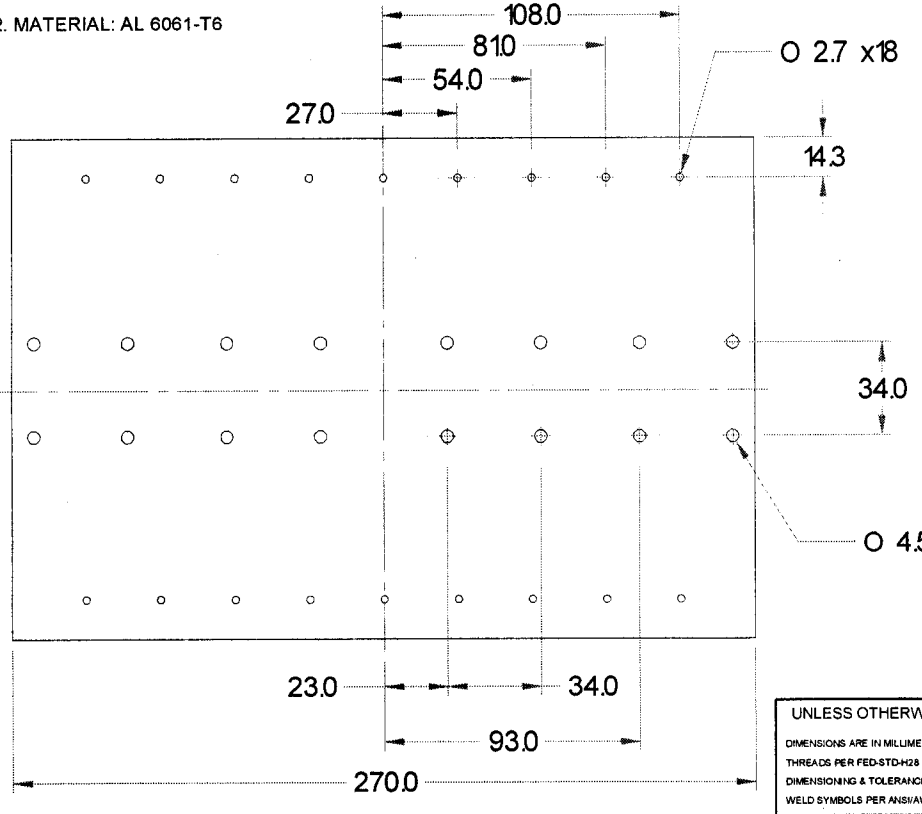

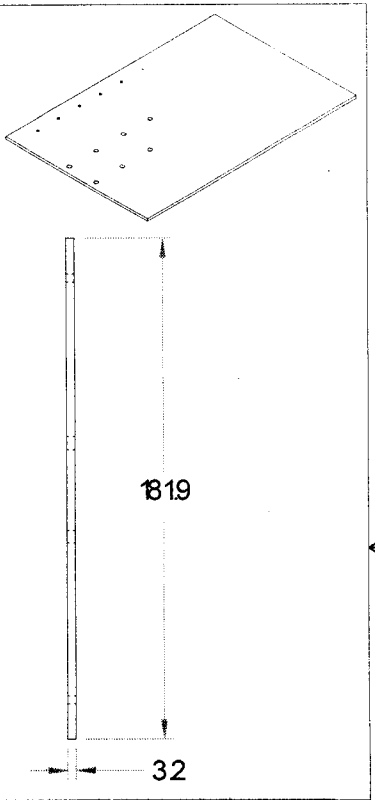

APPROVALS	DATE	SIGNATURES
DRAWING: J-P Deblois	(Y-M-D) 08-04-09	
DESIGN:	08-04-09	

UNLESS OTHERWISE SPECIFIED

DIMENSIONS ARE IN MILLIMETERS (mm)
THREADS PER FED-STD-H28
DIMENSIONING & TOLERANCING PER ASME Y14.5M-1994
WELD SYMBOLS PER ANSI/AWS A2.4-98

DIMENSIONAL TOLERANCES

LINEAR	ANGULAR
.X ± 0.1	X ± 1°
.XX ± 0.05	.X ± .5°
.XXX ± 0.025	.XX ± .25°

[X] NON FLIGHT
[ ] FLIGHT

THIRD ANGLE PROJECTION

Canadian Space Agency / Agence spatiale canadienne
6767 ROUTE DE L'AEROPORT SAINT-HUBERT, QC, CANADA J3Y 8Y9

PROJECT: Shock Overtesting Investigation

TITLE: Mid Panel

SIZE	DWG NO.	REV
A	CON-MS-04	P1

SCALE 1 : 1 | WEIGHT | SHEET 1 OF 1

DO NOT SCALE DRAWING

NOTES:

1. REMOVE ALL BURRS AND BREAK SHARP EDGES
2. MATERIAL: BRASS
3. QUANTITY: 8

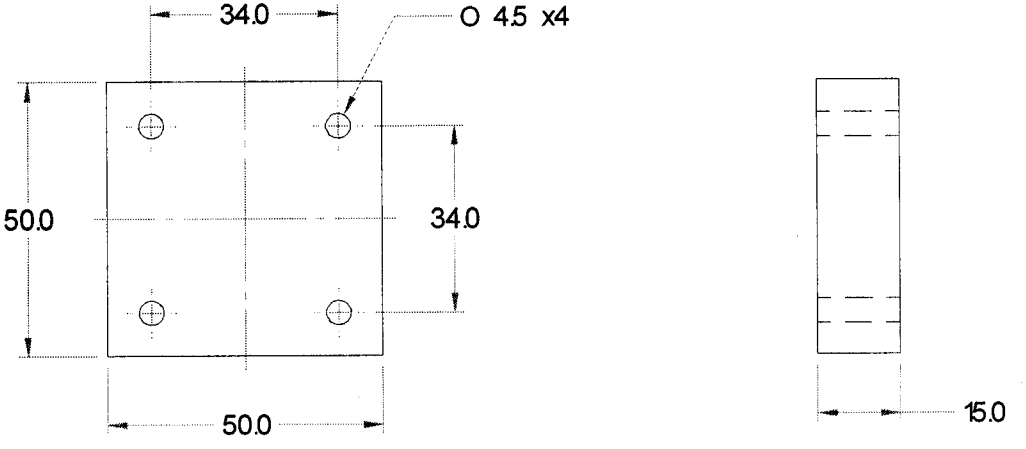

UNLESS OTHERWISE SPECIFIED
DIMENSIONS ARE IN MILLIMETERS (mm)
THREADS PER FED-STD-H28
DIMENSIONING & TOLERANCING PER ASME Y14.5M-1994
WELD SYMBOLS PER ANSI/AWS A2.4-98

DIMENSIONAL TOLERANCES

LINEAR	ANGULAR
.X ± 0.1	X ± 1°
.XX ± 0.05	.X ± .5°
.XXX ± 0.025	.XX ± .25°

[X] NON FLIGHT
[ ] FLIGHT
THIRD ANGLE PROJECTION

APPROVALS	DATE (Y-M-D)	SIGNATURES
DRAWING: J-P Deblois	08-04-09	
DESIGN:	08-04-09	

Canadian Space Agency / Agence spatiale canadienne
6767 ROUTE DE L'AEROPORT SAINT-HUBERT, QC, CANADA J3Y 8Y9

PROJECT: Shock Overtesting Investigation

TITLE: MS Mass

SIZE	DWG NO.	REV
A	CON-MS-05	P1

SCALE 1 : 1 | WEIGHT | SHEET 1 OF 1

DO NOT SCALE DRAWING

NOTES:

1. REMOVE ALL BURRS AND BREAK SHARP EDGES
2. MATERIAL: AL 6061-T6
3. QUANTITY: 2

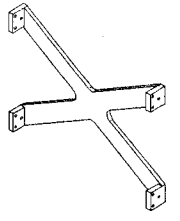

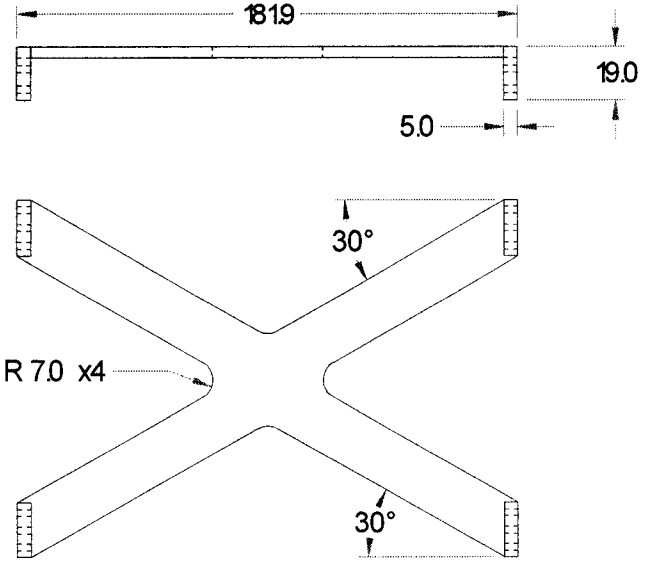

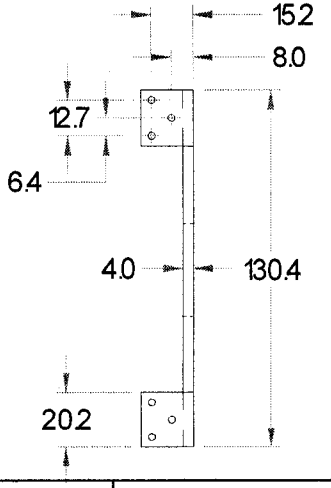

APPROVALS	DATE	SIGNATURES
DRAWING: J-P Deblois	(Y-M-D) 08-04-09	
DESIGN:	08-04-09	

UNLESS OTHERWISE SPECIFIED

DIMENSIONS ARE IN MILLIMETERS (mm)
THREADS PER FED-STD-H28
DIMENSIONING & TOLERANCING PER ASME Y14.5M-1994
WELD SYMBOLS PER ANSI/AWS A2.4-98

DIMENSIONAL TOLERANCES

LINEAR	ANGULAR
.X ± 0.1	X ± 1°
.XX ± 0.05	.X ± .5°
.XXX ± 0.025	.XX ± .25°

[X] NON FLIGHT
[ ] FLIGHT

THIRD ANGLE PROJECTION

Canadian Space Agency / Agence spatiale canadienne
6767 ROUTE DE L'AEROPORT SAINT-HUBERT, QC, CANADA J3Y 8Y9

PROJECT: Shock Overtesting Investigation

TITLE: X Stiffner

SIZE	DWG NO.	REV
A	CON-MS-04	P1

SCALE	WEIGHT	SHEET
1 : 2		1 OF 1

DO NOT SCALE DRAWING

NOTES:

1. REMOVE ALL BURRS AND BREAK SHARP EDGES
2. MATERIAL: AL 6061-T6

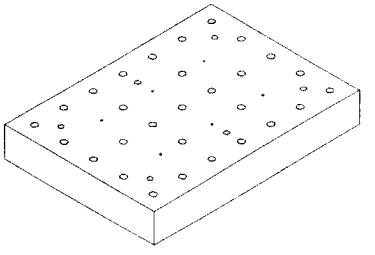

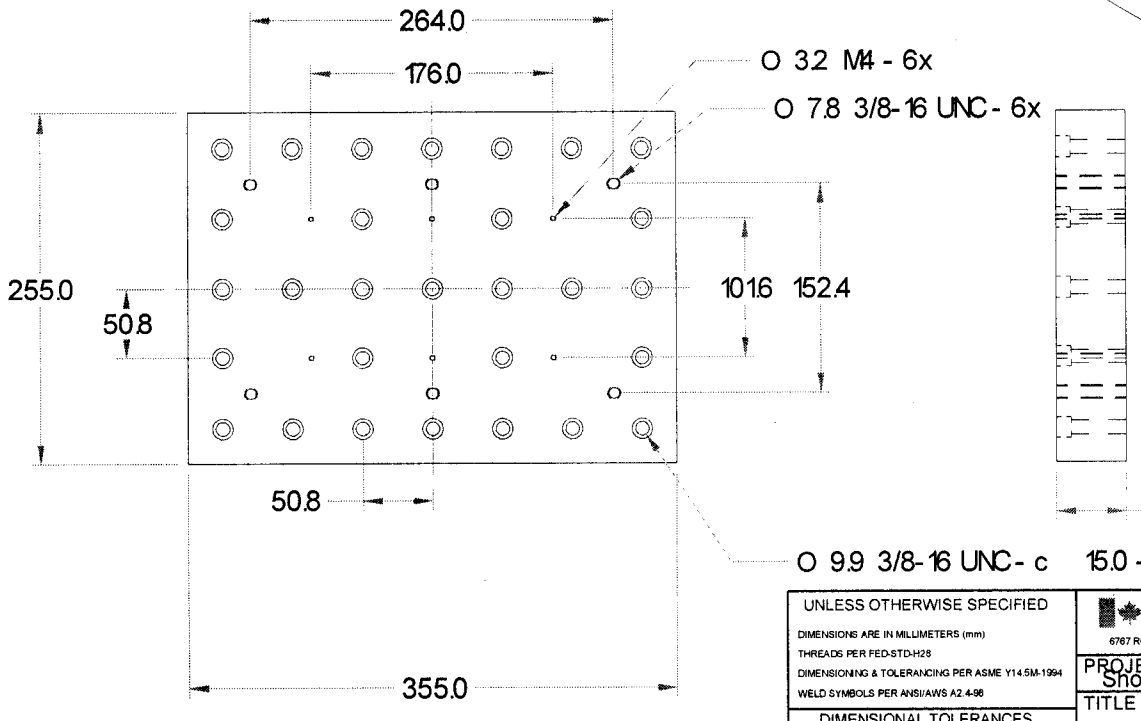

UNLESS OTHERWISE SPECIFIED
DIMENSIONS ARE IN MILLIMETERS (mm)
THREADS PER FED-STD-H28
DIMENSIONING & TOLERANCING PER ASME Y14.5M-1994
WELD SYMBOLS PER ANSI/AWS A2.4-98

DIMENSIONAL TOLERANCES	
LINEAR	ANGULAR
.X ± 0.1	X ± 1°
.XX ± 0.05	.X ± .5°
.XXX ± 0.025	.XX ± .25°

[X] NON FLIGHT
[ ] FLIGHT

THIRD ANGLE PROJECTION

APPROVALS	DATE (Y-M-D)	SIGNATURES
DRAWING: J-P Deblois	08-04-09	
DESIGN:	08-04-09	

Canadian Space Agency / Agence spatiale canadienne
6767 ROUTE DE L'AEROPORT SAINT-HUBERT, QC, CANADA J3Y 8Y9

PROJECT: Shock Overtesting Investigation

TITLE: Fixture DFL

SIZE	DWG NO.	REV
A	CON-FIX-03	P1

SCALE 1 : 4	WEIGHT	SHEET 1 OF 1